Infrared fibres in astronomical instrumentation

Haynes, Roger

Infrared Fibres in Astronomical Instrumentation

by

Roger Haynes

September 1995

A thesis submitted to the University of Durham in accordance with the regulations for admission to the degree of Doctor of Philosophy

To Maree Lee and my family

Acknowledgements

I would like to thank my supervisors Ian Parry, Jeremy Allington-Smith and John Major for their support and guidance, the staff and postgraduates of the Physics Department at Durham, and in particular George Dodsworth, Ian Lewis and Ray Sharples. Many thanks to my wife for her tolerance and patient editing. In addition, I would like to thank Fred Watson for his encouragement and acknowledge the support of the UKIRT staff at both the Royal Observatory Edinburgh and in Hawaii.

Preface

The work presented in this thesis was carried out between 1991 and 1995 while the author was a research student under the supervision of Dr I. R. Parry, Dr J. V. Major and Dr J. R. Allington-Smith in the Department of Physics at the University of Durham. None of the material presented has been previously submitted for a degree at this or any other University. Some of the work decribed was carried out as part of a collaboration, however, the author was responsible for the experimental results presented within. Some of the material has appeared in the following papers:

Haynes R., and Parry I. R., Proc. SPIE 2198, 572, (1994).

Haynes R., Sharples R. M., and Ennico K., SPECTRUM Newsletter of the Royal Observatories, no. 7, 4, (1995).

Abstract

For several years multi-object spectroscopy systems have been available for carrying out survey work in the visible region, but until very recently there has not been a system for the near infrared region. This thesis describes the design, manufacture and commissioning of the first multi-object fibre system for near infrared spectroscopy. SMIRFS (Spectroscopic Multi-object Infrared Fibre System) is a prototype system that has been designed at the Department of Physics in Durham to couple the Cassegrain focus of the United Kingdom InfraRed Telescope (UKIRT) to a cooled long slit infrared spectrograph (CGS4). Two different fibre bundles are available, each containing 14 fibres. One bundle is made from zirconium fluoride fibres, for K band spectroscopy and the second bundle is made from silica fibres, for J and H band spectroscopy.

During the design process of SMIRFS a number of issues were addressed. These included; the characteristics of infrared fibres, in particular their throughput and FRD, atmospheric features in the near infrared and suitable sky subtraction techniques, fibre preparation and evaluation, the use of microlenses for coupling slow focal ratio beams with fibres, and the thermal emissions from the warm material of the instrument. These, along with the design, manufacture and testing of the SMIRFS are described in detail, including the fibre evaluation results and estimates for throughput, instrument thermal background derived from the commissioning run data.

Finally, there is a brief discussion on the development of infrared fibre system for astronomy.

Table of Contents

CHAPTER 1: INTRODUCTION 11

1.1 Infrared spectroscopy 11
1.1.1 Spectrographs and detectors 11
1.1.2 Spectroscopic studies 12
1.1.3 Infrared surveys 13

1.2 Fibre spectroscopy 13
1.2.1 A brief history 13
1.2.2 Infrared fibres for spectroscopy 14

1.3 Project Plan 15
1.3.1 Fibre material 16
1.3.2 Coupling to the telescope and spectrograph 16
1.3.3 Fibre positioning 17
1.3.4 Coupling to the spectrograph 17
1.3.5 Field acquisition and guiding 17

1.4 Summary 18

CHAPTER 2: INFRARED OPTICAL FIBRES 19

2.1 Introduction 19

2.2 Basic properties of fibre 19
2.2.1 Basic structure 19
2.2.2 Mechanism of light guiding 19
2.2.3 Dispersion 21
2.2.4 Absorption losses 21
2.2.5 Focal ratio degradation (FRD) 22

2.3 Infrared fibre materials 24
2.3.1 Brief history 24
2.3.2 Transmission characteristics. 24
2.3.2.1 Silica fibres 24
2.3.2.2 Zirconium fluoride glass fibres 26
2.3.2.3 Chalcogenide glass fibres 27

2.4 Summary 27

CHAPTER 3: THE NEAR-IR SKY AND SKY SUBTRACTION 37

3.1 Introduction 37

3.2 The atmosphere in the near-IR 37

3.2.1 Atmospheric transmission 37
3.2.2 Non-thermal emissions 38
3.2.3 Thermal emissions 39

3.3 Sky subtraction **39**
3.3.1 Spatial separation (fibre pairs) 40
3.3.2 Temporal separation (beam switching) 40
3.3.3 Beam switching fibre pairs (cross beam switching) 40
3.3.4 Scattered dedicated sky fibres (mean sky subtraction) 41
3.3.5 Instrument considerations in sky subtraction 41
3.3.6 Infrared sky subtraction 42

3.4 Summary **42**

CHAPTER 4: INFRARED FIBRE PREPARATION AND EVALUATION TECHNIQUES **48**

4.1 Introduction **48**

4.2 Terminating fibres **48**

4.3 Polishing techniques **49**

4.4 Measurement of FRD **51**
4.4.1 Infrared FRD measurement 52
4.4.1.1 Scanning method using a heated filament 52
4.4.1.2. Scanning method using a infrared He/Ne laser (1.52μm) 53
4.4.1.3. Scanning method of output ring using an infrared He/Ne laser (1.52μm) 54
4.4.1.4 The future of Infrared FRD measurement 55

4.5 Throughput measurement **55**

4.6 Thermal emissivity calculations for the fibres **56**

4.6 Summary **58**

CHAPTER 5: MICROLENSES AND COUPLING WITH FIBRES. **64**

5.1 Introduction **64**

5.2 Coupling telescope and spectrograph **64**
5.2.1 Coupling at the fibre input 65
5.2.1.1 Direct re-imaging 66
5.2.1.2 Pupil imaging 67
5.2.2 Lens coupling at the fibre output. 67
5.2.3 Summary of fibre coupling methods 68

5.3 Types of microlenses **69**
5.3.1 Fibre tapers 69

5.3.2 Spherical lenses 70
5.3.3 Rod lenses 70
5.3.4 Graded index (GRIN) lenses 71
5.3.5 Lens aberrations and reflection losses 72
5.3.6 Choosing your microlens 72

5.4 Summary 73

CHAPTER 6: SMIRFS-AN INFRARED MULTI-FIBRE SYSTEM FOR UKIRT 77

6.1 Introduction 77

6.2 Design considerations 77
6.2.1 Aims 77
6.2.2 General considerations 78
6.2.3 SMIRFS Infrared fibres 79
6.2.4 SMIRFS microlenses 80
6.2.5 The field plate and fibre pointing 82
6.2.6 The slit projection unit. 83
6.2.7 The fibre slit 84
6.2.8 Guide fibre unit 85
6.2.9 Reflection losses in the system 85

6.3 Ray tracing the optical components of SMIRFS 87
6.3.1 Field curvature of UKIRT 87
6.3.2 Microlenses 87
6.3.3 The slit projection unit (SPU) 89

6.4 Technical description of SMIRFS 89
6.4.1 The field plate unit (FPU) 89
6.4.2 The slit projection unit (SPU) 90
6.4.3 The guide fibre unit (GFU) 91
6.4.4 The infrared fibre bundles and fibre slits 92
6.4.4.1 The fibre input 93
6.4.4.2 The fibre slit 94

6.5 Summary 95

CHAPTER 7: MANUFACTURE AND TESTING OF SMIRFS 112

7.1 Introduction 112

7.2 The SMIRFS fibre bundles 112
7.2.1 Pre-polish preparation 112
7.2.2 Fibre polishing 114
7.2.3 Fibre throughput measurements 117
7.2.4 Focal ratio degradation measurements 118
7.2.5 Microlens alignment 119

7.2.5.1 Alignment jig set up 119
7.2.5.2 Aligning the input microlenses 121
7.2.5.3 Aligning the output microlenses 122

7.3 The guide fibre bundle **122**
7.3.1 Fibre preparation 123
7.3.2 Fibre polishing 123
7.3.3 Final assembly of the guide fibre bundle 124

7.4 The slit projection unit (SPU) alignment **125**
7.4.1 Bench alignment procedure 125
7.4.2 SPU adjustments when mounted to CGS4 126

7.5 Summary **127**

CHAPTER 8: COMMISSIONING OF SMIRFS **134**

8.1 Introduction **134**

8.2 Set up and alignment **134**
8.2.1 The field plate unit (FPU) 134
8.2.2 Slit projection unit (SPU) 136
8.2.2.1 Alignment steps 136
8.2.3 Guide fibre unit (GFU) 137

8.3 Throughput of the SMIRFS system **139**
8.3.1 Fibre collecting area 139
8.3.2 Deriving throughput of the fibre bundles 140
8.3.3. Throughput results. 141
8.3.4 Relative fibre throughput using sky frames 143
8.3.4.1 Relative throughput results 143
8.3.5 Sources of throughput loss 145
8.3.5.1 Fibre pointing 145
8.3.5.2 Transmission losses 145
8.3.5.3 Fibre output beam alignment 146
8.3.5.4 Slit vignetting 146
8.3.6 Summary of throughput 147

8.4. Instrument thermal background **147**
8.4.1 Thermal background estimates from observations 147
8.4.1.1 Data reduction 148
8.4.1.2 The thermal background from SMIRFS vs CGS4 alone 148
8.4.2 Origins of the thermal background 149

8.5 Spectral resolution **150**

8.6 Effectiveness of sky subtraction **151**

8.7 K-band spectra of bright K & M Giants **153**

8.8 Data reduction 154

8.9 Summary 154

CHAPTER 9: FURTHER DEVELOPMENT OF IR FIBRES 166

9.1 Multi-object spectroscopy 166

9.2 Integral field spectroscopy 167
9.2.1 An IFU for UKIRT 167

9.3 K band fibre spectroscopy 168

9.5 Summary 169

CHAPTER 10: CONCLUSIONS 172

REFERENCES 175

Chapter 1: Introduction

During the early nineteenth century telescopes and the spectroscope evolved rapidly and since then astronomers have been using spectroscopy to study the dynamics and chemical composition of a multitude of astronomical objects. In the past these studies have been concentrated in the visible region but with the development of infrared array detectors there has been a significant increase in near-IR spectroscopy. In this thesis I hope to demonstrate that infrared fibres can play an important role in the future of this rapidly expanding field.

1.1 Infrared spectroscopy

1.1.1 Spectrographs and detectors

In recent years a number of near-IR spectrographs have been built to take advantage of the emergence of two dimensional infrared arrays based on InSb and HgCdTe technologies. Examples include instruments such as CSHELL at the NASA IRTF (Tokunaga *et al.*, 1990) designed to accommodate a 256x256 InSb array giving ~ 1-5 μm coverage at R < 40,000 and CGS4 at UKIRT (Mountain *et al.*, 1990) originally designed with a 58x62 InSb array which has recently been upgraded to a 256x256 InSb array giving ~ 1-5μm coverage at R < 20,000, where R is the resolution of the spectrograph and is given by

$$R = \frac{\lambda}{\Delta\lambda}$$

infrared array technologies have been developing rapidly in the past few years, 256x256 arrays are now commonplace in infrared instrumentation and 1028x1028 arrays will soon be available. Both HgCdTe (Hodapp *et al.*, 1994) and InSb (Fowler *et al.* ,1994) detectors will be available in this format and the next generation of infrared instruments for the new 8-10 meter class telescopes will be based on these. These include proposed spectrographs such as near-IR spectrographs for the Gemini telescopes (1-5μm and R < 30,000) and the Keck telescope (1-5μm and R < 100,000 with adaptive optics), also FOCAS for the SUBARU telescope which will have an optical and infrared arm (0.365-0.9μm and 0.9-1.8μm with R < 5000), ISAAC (1-5μm and R < 10,000) and CRIRES (2-5μm and R ≥ 100,000) for the ESO VLT. The detection limits for these instruments

will be enhanced over that of current spectrographs due to the increased collecting area and improved image quality of the telescopes. For example, with the Gemini near-IR spectrograph the expected magnitude limit for a 10σ detection per resolution after a 3 hour exposure is H ~ 21.7 and K ~ 21.0 with a 0.4 arcsec slit width (Davidge *et al.*, 1994).

1.1.2 Spectroscopic studies

Infrared spectroscopy provides the opportunity to study a number of different objects and features. The rest frame of optical features is shifted into the near-IR for distant galaxies at redshifts greater than 1 (Davidge *et al.*, 1994). These high redshift galaxies are important cosmologically because they were formed when the universe was relatively young, approaching the epoch of galaxy formation. Studying the spectra of these galaxies gives information on the stellar content and physical conditions within the galaxy. These infrared features provide comparisons to optical spectra of nearby galaxies. Important quasar optical emission lines are similarly shifted, which can be used to obtain redshifts for the quasar and as probes for the intervening medium. The approximate number density of faint galaxies in the K-band is ~ 40,000 per square degree for $K < 20$ and models indicate that 20-40% of these objects will have a redshift ≥ 1 (Broadhurst *et al.*, 1992). This suggests that there are sufficient objects available within a reasonable field of view to justify the development of infrared multi-object spectroscopic systems.

A number of atomic and molecular features occur in the infrared region, for example CO, H_2 and Fe transitions. These can be used for a multitude of different studies. For example, there have been studies using the profiles of high resolution CO emission features in young stellar objects to compare accretion disk and neutral wind models (e.g. Carr *et al.* and Chandler *et al.*,1994). H_2 emission has been applied to the study of shells of planetary nebulae (e.g. Graham *et al.*, 1994). Fe^{+} and Fe^{++} emission features have been used in the study of supernovae (e.g. Spyromilio *et al.* 1994). In the study of low mass sub-stellar objects such as M dwarfs and brown dwarfs a number of important feature occur in the infrared. These include the H_20 bands, CO, Ca and Na which can be used to help identify and determine the temperature of brown dwarf candidates (Steele *et al.*, 1994). The approximate number density of brown-dwarf candidates within

Pleiades like star clusters would be ~ 50 per square arcmin for K < 21 (Davidge *et al.*, 1994).

1.1.3 Infrared surveys

There are two large infrared imaging sky surveys due to be completed by ~ 1998: DENIS (Epchtein, 1994) and 2MASS (Kleinmann *et al.*, 1994). These should provide a number of interesting sources which will require follow up studies using infrared spectroscopy. DENIS is an all sky survey of the southern hemisphere in the I, J and K_s bands using a camera with 3 different channels, one for each waveband, based at the ESO 1-meter in Chile. The magnitude limits for the survey were to be I ~ 18, J ~ 16 and Ks ~ 14. The study was due to start in early 1994, last for 4 years, and be sensitive to evolved objects such as red dwarfs, late giant stars and spiral galaxies. 2MASS is aimed at mapping the whole sky in three wavelength bands, J, H and K_s using two matched telescopes situated at Mt. Hopkins and Cerro Tololo. The camera is to be a NICMOS3 HgCdTe 256x256 array that will sample the sky from K_s ~ 4-14. It should commence in 1996 and detect ~ 100 million stars and ~ 1 million galaxies. The survey is designed to develop on the Two Micro Sky Survey made in 1969 (Neugebauer & Leighton, 1969) which had a limit of K ~ 3. The surface density of, for example, stellar objects in the 2MASS survey is expected to be ~ 10,000 per square degree at K = 12 at Galactic co-ordinates l = 53°, b = 0°. With number densities such as these, infrared multi-object fibre systems would significantly reduce the time overheads for follow up spectroscopy.

1.2 Fibre spectroscopy

1.2.1 A brief history

A multitude of spectroscopic multi-object fibre systems offering large multiplex gains for spectroscopic studies have been developed and built since the first system (MEDUSA) was produced at the Steward Observatory in 1979 (Hill *et al.* 1982). This was a plug plate system which was closely followed by a number of similar systems different observatories. At the Fiber Optics in Astronomy conference Hill (1988) discussed "The History of Multiobject Fiber Spectroscopy" in detail. By this time plug plate systems such as FOCAP at the AAT (Gray ,1983), OPTOPUS at ESO (Lund & Enard, 1982) and FLAIR at the UK Schmidt (Watson, 1988) had been developed as well as the first

robot positioning systems: MX (Hill and Lesser, 1986) and AUTOFIB (Parry and Sharples, 1988). Since then there have been advances in wide field prime focus systems, such as AUTOFIB2 for the WHT (Parry *et al.*, 1994) and 2df for the AAT (Taylor *et al.*, 1994) with up to 400 fibres in a 2 degree field.

1.2.2 Infrared fibres for spectroscopy

The application of fibres in the near-IR region is a recent development. At the "Fiber Optics In Astronomy II" SPIE conference in 1991 two papers (Levin *et al.* and Dallier *et al.*) discussed instruments that had used fibres for infrared spectroscopy. The first paper concerned IR-DensePak (Levin *et al.*,1993) which was an image slicer composed of 25 ZrF_4 glass fibres packed into an square arrangement at the input end and reformatted into a slit at the output. It was only 6cm long and was used to demonstrate spectral mapping using the infrared grating spectrometer (CRSP) at the Kitt Peak 1.3m and 2.1m telescopes. The group developed a second bundle for the 0.9m telescope on the NASA Kuiper Airborne Observatory. They also measured spectral response at room temperature and 88°K as well as performing FRD measurements (see chapters 2 and 4) at input focal ratios from f/3 to f/12. Their conclusions from this work were "that fluoride fibers and bundles can provide the same new options for infrared. focal plane array instruments that Si fibers have shown for visible instrumentation using Si CCD arrays." (Levin *et al.*, 1993: p.301). The Meudon group (Dallier *et al.* 1993) discussed the use of a 20m length of ZrF_4 glass fibre to link a "warm" Czerny-Turner type spectrograph to the 2m telescope of the Pic du Midi (south of France). They looked at the FRD and throughput of ZrF_4 fibres supplied by Le Verre Fluore in France and Infrared Fiber Systems (IFS) in the USA. The IFS fibre displayed the more favourable FRD characteristics. Since then we have developed SMIRFS, a Spectroscopic Multiobject InfraRed Fibre System for UKIRT (Haynes & Parry, 1994 and Haynes *et al.*, 1995), at the University of Durham. This instrument is, I believe, the first infrared multi-object system to have been developed and is described within this thesis. There have also been further developments by the Meudon group such as ISIS IR (Dallier *et al.*, 1994 and Dallier, 1995).

The latest version of ISIS IR is designed to work with one of the RedEye cameras at the CFHT. It is basically a 'warm' grating spectrograph that can deliver resolutions of ~

400, 2000 and 10000 in both the J and the H bands. The detector is based on a 256x256 NICMOS3 HgCdTe array with pixel scales of ~0.5 arcsec/pixel. The spectrograph is floor mounted and is fed by a 15m long fibre bundle. The input of the bundle is a roughly hexagonal array of 51 object fibres surround by a ring of 10 sky fibres. The bundle is made from Polymicro infrared optimised silica fibres. The hexagonal array is ~7.4 arcsec across with 0.7 arcsec fibres and the sky fibre ring is 21 arcsec across. This can be increased by a factor of 1.7 by a focal reducer. The bundle is reformatted into a slit at the output to feed the spectrograph. The packing efficiency of the fibres is ~ 60% and their internal transmission efficiency ~ 94% in J and ~ 92% in H. The limiting magnitude on the CFHT for a 1 hour exposure (1arcsec object, 10σ detection) is ~ 16-17 in J and ~ 15 in H for R ~ 2000.

1.3 Project Plan

Using optical fibres in infrared spectroscopy in astronomy was made possible by the development of infrared fibres for the telecommunications industry in their effort to reduce fibre attenuation over very long lengths of cable. My project was to investigate the properties and suitability of such fibres, then develop a prototype fibre system along the lines of the early visible wavelength fibres systems, but to work at wavelengths between ~1-3 μm. This would allow access to the J, H and K bands. It was felt it could be possible to get down to wavelengths as long as 3μm without cooling the fibres, however beyond this thermal emission would make their use impractical. The budget for the whole system was limited to £10,000 from development to arrival at the telescope. Due to the limited budget it was thought to be impractical to develop a complex or cooled fibre system, so a simple plug plate system was to be developed to fit, as an add on, to a current near infrared spectrograph. The spectrograph chosen was the CGS4 cooled grating spectrometer at UKIRT with its long slit capability and 256x256 InSb array detector. The wavelength coverage of CGS4 was 1-5μm with resolving powers varying from about ~ 400 to 40,000 depending on the grating and camera configurations.

1.3.1 Fibre material

The type of optical fibres used for fibre spectroscopy at visible wavelengths were not suitable for this application as significant absorption features occur in the 1-3 μm region. These would significantly reduce the signal transmission particularly beyond 1.8 μm. Preliminary investigations suggested there were a number of fibre materials available that transmitted in the near-IR, of which two warranted further investigation. First of these was a low OH^- silica fibre optimised for near-IR transmission. This was a relatively cheap fibre that was quoted to have reasonable transmission characteristics from 1-1.8 μm, however, beyond 1.8 μm the transmission fell off sharply. The second fibre material was zirconium fluoride (ZrF_4) which was quoted as having good transmission characteristics over the whole region of interest (1-3 μm) and beyond. However, ZrF_4 fibre was relatively expensive costing ~ £85 per meter for 200 μm core fibre as opposed to ~ £3 per meter for the same sized low OH^- silica fibre.

The initial set of tests would involved measuring the transmission with wavelength and FRD characteristics of the different fibre materials from a number of different manufactures. Information and results derived from investigation and analysis of these two fibre types was to provide valuable information for the design of the prototype system and any future near-IR fibre systems.

1.3.2 Coupling to the telescope and spectrograph

A well publicised feature of optical fibres was their very poor transmission of slow focal ratio beams which was particularly relevant to this project as the CGS4 spectrograph was designed to accept the f/36 beam provided by the UKIRT. Previous work suggested that with an input beam of f/36, typically less than 20% of the energy would be confined within an f/36 beam at the output. This would lead to losses of over 80% for the particular system suggested if direct fibre coupling was employed. However, it was also well publicised that faster focal ratio beams propagate much more efficiently. It was therefore necessary to investigate various forms of optical coupling techniques that would couple the f/36 telescope beam to the fibre at a faster focal ratio that would propagate efficiently. Then this faster fibre output beam would be coupled back to f/36 to suit the spectrograph. One technique that looked particularly promising was the use of microlenses and this was to be compared with other coupling techniques. Both the

effects on overall efficiency and the cost were considered important. However, it was thought that a significant portion of the project budget could be spent on the fibres and coupling optics, as they were the areas of new development.

1.3.3 Fibre positioning

As the main drive of the project was to investigate the suitability of fibres for use in near-IR spectroscopy it was decided that the fibre positioning system should be relatively simple such as a plug plate system. This particular technique had been very successfully used in a number of previous fibre systems developed by various different groups. It had the advantages that, for small fibre numbers we were considering, it provided a solution that would allow both more effort to be spent in the other areas of the project and it was relative cheap.

1.3.4 Coupling to the spectrograph

As previously stated, it was decided that the fibre system would be coupled to a spectrograph that was already in use. However, the CGS4 spectrograph was not designed for a fibre system and it was necessary to design a way of getting the light from the fibre output into the spectrograph. This was made more complicated as CGS4 was a cooled grating spectrograph with most of the components enclosed within the dewar. It was not going to be feasible to have the fibres inside the dewar so various methods were to be investigated to project the light from the fibres into CGS4 with minimal physical disruption, down time and cost.

1.3.5 Field acquisition and guiding

It was felt that the simplest and most cost effective solution to acquisition and guiding was to use guide fibres much in the same way as for many of the visible wavelength fibre systems. It was realised early on in the project that it would not be feasible to develop a guide system based on an infrared camera as one was not readily available to buy or borrow. Therefore the effort was to be focused on developing a guide system based on visible light. Again cost was an important consideration.

1.4 Summary

In recent years there have been significant developments in infrared instrumentation due to the development of large infrared arrays. Currently instruments are primarily based on 256x256 arrays but the next generation of instruments for the 8-10 meter class telescopes will use 1024x1024 HgCdTe (~1-2.5μm coverage) and InSb (~ 1-5μm coverage) array technology. Infrared spectroscopy offers the opportunity to study the redshifted optical region of high redshift ($z > 1$) objects. There are a number of atomic and molecular features in the near-IR and it offers a useful opportunity to study low mass sub-stellar objects such as brown dwarf candidates. There are two infrared imaging surveys covering the whole sky which should be completed by 1998. These should provide a number of follow up programs for infrared spectroscopy. Multi-object spectroscopy using fibres has progressed a long way at visible wavelengths with large field instruments and hundreds of fibres. However, very little has been done in the infrared which, with the development of large array and infrared fibres, offers significant development potential for both integral field and, given the number densities, multi-object fibre systems. A project was devised to take advantage of this opportunity that would be a prototype system that used optical fibres optimised for near infrared transmission. It would be a separate unit that would provide a multiple object fibre capability for the CGS4 spectrograph at UKIRT designed to access the J, H and K bands. Not only would it provide the multi-fibre capability with its potential multiplex advantages over single long slit spectroscopy but also valuable information for the development of future system for the near-IR based on optical fibres.

Chapter 2: Infrared optical fibres

2.1 Introduction

The manufacture, physical and chemical characteristics as well as some of the optical properties of infrared fibres are discussed in a number of textbooks such as Katsuyama & Matsumura (1989), Klocek & Sigel (1989), France *et al.* (1990). Also Nelson (1988) and Heacox & Connes (1992) discuss the properties of fibres in detail. What follows in this chapter is a brief description of the basic structure of optical fibres, how light propagates along the fibre, the sources of attenuation loss and focal ratio degradation within fibres. The attenuation characteristics of a number of silica fibres along with zirconium fluoride and chalcogenide fibres are then looked at in detail to determine their suitability for use in the infrared.

2.2 Basic properties of fibre

2.2.1 Basic structure

The basic structure of an optical fibre is a series of concentric cylinders. The central section is composed of a relatively high refractive material and is known as the fibre core. This is surrounded by a lower refractive index material known as the cladding, which in turn is sheathed in a protective layer known as the buffer. The buffer material is available in a number of different compositions to suit different physical and chemical environments.

Fibres can be divided into three basic types: step-index multimode fibres in which the core has a uniform refractive index, graded-index fibres in which the core has a radial refractive index gradient which is relatively high in the centre of the core and drops off toward the edge of the core, and single mode fibres which are similar in structure to step-index multimode fibres but the fibre core has such a small diameter that only one optical mode can propagate down the fibre. In this section step-index fibres will be discussed but similar principles can be applied to graded-index fibres.

2.2.2 Mechanism of light guiding

The fibre is a form of circular dielectric waveguide down which different modes can propagate. The modes describe the propagation vectors of the different electromagnetic

waves that can exist in the waveguide. The number of modes that can propagate along a fibre is given by

$$M = (2\pi r)NA / \lambda$$

where r is the radius of the fibre core, NA is the numerical aperture of the fibre and λ is the wavelength of light. Hence the relatively small core size of single mode fibres.

However if the wavelength of the light is considerably shorter than the core diameter, as with multimode fibres, it is more convenient to use geometrical optics. Figure 2.1 shows the basic structure of a step index fibre.

When a ray strikes the fibre core at some angle θ, some will be reflected and the rest will be refracted into the fibre core. The refractive index of the core (n_1) is greater than that of the cladding (n_2), so if the angle of the light ray in the core α is less than the critical angle α_c , complete reflection occurs. Since subsequent reflections occur at the same angle, the light continues to propagate along the fibre core. If on the other hand the ray strikes the core/cladding boundary at an angle greater than α_c , only partial reflection takes place and some of the energy is lost into the cladding by refraction. After successive partial reflections most of the energy of this ray is lost in the cladding. Thus only those light rays which are incident on the fibre face with angle θ smaller than the critical angle θ_c will be propagated by the core.

The critical angle at the core cladding boundary is

$$\alpha_c = \cos^{-1}(n_2 / n_1)$$

where n_1 is the refractive index of the core and n_2 is the refractive index of the cladding.

The maximum acceptance angle of the fibre is

$$2\theta_c = 2\sin^{-1}(n_1 \sin\alpha_c)$$

The fibre manufactures usually express this in terms of the numerical aperture given by

$$NA = \sin\theta_c = \sqrt{n_1^2 - n_2^2}$$

2.2.3 Dispersion

Dispersion in fibres derives from two sources, intermodal dispersion and intramodal dispersion. The effect of dispersion is to spread out a short pulse of light as it propagates down the fibre. Intermodal dispersion is a consequence of the different path length of the modes that propagate along the fibre. Intramodal dispersion is a consequence of the change in refractive index of the fibre core with wavelength, which causes variations in a mode's group velocity. Refractive index change, and hence intramodal dispersion, is more severe at shorter wavelengths. In multimode fibres the intermodal dispersion tends to dominate, but it can be reduced by using graded index fibres. Here the centre of the fibre core has a higher refractive index than the outer regions. Thus modes propagating in the outer regions of the core, with longer path lengths, travel at higher velocities thereby reducing the pulse dispersion.

2.2.4 Absorption losses

Absorption losses in optical fibres are due to intrinsic absorption of the fibre material, absorption by impurities and atomic defect absorption. Intrinsic absorption derives from excitation of both electron transitions in the material band-gap and lattice vibrations in the fibre material. Band-gap absorption follows an $e^{1/\lambda}$ law and occurs mainly in the ultraviolet region. Lattice vibration absorption follows an $e^{-1/\lambda}$ law and occurs more prominently in the infrared. The fundamental vibrational frequencies are related to the mass and the bond strength of the molecules. Silica has a relatively light molecule (SiO_2 - molecular mass 30) so absorption is significant in the infrared whereas zirconium fluoride has a more massive molecule (ZrF_4 - molecular mass 76) and so is transparent further into the infrared region. Impurity absorption results from the excitation of the impurities in the fibre material. These are often transition metal ions or OH ions. These effects tend to dominate at visible and near-IR wavelengths. OH absorption is particularly significant towards the red end of the visible and the near-IR. It is therefore important to ensure low OH impurity levels in fibre materials designed for these regions. Atomic defect absorption can be induced from external sources such as large temperature variations, intense radiation and chemical environment. In less severe cases the fibre can recover from the effects of these harsh environments.

There are a number of intrinsic scattering losses in fibres. Small particles or inclusions caused by variations in the cooling rates of the glass as it solidifies alter the refractive index of the material. If these variations occur on a scale that is small compared to the wavelength of light, Rayleigh scattering results scaling as ~ λ^{-4}. If the fluctuations occur on scales comparable to the wavelength of the light then these result in Mie scattering. Usually, Raman and Brillouin scattering are relatively small, however high attenuation can result if the optical power is sufficient.

Other scattering losses due to structural imperfection tend to be wavelength independent. They can be brought about by irregularities in the core cladding boundary, pores or bubbles in the core or cladding, microbending and variations in the core diameter if this is not maintained to within ~ 1μm. There will also be Fresnel reflections from the fibre end face as a result of the refractive index changes at this boundary (usually air/glass) and scattering at the ends due to a poor finish.

2.2.5 Focal ratio degradation (FRD)

Ideally, if the input face of a fibre is illuminated with a parallel beam from a laser at some arbitrary angle θ, that is less than the numerical aperture of the fibre, instead of appearing as a single beam at the output, it is emitted as a hollow cone of angle θ. So fibres have the property of azimuthal scrambling the input image. This azimuthal scrambling occurs even with a very short length of fibre and is effectively perfect. It is not affected by input angle. In the case of real fibres not only is the beam azimuthally scrambled but there will also be a spread of the cone angles Δθ centred about the peak intensity at θ. This is shown in figure 2.2. This has the effect of speeding up the input beam as it propagates along the fibre so it will emerge from the fibre output at a faster focal ratio than that at which it was injected. This is known as focal ratio degradation or FRD. This is not usually specified by the fibre manufactures but has been discussed by Ramsey (1988), Guerin (1988) and Carrasco (1992). Techniques for the measuring of FRD and FRD results for the SMIRFS fibres are discussed in chapters 4 and 7.

FRD can originate from a number of sources: microbends, macrobends, diffraction broadening and scattering. Microbends are small scale deformations in the cylindrical

shape of the core which cause the light to propagate at a different reflection angle. This is shown in figure 2.3. This may also be seen as modal transfer where the energy of one propagating mode is transferred to another mode. Macrobending is similar to microbending but the deformation is on a scale very much larger than the fibre core. There will be a certain amount of inherent microbending and macrobending within a fibre but it has been noted (Angel *et al*, 1977 and Heacox, 1986) that angular broadening from mechanical deformation ($\Delta\theta_m$) as a result of bending the fibre is approximately given by

$$\Delta\theta_m = \frac{D\theta}{R}$$

where D = fibre core diameter, θ = the incidence angle and R = the bend radius of the fibre. However it should be noted that the mechanical deformation due to localised stressing from crimping or crushing can have a considerable effect on the FRD induced in a fibre.

The diffraction broadening ($\Delta\theta_d$) can be calculated from

$$\Delta\theta_d = 2.44 \times \frac{\lambda}{D}$$

This is only really significant for long wavelengths and small cored fibres. Scattering can be due to small scale imperfections within the core material that lead to Rayleigh scattering or scattering due to imperfections at the fibre face.

An important feature of FRD is that the effects are significantly worse at small input angles than at large input angles. Thus fast beams propagate down fibres with much more efficiency than slow beams. For short lengths of fibre (~1m) that display relatively good FRD characteristics an input beam of f/36 will typically have less than 20% of the energy of the output beam confined within f/36. For faster input beams of f/5 more than 90% of the energy can be confined within f/5 at the output; however for poor quality or long lengths of fibre the FRD can be significantly worse.

The limit on the beam speed that will propagate down the fibre is set by its numerical aperture. For a typical glass clad silica fibre the NA is ~ 0.2 which corresponds to a

beam of ~ f/2.5 or the half angle of the acceptance cone θ_{max} ~ 11.5°. If the input angle of a propagating ray is scattered to an angle greater than θ_{max}, the ray will not propagate down the fibre and will be lost in the fibre cladding. If the input beam is close to the maximum defined by the NA then FRD effects will scatter a significant proportion of the rays to an angle greater than θ_{max} and therefore a significant amount of the energy of the beam will be lost in the cladding. The most efficient propagation of input beam is generally agreed to be in the region of f/3 - f/4 for a typical NA ~ 0.2 (Baudrand *et al.*,1994).

2.3 Infrared fibre materials

2.3.1 Brief history

Optical fibres have primarily been developed for telecommunication applications and sensing systems. The telecommunications industry required fibres which could transmit information over vast distances with negligible transmission losses. This led to the development of low loss silica based fibres with a predicted intrinsic limit as low as 0.2 dB/km. The development of infrared fibres was partially motivated by the possibilities of ultra-low loss fibre with attenuation of less than 0.01dB/km. A number of different materials have been studied such as heavy-metal oxides, halides and chalcogenides. The most promising of these materials for near-IR applications are zirconium fluoride based fibres which have a predicted intrinsic attenuation of less than 0.01dB/km at wavelengths in the 2-4 μm region. Silica fibres attenuate strongly in this region.

2.3.2 Transmission characteristics.

For the SMIRFS project (Haynes & Parry, 1994 and Haynes *et al.* 1995) the wavelength regime was in the 1-2.5 μm region, covering the J , H and K bands. For this both silica (Nelson, 1988) and zirconium fluoride (Levin *et al*, 1988) fibres were considered as they display attenuation characteristics that provide reasonable transmission over some or all of this wavelength range.

2.3.2.1 Silica fibres

With silica fibres it is possible to modify the characteristics of the fibre to suit different wavelength regions; these are available with core sizes typically in the range of 50μm to

1 mm. Figure 2.4 shows the difference in attenuation between the FH fibre series which has a high OH silica core (800-1200ppm) and FL fibre series which has a low OH silica core (< 2ppm). These fibres are supplied by Polymicro Technologies Incorporated of Phoenix, Arizona. As seen in this graph the presence of the OH radical in the core material causes significant attenuation peaks beyond about 0.7μm. This results from the excitation of this radical which has fundamental resonance at 2.73μm with overtones at 1.37, 0.95 and 0.72μm. The reduction of the OH^- content of the silica core material has a significant effect on the attenuation. Figure 2.5 shows the attenuation curves for three different low OH^- Polymicro fibres. FL = Low OH^-, FI = Ultra-Low OH^- and FB = Blue Enhanced Low OH^-. These fibres are not significantly different except for the FB series which shows a small increase in attenuation beyond 1μm and the peak at ~ 600nm is smoothed out. The feature that should be noted for infrared applications is the sharp turn up in attenuation beyond 1.8μm where the scale changes from dB/km to dB/m. Between 0.4μm and 1.8μm even the high OH^- fibres have an attenuation of less than 0.2 dB/m which corresponds to a transmission per meter of approximately 95%. Beyond 1.8μm the attenuation for the FI fibres rises rapidly to ~ 3 dB/m at 2.5μm (transmission per meter ~ 50%). This attenuation is the result of intrinsic attenuation mechanisms in the silica, mainly multiphoton or lattice vibrations.

A feature of silica fibres which is not of such importance for infrared applications, but could be of importance for systems designed to work from the ultra-violet through to the infrared, is the UV attenuation. This can be seen to rise rapidly shortward of ~ 400nm. There are high OH^- fibres available such as the FH and FV series of Polymicro fibres but these do not have very good transmission toward the infrared. Figure 2.6 shows the attenuation characteristics of the Polymicro FH = High OH^- and FV = UV Enhanced High OH^- fibres. A possible solution to this problem would be to use Low Na, Low OH^- fibres. These fibres have similar transmission characteristics to the FI Polymicro fibres but have enhanced UV characteristics with attenuation < 0.5dB/m at about 320nm.

These fibres can be supplied with a range of buffer materials that protect the fibre cladding surface (Nelson 1988). The more common are acrylate, silicone and polyimide.

The polyimide buffer is a hard, typically thin, buffer that provides good protection against harsh chemical and thermal environments. Due to the hard nature of the buffer these fibres are likely to be more susceptible to stresses such as pinching which can be transmitted to the fibre core producing FRD. Silicone buffers are typically thicker and softer than the polyimide buffer but can offer good chemical and thermal protection. The UV curing acrylate buffer is a relatively soft and thick buffer that can be relatively easily removed if necessary using a methylene chloride solution such as a paint or varnish remover. It is also possible to obtain double buffered fibres such as a polyimide layer coated with acrylate. Hermetic coatings are possible, providing better long term durability.

2.3.2.2 Zirconium fluoride glass fibres

Silica fibres are adequate for application shortward of 1.8μm but if fibres of any significant length are to be used beyond ~ 1.8μm then it is necessary to use a different core material for the fibres. Zirconium fluoride (ZrF_4) fibres have good transmission characteristics from 1 - 4 μm and are available in a range of core sizes, typically 70μm to 1mm, with a refractive index of ~ 1.52. Figure 2.7 shows the typical attenuation characteristics in the 1-4μm region for IRGUIDE PJ 200/250 zirconium fluoride glass fibre supplied by Le Verre Fluore of France. The fibre has an attenuation of ~ 0.1 dB/m at 1μm (98% transmission/m) which drops to a minimum of ~ 0.01 dB/m at 2.6μm (~ 99.8%) and then starts to increase to reach 0.1dB/m at ~ 3.6μm, reaching 1 dB/m at ~ 4.2 μm. Thus it is possible to use fibres of up to tens of meters in length within this wavelength region without experiencing crippling attenuation losses.

Though the tensile strength has improved over the years and despite buffer coatings such as acrylate and polyimide, ZrF_4 glass fibres are not as mechanically durable as silica fibres. They tend to break relatively easily if kinked or roughly handled. This is a significant consideration as ZrF_4 fibre is about 30 times the price of the silica fibre.

Like the silica fibre, the infrared response is adversely affected by the OH^- radical which must be kept to a few parts per million. However, unlike the silica fibres, these fibres are susceptible to attack by moisture which degrades the optical quality after manufacture. This means that conventional polishing techniques using water suspensions cannot be

employed and the cleaning of the fibre faces is best done with a soft tissue and an alcohol such as methanol. The acrylate buffer offers some mechanical and chemical protection but it is worthwhile providing additional protection against mechanical and moisture attack if feasible.

2.3.2.3 Chalcogenide glass fibres

Though chalcogenide fibres do not display the kind of transmission characteristics available with ZrF_4 fibres, for short lengths of fibre they do offer coverage from ~ 2-10μm. Figure 2.8 show the attenuation curve for an unclad chalcogenide glass fibre supplied by Infrared Fiber Systems Inc., USA. This fibre has an attenuation of about 10dB/m at 2μm which drops to a minimum of about 1dB/m in the region of 6μm and then slowly rises to about 10dB/m again at 10-11μm. These fibre are even more prone to impurities and scattering defects than the fluoride glasses (which in turn are more susceptible than silica fibres), leading to relatively high loss. Also the refractive index is ~2.6 which results in large Fresnel reflection losses at the fibre faces.

2.4 Summary

The optical characteristics of a fibre can be specified by its numerical aperture, attenuation and FRD. The numerical aperture specifies the maximum acceptance angle of a ray that will propagate down the fibre and is derived from the difference between the refractive index of the core and cladding materials of the fibre. The attenuation of the fibre is specified per unit length and is related to various loss mechanisms within the fibre such a scattering and absorption, also there are both Fresnel reflections and scattering losses at the fibre faces. Focal ratio degradation (FRD) is an effect that speeds up a beam as it propagates down a fibre. The effect is far greater at slower beam speeds. This is the result of intrinsic fibre properties but can also be affected significantly by external mechanisms such as bending and stresses such as pinching.

Silica fibres are available to suit different wavelength regions from the UV through to the infrared, however the attenuation of these fibres limits their usefulness to ~ 0.2 to 2.3 μm beyond which the fibres start to attenuate heavily (> 1dB/m). Zirconium fluoride fibres display very low attenuation in the near-IR region, less than 0.1dB/m from ~ 1-

3.6μm. Chalcogenide fibres can cover the region from ~ 2-10μm but the attenuation tends to be relative large reaching a minimum of ~ 1dB/m at about 5-6μm.

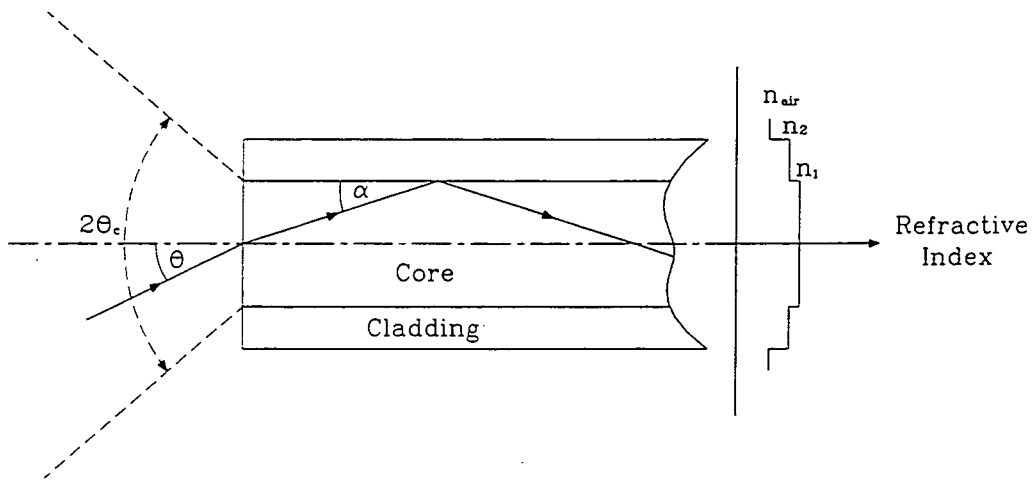

Figure 2.1 The basic structure and refractive index profile of a step index fibre. The maximum acceptance angle of the fibre is $2\theta_c$, θ is the input angle and α is the reflection angle at the core/cladding boundary. The refractive index of the core, cladding and air are respectively given by n_1, n_2 and n_{air}.

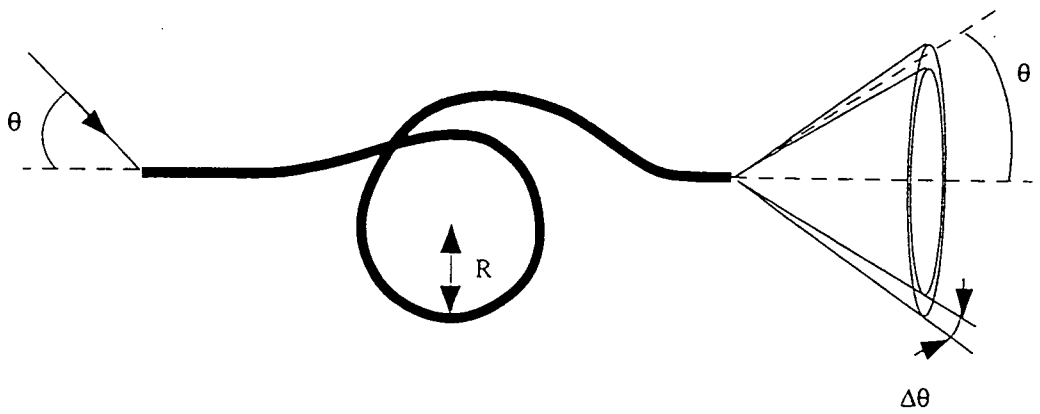

Figure 2.2 The azimuthal scrambling and FRD induced in a fibre. The spreading of the output cone is given by $\Delta\theta$, θ is the input beam angle and R is the bend radius of the fibre.

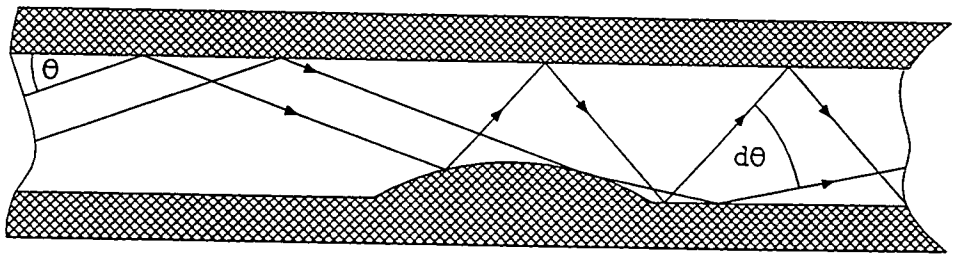

Figure 2.3 Beams spreading as a result of microbends in fibres. Prior to the microbend the two rays propagate at the same angle θ to the core/cladding boundary. After the microbend the propagation angle of the two rays differ by dθ.

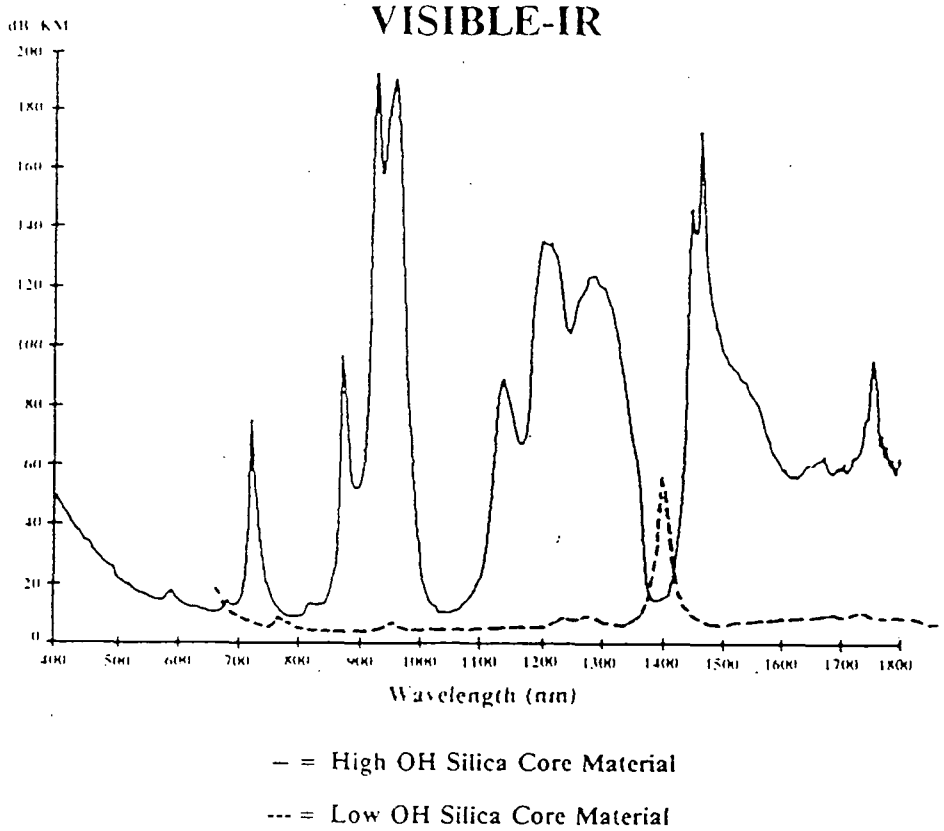

Figure 2.4 The manufacturers spectral attenuation curves for the High OH (FH series) and Low OH (FL series) silica core fibres supplied by Polymicro Technologies Incorporated.

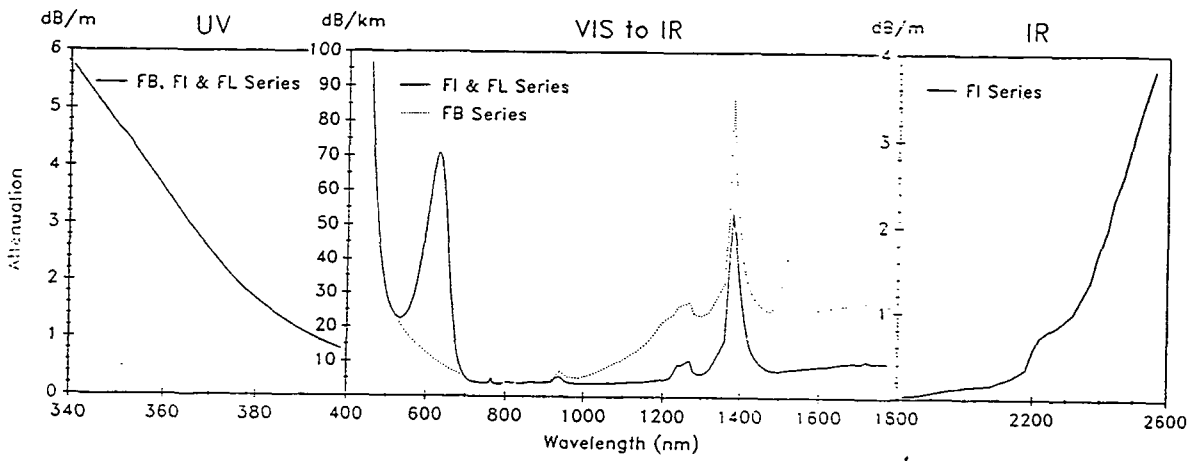

Figure 2.5 The manufacturers spectral attenuation curves for the Low OH silica core fibres supplied by Polymicro Technologies Incorporated. The FL series are Low OH, the FI series are Ultra Low OH and the FB series are Blue Enhanced Low OH fibres.

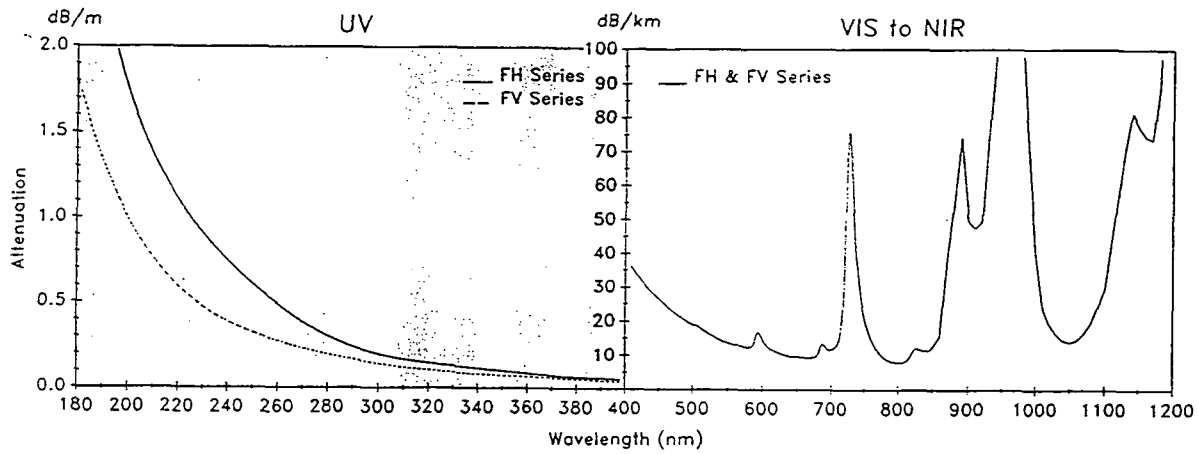

Figure 2.6 The manufacturers spectral attenuation curves for the High OH silica core fibres supplied by Polymicro Technologies Incorporated. The FH series are High OH fibres and the FV series are UV Enhanced High OH fibres.

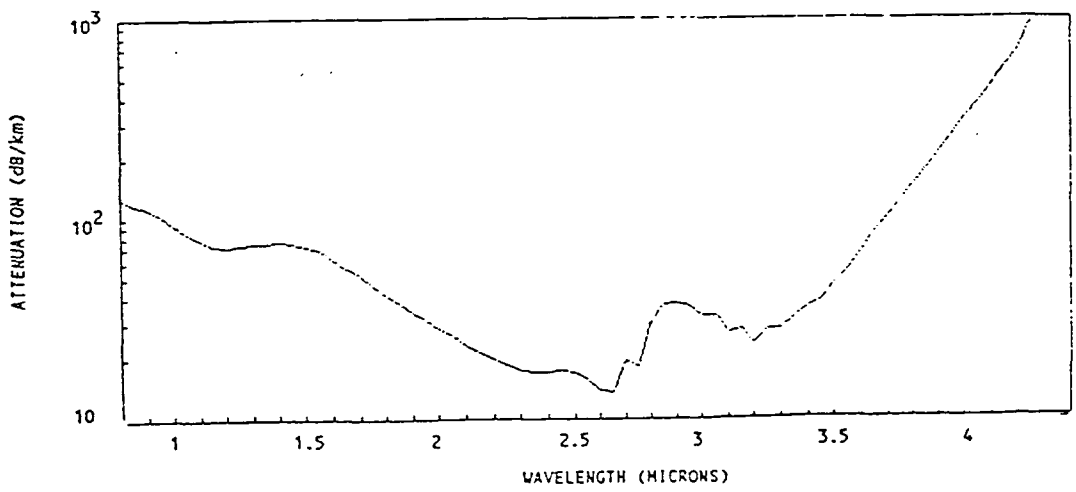

Figure 2.7 The manufacturers spectral attenuation curve for the IRGUIDE PJ 200/250 zirconium fluoride fibre supplied by Le Verre Fluore.

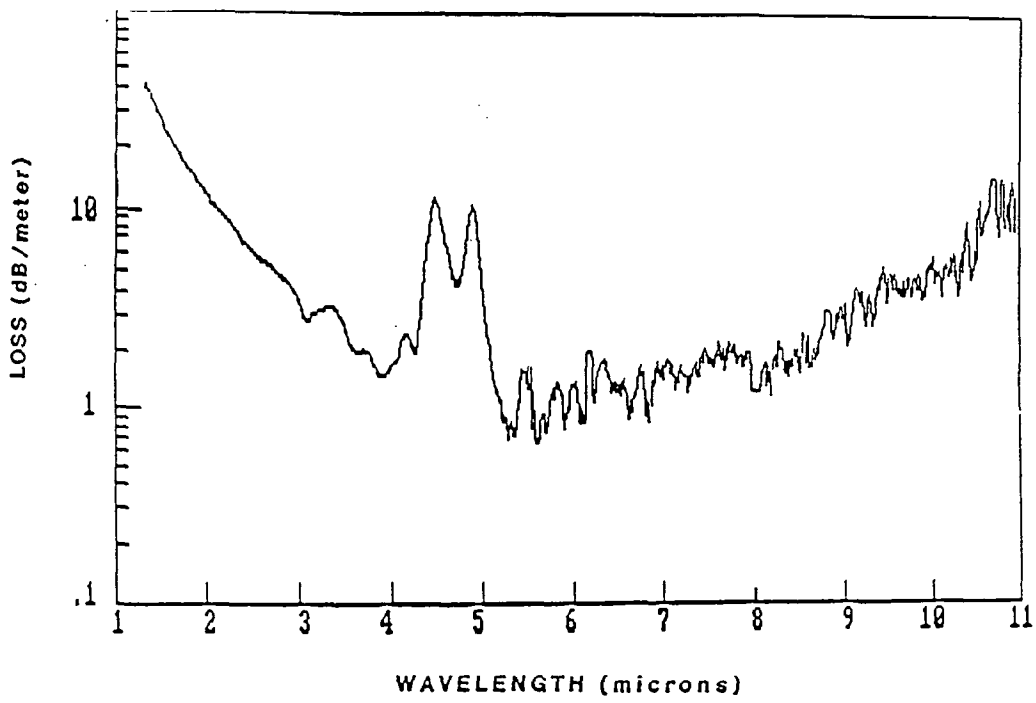

Figure 2.8 The manufactures spectral attenuation curve for the chalcogenide fibres supplied by Infrared Fiber System Incorporated.

Chapter 3: The near-IR sky and sky subtraction

3.1 Introduction

In the near-IR the atmosphere above the telescope has a significant effect on the signal through three different mechanisms. These are atmospheric absorption, non-thermal emissions and, beyond about 2μm, thermal emission. The non-thermal emissions in particular can vary significantly on quite short time and spatial scales which have implications for sky subtraction. In this chapter I will briefly discuss the properties of the atmosphere in the near-IR (1-2.5μm) and review some sky subtraction techniques that are employed in fibre spectroscopy.

3.2 The atmosphere in the near-IR

At optical wavelengths the intensity of the background night sky is derived from a number of sources such as zodiacal light from dust scattering, auroral emissions, non-thermal emissions and faint astronomical sources. In the near-IR the most dominant features are atmospheric transmission, non-thermal and thermal emissions.

3.2.1 Atmospheric transmission

Figure 3.1 shows the typical atmospheric transmission at Mauna Kea in the near-IR (1-2.5μm). There are essentially three atmospheric windows, the first is the J band centred at ~ 1.25μm, the second is the H band at ~ 1.65μm and the third is the K band at ~ 2.2μm. The bands are separated by regions of high atmospheric absorption caused predominately by water vapour (H_2O) and carbon dioxide (CO_2); as the concentration of H_2O and CO_2 increase so does atmospheric absorption. The concentration of these gases vary considerably with atmospheric conditions and telescope site. A good infrared site, such as Mauna Kea, is at high altitude where the atmosphere is relatively dry and free from low cloud.

The infrared atmospheric windows are defined by a series of Johnson broad bandpass filters, that encompass the regions of "good" throughput. Other filters are available which overlap with the K band filter. Table 3.1 shows the central wavelength and bandpass of these filters.

Waveband	Central Wavelength (μm)	Bandwidth (μm)
J	1.25	0.3
H	1.65	0.3
K	2.2	0.4
K'	2.1	0.4
$\mathbf{K_{short}}$	2.15	0.3

Table 3.1 The central wavelength and bandpass of the near-IR filters.

Beyond these wavelengths one enters the thermal infrared region in which the thermal emissions from "warm" objects such as the atmosphere and the telescope dominate the signal.

3.2.2 Non-thermal emissions

In the near-IR the dominant contribution to the airglow is due to emissions from vibrational-rotational transitions of OH^- radicals in the upper atmosphere. There is also significant O_2 emission at 1.27μm. Figure 3.2, 3.3 and 3.4 (Ramsay *et al.*, 1992) show the OH^- emission lines in the J, H and K windows respectively. It can be seen that there are a great number of lines, many of which are blended from more than one transition. However, the increase in background signal seen in the K band spectra beyond ~ 2.1μm is not due to OH^- transitions but to thermal emissions which will be discussed later.

The absolute and relative intensities of these lines change systematically with airmass, and with the observing time during the night as well as the time of year. During the ALOHA-90 campaign on Mauna Kea the 4-2 OH^- emission lines were found to vary by 25% rms during the course of the night and by 25% rms from night to night. However, on one particular night the OH^- emissions dropped by ~ 2.5 times during the course of 5 hours (Content R., private communication, 1995). Ramsey *et al.* (1992) observed fluctuations in emission line intensity from 3 to 10% with periods from 5 to 15 minutes and global decrease in emission of 46±5% over a period of about 3 hours. This decrease

was more significant at the beginning of the night and levelled off towards the end of the night.

The fluctuations in intensity of OH^- emissions result from variations in the concentrations of the components that affect the OH^- excitation. The long term fluctuations are thought to be due to the slow diffusion of the atmospheric constituents, whereas the short term variations are thought to be due to variation in temperature and density caused by the passage of gravity waves through the ionosphere. There will also be spatial variations in emission line intensity due to local fluctuations in density, temperature and composition as well as global changes with zenith angle or airmass. Ramsey *et al.* (1992) noticed no significant variations in emission intensity along the length of the ~ 90 arcsec slit of the CGS4 spectrograph at UKIRT, however over larger fields the variations will increase.

3.2.3 Thermal emissions

As well as the OH^- emission line another feature that affects the background signal from the atmosphere is thermal emission. The atmosphere is not totally transparent and various components of the atmosphere absorb light on its path to the telescope. Some of the more significant absorbers in the near-IR are H_2O, CO_2 and O_2. The amount of thermal emission from the atmosphere depends upon its temperature and its emissivity which in turn depends on its transparency. The effective temperature of the majority of the atmospheric components is ~ 228K, but the water vapour is ~ 253K. However, the typical temperatures inside the dome would be ~ 0°C (273K) and the telescope optics will typically have an emissivity of $\varepsilon \sim 0.15$, so the thermal emission from the telescope will dominate over the atmospheric thermal emission (McCaughrean, 1987). From figure 3.4 it can be seen that the thermal emission starts to have a significant contribution to the signal beyond about 2.1μm.

3.3 Sky subtraction

The importance of good sky subtraction with fibres and various sky subtraction techniques have been discussed in a number of papers, for example, Parry & Carrasco (1990), Wyse & Gilmore (1992), Barden *et al.* (1993) and Mignoli & Cuby (1994).

The limitations to sky subtraction derive from a number of different sources such as the inhomogeneities of the sky, scattered light within the spectrograph, non-uniformities across the detector, wavelength stability and fibre transmission. The spatial and temporal variations in the night sky have an influence on the most suitable observing strategy to use. There are essentially four different techniques: spatial separation, temporal separation, beam switching fibre pairs, and scattered dedicated sky fibres.

3.3.1 Spatial separation (fibre pairs)

This is essentially a single observation which simultaneously monitors object + sky with one fibre and the adjacent sky using the other fibre in a pair. The sky fibre signal is subtracted from the object fibre signal. This has the advantage that the sky is monitored close to the object sky which reduces the effects of spatial variations and simultaneous observation eliminates temporal variations. The disadvantage is that 2 fibres are dedicated to each object observed which reduces the multiplex gain. Moreover accurate measurements of the relative transmissions by the two fibres are required.

3.3.2 Temporal separation (beam switching)

In this case there are two equal length observations, one in which the fibres are all dedicated to the objects and the second in which the fibres a dedicated to blank sky offset from the original telescope position. The sky exposure is then subtracted from the object exposure. This has the advantage in that there is less dependence upon the relative fibre throughput as the same fibre is used for each observation. Also there is less constraint to a fixed offset which can lead to contamination of the sky observations in some circumstances. However, there is an extra time overhead of two exposures that double the observing time. There is still susceptibility to small scale spatial variations and, in this case, temporal variation as well.

3.3.3 Beam switching fibre pairs (cross beam switching)

This technique combines the beam switching technique with that of the fibre pairs. There are essentially two observations. In the first exposure one of the fibre pair (A) is dedicated to the object and the other fibre in the pair (B) is dedicated to the adjacent sky. In the second exposure the telescope is offset so the fibre B is now dedicated to the object and fibre A is dedicated to sky adjacent to the object. The sky exposure for each

fibre is subtracted from the object exposure for the same fibre and then the signal from fibres A and B are combined. The technique should minimise the effects of relative fibre throughput determination and temporal variations as the sky is continuously monitored. However, there is still the 50% overhead in the number of fibres required.

3.3.4 Scattered dedicated sky fibres (mean sky subtraction)

In this technique a number of fibres dedicated to sky are distributed in the field. The number of fibres required is discussed in detail by Wyse & Gilmore (1992) but for N fibres the number of sky fibres is $< \sqrt{N}$. The estimate of the mean sky can then be derived and subtracted from the object fibre spectra. This method has less shot noise than the single fibre subtraction used in beam switching. Also the fibre or time overheads are less than in the previous methods but the technique is susceptible to larger scale spatial variations.

Another variation on this technique is to combine it with beam switching to areas of blank sky which double the time overhead but requires less fibres than beam switching with fibre pairs. Using fibres pairs allow fibres to be placed close together in the field which can sometimes be an advantage whereas discrete fibres can rarely be placed closer than ~ 20 arcsec due to mechanical constraints.

3.3.5 Instrument considerations in sky subtraction

In most of the techniques discussed it is necessary to obtain good estimates of the relative fibre throughputs. This is not trivial as the throughput can vary with telescope angle due to misalignment caused through fibre stress and flexing of the support structure. The intrinsic fibre throughput also differs from fibre to fibre due to differences in the fibre surface finish, FRD characteristics and transparency. An estimate for the relative fibre throughputs can be gained from flat field exposures.

There are a number of other features that affect the accuracy of sky subtraction with fibres such as: scattered light within the spectrograph, wavelength calibration, variation in fibre to fibre spectral response, both spatial and temporal variation in the detector. Wyse & Gilmore (1992) show that the amount of uniform scattered light in a frame can constitute a significant proportion of the total intensity and that light from a bright source can be spread across adjacent fibre spectra. Localised scatter can be determined

by illuminating each fibre with a bright source and observing the extracted fibre profile and the uniform scattered light can be estimated from the "dead" areas of the fibre slit.

Basic operations such as bias and dark subtraction are necessary as well as cosmic ray removal which can be identified by taking more than one frame. Also small mismatches in wavelength calibration can lead to large residuals when subtracting sky spectra with strong emission lines. This is of particular relevance in the near-IR which is dominated by large numbers of strong emission lines. The calibration can be achieved using calibration lamp lines, or the sky lines themselves.

3.3.6 Infrared sky subtraction

Essentially the techniques used for sky subtraction should be the same as those used in the optical region. However in the near-IR the dominant contribution to the night sky is from non-thermal emission lines. This is more significant below 2μm beyond which the continuum from thermal emission starts to becomes more dominant. This makes good wavelength stability essential if there is to be effective sky subtraction without significant residuals. The ultimate goal of sky subtraction is to reduce the error in the final spectrum down to just photon noise. This is not achievable in practice, but every effort is made to reduce the sky residuals in the final spectrum thus maximising the S/N. The global and relative non-thermal emission line intensities are known to vary significantly on short time scales of a few minutes but not significantly on small spatial scales (Ramsey *et al.* 1992). This suggests that the observing technique should be one that minimises the temporal variation such as simple spatial separation using fibre pairs or scattered fibres. However, this requires very accurate estimates for the relative fibre throughput. One way around this is simply to scale the wavelength calibrated emission lines in the sky spectra to those in the object + sky frame and then subtract the two frames. Alternatively, a combination of beam switching on relative short time scales and dedicated sky fibres techniques could be employed.

3.4 Summary

The main features of the "sky" in the near-IR are absorption by water vapour and carbon dioxide, non-thermal emissions from the OH^- radicals and thermal emissions. The atmospheric absorption restricts the wavelength regions into three bands, the J band ~

1.2 to1.3 μm, the H band ~ 1.55 to 1.75 μm and the K band ~ 2.0 to 2.4 μm. Within these bands the most dominant feature is non-thermal line emission which displays significant temporal variations on both short (few minutes) and long time scales (the course of the night and time of year) but little spatial variation over small scales (1 arcminute or so). Beyond about 2μm the thermal emissions from the sky, telescope and instrumentation start to become significant and are dependent on the emissivity and temperature object.

The sky emissions along with instrument "sky" greatly reduce the signal to noise in the object spectra so accurate sky subtraction techniques are required. The instrument sky subtraction involves the standard bias and dark subtraction, cosmic ray removal and scattered light subtraction which can make up significant proportion of the total intensity at the detector. Accurate wavelength calibration is essential, otherwise large residuals can result from subtraction of the emission lines. A number of different observing techniques are available but for infrared fibre spectroscopy I believe the more suitable techniques would be those that simultaneously monitor both the sky and the object and therefore minimise the temporal variations. This is necessary because of the large and relatively rapid variation in the emission line intensities. However, these techniques do raise the problem of relative fibre throughput, so a variation of beam switching technique may be necessary.

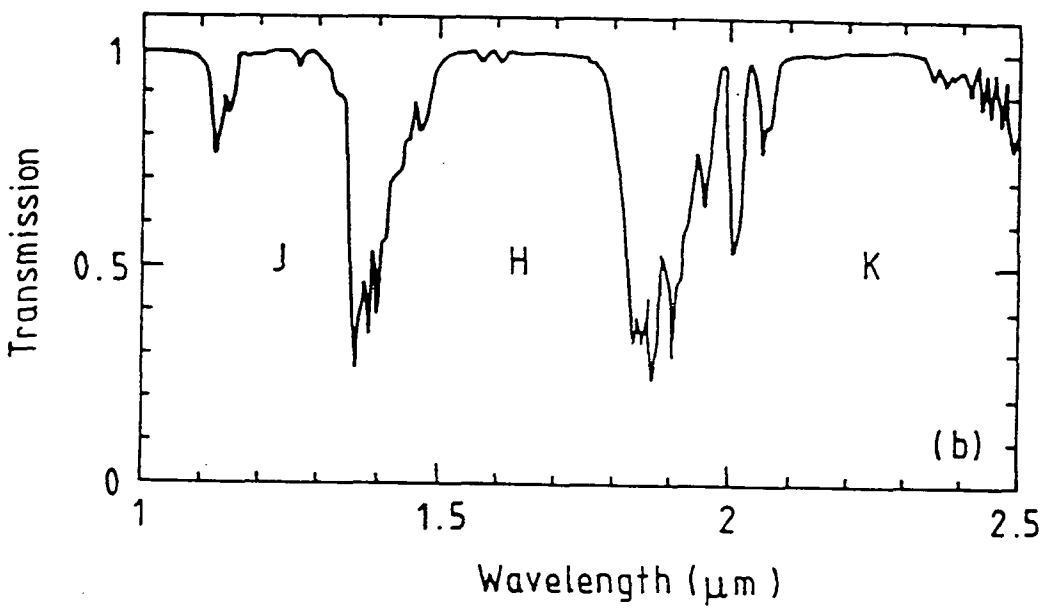

Figure 3.1 The transmission of the atmosphere above Mauna Kea in the near-IR. The three main wavebands used in this region are J (~1.25± 0.15μm), H (~1.65±0.15μm) and K (~2.2±0.2μm).

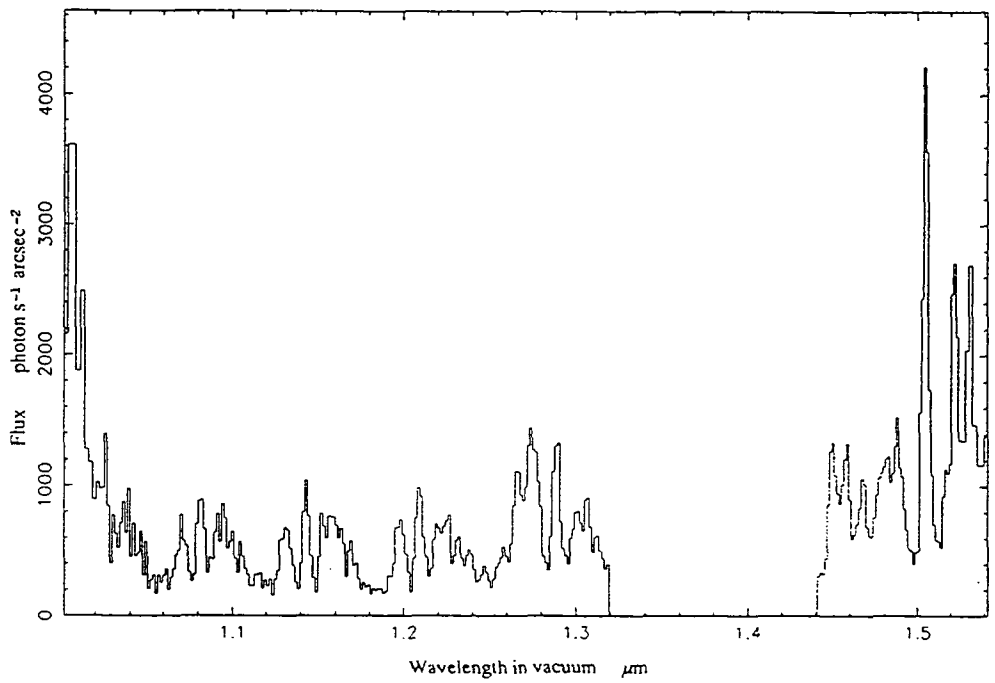

Figure 3.2 Spectrum of the atmospheric OH^- emission in the J window taken using CGS2 (Ramsey *et al.*, 1992).

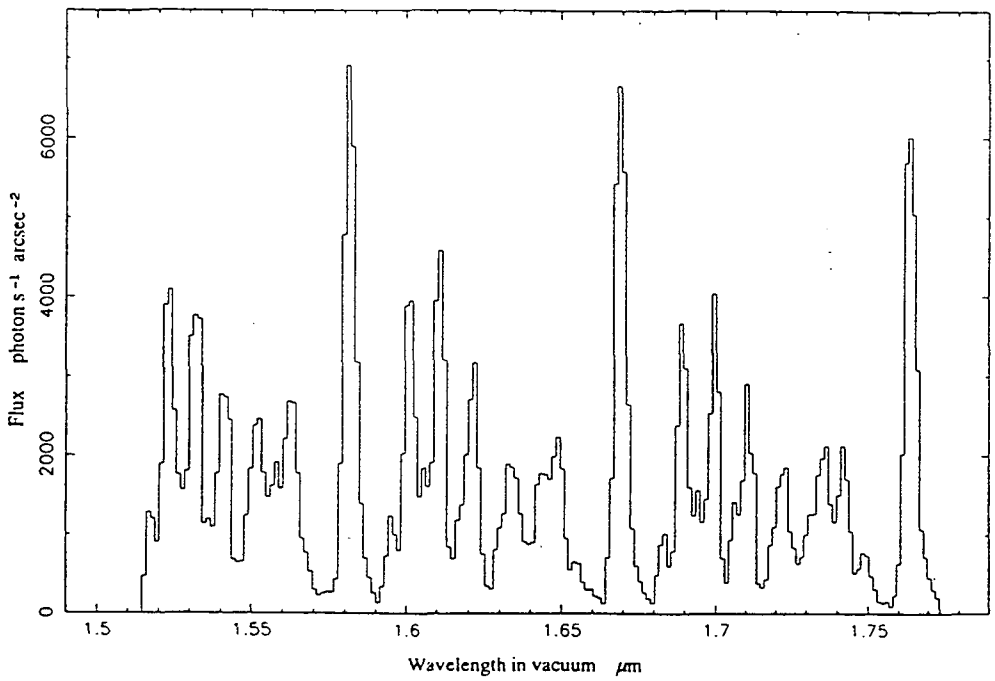

Figure 3.3 Spectrum of the atmospheric OH^- emission in the H window taken using CGS2 (Ramsey *et al.*, 1992).

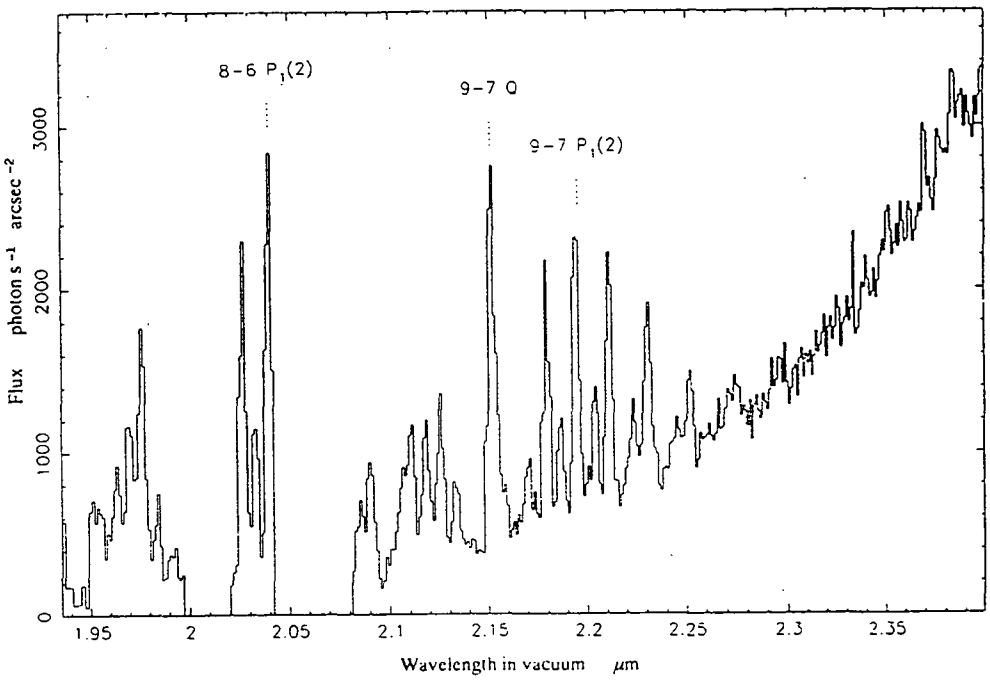

Figure 3.4 Spectrum of the atmospheric OH^- emission in the K window taken using CGS2 (Ramsey *et al.*, 1992).

Chapter 4: Infrared fibre preparation and evaluation techniques

4.1 Introduction

Fibres have their own inherent throughput loss and focal ratio degradation (FRD) mechanisms (see chapter 2) but the fibre preparation can have a considerable effect on these and other fibre characteristics. It is therefore necessary to take great care in fibre preparation and to monitor the preparation by taking throughput and FRD measurements of the fibres. A fibre is particularly vulnerable during the preparation stage. Any damage at this stage will show up in the test results.

This chapter considers fibre termination which can radically affect the FRD characteristics of the fibre and also considers fibre polishing which affects the throughput of the fibre. These are both important characteristics in fibre spectroscopy and experiments for measuring both FRD and throughput of the fibres are described. Finally there is a section on thermal emissivity calculations for fibres. When working in the near-IR particularly beyond about 2μm, emissivity can become an important issue.

4.2 Terminating fibres

Local stress induced by the fibre termination will increase the FRD in the fibre. Further the quality of the surface finish can effect the throughput of the fibre through scattering loss and may affect the FRD if the fibres become rounded off at their ends. The round off is equivalent to placing a lens in front of the fibre and will increase the focal ratio of the beam that propagates down the fibre which combines with other FRD effects to speed up the output beam.

For some applications it may be sufficient to cleave a fibre; this can produce a good finish over most of the fibre surface but smooth cleaving rarely occurs and the surface is usually ragged at one of the edges. This can lead to structure in the fibre output image which degrades wavelength stability in spectroscopic applications. The angle of the cleave to the fibre axis is also difficult to control. This is usually close to perpendicular but it cannot be guaranteed. Polishing the fibre faces produces more consistent results. This requires more effort but very good finish qualities can be achieved over the whole

fibre face, with good surface flatness and good perpendicularity between the fibre face and axis. To polish the fibre it is necessary to hold the fibre rigidly to prevent the fibre flexing or shattering during polishing. This may be achieved in a number of ways such as fixing in wax, which can latter be removed, or clamping directly into a polishing jig. In most cases the fibre will be fixed into place at a later stage. This needs to be achieved without causing local stressing to the fibre at the point of fixing which will induce FRD. A common method is to encase the ends of the fibre in a metal ferrule that can be held firmly without transferring the stress to the fibre inside. The ferrule provides both stress protection for the fibre and holds the fibre rigid for polishing. The most common means of attaching the ferrule is to use an adhesive. Yet, if the adhesive expands or contracts in the ferrule it induces local stress on the fibre walls and hence increases FRD, therefore the amount of adhesive should be keep to a minimum.

An example of adhesive induced stress can be seen in figure 4.1. This shows how the focal ratio of a fibre's output beam changes as the epoxy cures. The fibre was fixed inside a steel ferrule for polishing using Bostic, which dissolves in acetone. After polishing the fibre the ferrule was removed and replaced with a second ferrule glued on with Araldite Rapid which is a quick set epoxy. Slow setting epoxies are normally preferred as it is agreed that these induce less stress than their quick setting counterparts. The fibre output for a fixed input of f/5 was then monitored for about 4 hours. It can be seen that in the first 30 minutes the output degraded from about f/3.9 down to f/3.55 but did not degrade further. It should be noted that this fibre did not display particularly good FRD characteristics even at its best.

4.3 Polishing techniques

A number of different polishing techniques were investigated in an attempt to determine the most effective method for polishing silica and zirconium fluoride fibres. In each case the test fibres were mounted in a polishing jig. The polishing jig is shown in figure 4.2. The jig consisted of stainless steel ring with a mean diameter of ~ 100mm and ~ 15mm across. This had eight approximately 3mm wide radial slots in it that allowed the movement of the polishing slurry into and out of the steel ring. The lower steel ring was rigidly attached to the upper plate of the jig by 4 steel columns. Between the lower steel

ring and the upper plate of the jig there was a spring mounted plate to which was attached the fibre clamping mechanism. The spring mechanism was in the column section attached to the top plate of the jig. A knurled knob allowed the adjustment of the spring pressure. The clamp or polishing head consisted of a series of V-grooves into which the fibre ferrules were fitted and a flat block which clamped the fibres into the V-grooves. A slice of rubber sheet was glued to the face of the block to reduce the stress on the ferrules. The bottom ring provided a large surface that distributed most of the weight of the jig and the spring loaded mechanism allowed the force exerted by the fibres on the polishing medium to be adjusted from zero upwards. As the area of the end of a fibre could be small (< 0.2 mm^2) the amount of pressure exerted by a fibre on the polishing medium could be very large. Sometimes it was necessary to place blank steel rods in the polishing head. This had two purposes: the first was to distribute some of the force exerted by the polishing head when small fibres were used, and, secondly, if only one or two fibres were being polished they acted to stabilise the head which could sometimes be vibrated in the jig as the fibres skimmed across the polishing medium.

The polishing jig could be used to polish the fibres by hand or it could be used with the lapping machine. For the latter, the polishing medium was on a rotating disk and the polishing jig was moved back and forwards across one half of the disk. It did not cross the centre of the rotating disk as the forces exerted caused the jig to vibrate and could damage the fibres. The jig was placed inside a ring and the ring was attached to the end of an arm that slowly oscillated across the rotating disk. This ring had rollers that allowed the jig to rotate about its axis from the forces generated by the rotating action of the polishing medium. The speed of the disk could be adjusted to suit the polishing requirements.

A number of different polishing cloths and grades of polishing powder were experimented with. For silica fibres the most effective procedure was first to polish the fibres flat using a cast iron polishing disk with 1μm Aluminium Oxide polishing powder in a water suspension. This left a dull finish on the face of the fibres. This was then polished to give a good surface finish using a 0.3μm AlO_2 polishing suspension on a SCAN polyurethane plastic polishing cloth coated with cerium oxide filler. The polishing cloths were mounted on polishing disks which had plate glass tops, providing a good flat

surface. Polishing time was critical; if the fibres were polished for too long the ends of the fibres started to round off. If the polishing time was too short the surface finish of the fibres was poor resulting in throughput losses. The surface finish and flatness was checked using an interferometer. If the round off of the face of the fibres was too severe then the procedure had to be started again with the cast iron disk and the 1μm AlO_2 polishing suspension.

This polishing technique was suitable for Silica fibres but not for Zirconium Fluoride as that material is slightly hygroscopic and the water will leech ions from the material degrading the optical properties of the glass. A number of different oil suspensions were experimented with but they proved to be impractical. The process tended to be very messy and difficult to clean and the powder tends to clump together in the oils, producing poor suspensions. In the end a dry polishing technique was chosen for ZrFl fibres using 3M Aluminium Oxide polishing papers. A detailed description of this technique is provide in the SMIRFS fibre preparation section of chapter 7 but it basically involves the use of different grades of polishing paper to improve the surface quality until the desired finish is achieved. These polishing papers were mounted on plate glass to provide a cheap, relatively flat and blemish free surface. As the polishing papers tend to tear and break up, hand polishing was found to be best. This gave greater sensitivity to the process since one could feel any cloth damage through the jig and avoid that area of the paper. This technique was also used for the SMIRFS silica fibres. Also, when using the polishing papers one may flush the surface with water to ease the polishing action and remove the polishing debris but this was not found to be necessary with the SMIRFS silica fibres and was undesirable for the ZrFl fibres.

4.4 Measurement of FRD

A number of different methods for the measurement of fibre FRD have been developed over the years by groups working with fibres (e.g. Gray 1983, Powell 1983, Barden 1987, Ramsey 1988, Parry & Carrasco 1990). However, the results from experimenters are sometimes inconsistent. This "has been attributed, in part, to the lack of a standard way of calibrating the fibres" (Parry & Carrasco 1990, p703).

Initially attempts were made to measure the FRD of the infrared fibres in the near-IR region, however, the technique employed for the measurement of FRD for the SMIRFS fibres was the visible wavelength laser method described by Carrasco (1992). The experimental set-up is shown in figure 4.3. A laser beam is incident at the fibre face at some input angle θ_i that corresponds to the maximum angle of an input beam of a certain focal ratio. As long as the input angle is larger than the spreading induced by the FRD, it produces a hollow cone pattern at the output due to the azimuthal scrambling properties of fibres. The output cone is projected on a screen which is then imaged on a CCD camera. A frame grabber is then used to grab the image which is then reduced in software to give FRD information about the fibre. From the profile of the ring projected by the output cone the FRD produced by the fibre for different input beam angles can be calculated.

4.4.1 Infrared FRD measurement

A number of attempts were made to measure the near-IR FRD characteristic of sample lengths of both Ultra Low OH^- silica fibre supplied by Polymicro Industries Ltd and zirconium fluoride fibre supplied by Le Verre Fluore.

4.4.1.1 Scanning method using a heated filament

Initially we used a black body source to provide illumination, however this quickly failed and was considered too expensive to replace within the project budget. As an alternative a tungsten halogen filament was used to illuminate the fibre. This was run at a lower voltage than the rated working voltage, nominally 12 volts, in an attempt to reduce the temperature of the filament and thus optimise the emission between 1 - 2.5 μm. Using a 1.5 - 2.5 μm filter the voltage that gave the maximum signal at the detector was found to be ~ 10V, below this the signal was found to drop off rapidly. (Note: λ_{max} of a black body at 1000°C is approximately 2.3μm, however tungsten halogen filaments are typically operated at about 4500°C with a λ_{max} ~ 0.6μm.) The detector was a single element PbS detector that had good response characteristics between 1 - 2.5 μm after which it rapidly dropped off. This was linked to an optical chopper and a lock-in amplifier to improve the S/N of the system by up to 10 times over simple DC coupling. The layout of the apparatus is shown in figure 4.4. The detector was mounted on a

rotation stage so it could scan the profile of the output beam from the fibre and the lenses were made from $CaFl_2$ as silica based glasses have poor transmission in the 1 -2.5 μm region. Optical alignment of the apparatus was performed using the visible light from the tungsten halogen source, with the 1.5 - 2.5 μm filter removed. The optimal infrared focus of the $CaFl_2$ lenses was found by peaking up on the output signal from the fibre with the filter replaced in the system. It was necessary to increase the voltage of the source to ~ 12 volts to perform the initial alignment and then return it to ~ 10 Volts to perform the infrared focusing. (Note: the system was left to temperature stabilise for at least 10 minutes before the infrared focusing was attempted to avoid signal intensity variation brought on by changes in the filament temperature of the source.)

The drawback that was found with the above set up was the presence of significant filament structure in the beam that illuminated the fibre. This structure appeared to propagate along the fibre as a result of incomplete radial scrambling within the fibre resulting in significant structure in the output profiles. What was expected from similar experiments at visible wavelengths was smooth structure resembling a top hat function convolved with a Gaussian. The extra structure in the infrared profiles made the data reduction considerably more complex and this was thought to be impractical at the time. Attempts to reduce the filament structure in the input beam, using a diffuser for example, had the effect of reducing the signal to levels where it was barely detectable without significantly reducing the resolution of the scanning. This made the accurate scanning of the output profile impractical, so at the time along with the problems of aligning an essentially invisible beam, the technique was droped as a viable measurement technique. However with a more intense light source with less inherent structure, like a heated ceramic rod or similar device it may be a usable measurement technique. Such ideas were considered, but were ruled out on budget grounds.

4.4.1.2. Scanning method using a infrared He/Ne laser (1.52μm)

A second experiment was set up to measure the infrared FRD characteristics of the near-IR optimised fibre samples, this time using a infrared He/Ne laser (1.52μm). The apparatus was essentially the same as in figure 4.4 however the tungsten halogen lamp and infrared filter were replaced with the infrared laser and a microscope objective to

disperse the collimated laser beam. This was then focused on the fibre face using the pair of $CaFl_2$ lenses. The resulting output profiles showed significant structures and again were not the smooth top hat like function expected. At the time it was thought that this was due to laser induced speckle-like patterns, originally noticed when setting up the apparatus using a visible He/Ne laser (632.8nm). Recent work at Durham has suggested that some of this structure may have been a result of incomplete modal scrambling within the fibres which can be a significant feature in short lengths of fibre of the order of a meter or so. It was noted that the results were very repeatable if the fibre remained in a fixed position, however if the length of fibre was moved or put under localised stress the output profiles changed shape significantly. It had been noticed when using the visible He/Ne laser that the speckle structure in the fibre output beam shifted about significantly if the fibre was even touched or the bench knocked. Again due to the extra complexity involved in the data reduction this technique was abandoned.

4.4.1.3. Scanning method of output ring using an infrared He/Ne laser (1.52μm)

The third attempt at measuring the infrared FRD characteristics of fibre was based on the visible wavelength laser method described by Carrasco (1992) and described briefly earlier in this section, the experimental set up of which is shown in figure 4.3. The difference between the two techniques was the use of an infrared He/Ne laser at the input of the fibre and a PbS detector instead of the CCD camera. As the PbS detector was a single element device it was necessary to scan across the output profile of the fibre as opposed to taking a single frame of the ring formed by the output cone of the fibre on the face of the CCD. Both experimental set-ups had significant speckle-like structures in the output profiles. In the case of the CCD it was possible to integrate the profile around the ring which has the effect of smoothing the effects of the speckle. It is thus possible to gain a smooth profile structure. However, in the infrared case as the scanning only takes a small cut of the profile it is not possible to smooth out the effects of the speckle, thus the resulting highly peaky structure present in the fibre output profiles made determining the FWHM of the profile very difficult. This therefore made an estimate of the FRD produced by the fibre highly speculative. It was felt that the sort of errors that could be introduced into the FRD assessment by the presence of the speckle structure were sufficiently high that it was not worth pursuing the technique.

However, if an infrared array were available, the technique could be significantly improved by integrating the profile around the whole of the output ring and therefore would produce the kind of reliable results gained using the technique in the visible wavelength region. Again due to the cost of infrared arrays it was not possible to pursue this particular avenue on budgetary grounds.

4.4.1.4 The future of Infrared FRD measurement

Though the experiments described above were not successful, with greater investment in equipment and time it should be possible to develop successful systems for infrared FRD measurement based on the modification mentioned. The results gained from the various attempts at FRD measurement suggested that there was not a significant difference between the FRD measured in the infrared than in the visible region, however I must emphasise that the result are very speculative as the previously described experiments were fraught with possible sources of error.

4.5 Throughput measurement

The apparatus for throughput measurement is shown in figure 4.5 and is an adaptation of the set up used for direct measurement of FRD described by Carrasco (1992). It consisted of a tungsten light source containing a simple collimating mechanism. Some results from the SMIRFS fibre bundles are presented in Chapter 7. The beam was projected through a reflective glass diffuser to remove the lamp filament structure. The light passed through a filter; for SMIRFS this was an RG830 filter that transmits longward of ~ 0.83μm. It was then optically chopped at ~ 280 Hz. The chopper provided a reference signal that was used in conjunction with a lock-in amplifier to reduce DC drift and noise of the system. The light passed through a pinhole that was then re-imaged onto the fibre face by a pair of lenses. The first lens was used to collimate the beam and was a simple achromat with a 400mm focal length. The second lens focused the collimated beam onto the fibre face and was a 50mm focal length f/1.2 Pentax camera lens. The iris could be used to set the rough focal ratio of the fibre input beam. It was important to ensure that the input beam was significantly less than the numerical aperture of the fibre so light would not be lost in the fibre cladding. This pair of lenses provided a de-magnification of the pinhole of a factor of ~ 8, thus for SMIRFS

the 1000μm pinhole (A) was reduced to ~ 125μm and projected onto a 200μm fibre core. A 50/50 beam splitter was placed between the pinhole (A) and the first lens and was used to project light reflected from the fibre's input face back onto a CCD camera. This was then used to align and focus the pinhole image on the fibre face. The adjustments were provided by the X, Y, Z stage which was part of the fibre positioning head. At the fibre output the beam was collimated by a third lens and projected onto the detector which was a Newport photodiode (818-SL) with a relatively large surface area. The third lens was a 16mm focal length triplet combination. The signal from the fibre was compared to that from a pinhole (B), of an equivalent diameter to that of the fibre core, which replaced the fibre. The detector had to be moved to achieve this so the third lens was mounted in the same unit as the detector. The experiment was very sensitive to detector position so every effort was made to ensure the detector positions for the pinhole (B) and the fibre were readily repeatable. The signal from the detector was phase locked with the reference signal from the optical chopper to provide a relatively stable output signal that was reasonably independent of the lighting conditions in the room. The lamp power supply was chosen for its good temporal stability characteristics. The response of the detector started to fall off sharply beyond 1.0μm, so with the SMIRFS fibres the wavelength coverage of the measurements was ~ 0.85 to 1.0 μm. The results in chapter 7 provide an example of the typical throughput and FRD for well prepared fibres.

4.6 Thermal emissivity calculations for the fibres

When working at wavelengths beyond about 2μm thermal emissions from objects become an important consideration. A fibre will emit infrared radiation from all it surfaces particularly from its ends. The wavelength at which the emission peaks is characterised by its temperature. This emission will generate noise on the signal transmitting down the fibre. At a given wavelength, λ, the emission is $\varepsilon_{out}(\lambda)$ of the blackbody radiation of that wavelength and temperature. Zur and Katzir (1991) show that for a step index fibre with uniform core absorption

$$\varepsilon_{out}(\theta,\lambda) = \frac{\alpha_{ab}(\theta,\lambda)}{\alpha_t(\theta,\lambda)}\{1-\exp[-\alpha_t(\theta,\lambda)L]\}, \qquad for \qquad \theta \le \theta_c$$

$$\alpha_t = \alpha_{ab} + \alpha_{sc} \quad m^{-1}$$

where α_t is the total attenuation coefficient, α_{ab} is the attenuation due to absorption, α_{sc} is the attenuation due to scattering, θ_c is the critical angle as defined by the numerical aperture of the fibre and L is the length of the fibre. It has been assumed that the refractive index either side of the fibre face is the same and that there are therefore no successive reflections at the fibre end faces. Also

$$T = e^{-\alpha_t L}$$

where T is the transmission of the fibre. The emissivity of the fibre would be largest when all the attenuation in the fibre is due to absorption i.e. $\alpha_{sc} = 0$ and $\alpha_t = \alpha_{ab}$. Thus

$$\varepsilon_{out} \leq 1 - e^{-\alpha_{ab} L} \qquad \text{and} \qquad T = e^{-\alpha_{ab} L}$$

so

$$\varepsilon_{max} = 1 - T$$

When calculating the estimates for the thermal contribution to the background signal for the SMIRFS fibres in the infrared it was sufficient to approximate the fibre emissivity be equal to [1 - fibre transmission].

Table 4.1 shows the calculated estimates for the effective magnitude of the thermal emission from a 1m long fibre of area 3 arcsecs^2 at different wavelengths. Also included are the figures for a blackbody and the typical sky background figures for UKIRT calculated for an equivalent area and solid cone angle (f/36) as the fibre. The figures for the fibre and the blackbody were derived for a temperature of 0°C and the fibre results do not include a contribution from any source other than the fibre optic cable. The transmission figures were derived from the manufacturer's throughput data provided with the fibres.

Wavelength μm	**Fibre Material**	**Emission from Fibre (Mag)**	**Emission from Blackbody (Mag)**	**Emission from UKIRT Sky (Mag)**
1.25	ZrFl	38.4	33.3	16.6
1.65	ZrFl	27.8	22.7	15.2
2.2	ZrFl	20.8	14.3	14.4

Table 4.1 Effective magnitude of emission from a 3 arcsecs^2 thermal source.

These figures show that the contribution from the fibre will be very small when compared to that of an equivalent blackbody and that at UKIRT the background contribution from the sky dominates the thermal background from a blackbody source down to the K band.

4.6 Summary

In fibre spectroscopy both the fibre FRD and throughput are very important. Though fibres have inherent FRD and throughput loss mechanisms the performance of the fibres can be significantly affected by the fibre preparation. The way in which fibres are terminated can significantly increase the FRD of the fibre if local stressing is induced. The throughput of the fibres is sensitive to end losses which are affected by the finish quality of the fibre face and hence are affected by the polishing. It is also possible that during polishing the fibre face becomes rounded and will act like a lens and change the focal ratio propagating down the fibre, increasing the FRD effects. Fibre termination and polishing techniques should be tailored to keep the undesirable effects to a minimum. Particular attention should be paid to adhesives used in conjunction with the fibres as these can induce stress and therefore FRD. A number of different techniques for the measurement of throughput and FRD have been developed over the years. The techniques used for the testing of the SMIRFS fibre bundles are discussed.

Finally, the use of fibres in the infrared raises another issue that is not a consideration when working in the visible and that is the thermal emissions from the fibre material. The thermal emission from a 1m long fibre at 0°C was calculated for the J, H and K bands. The same was done for a blackbody and the typical sky background at UKIRT. The thermal emission from the fibre is small in comparison, which implies that it is not necessary to cool fibres for use in the J, H or K bands.

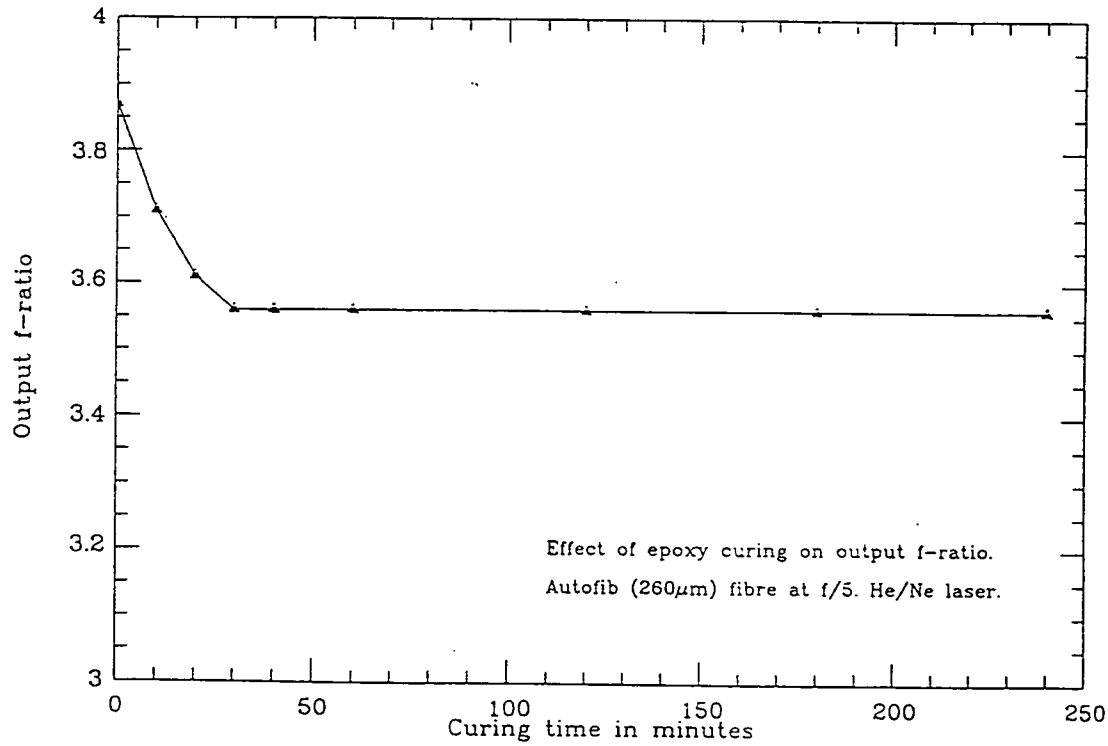

Figure 4.1 The effects of adhesive induced stress on the focal ratio of a fibre's output beam. The output beam was measured as the epoxy, used to glue the fibre inside a steel ferrule, cured.

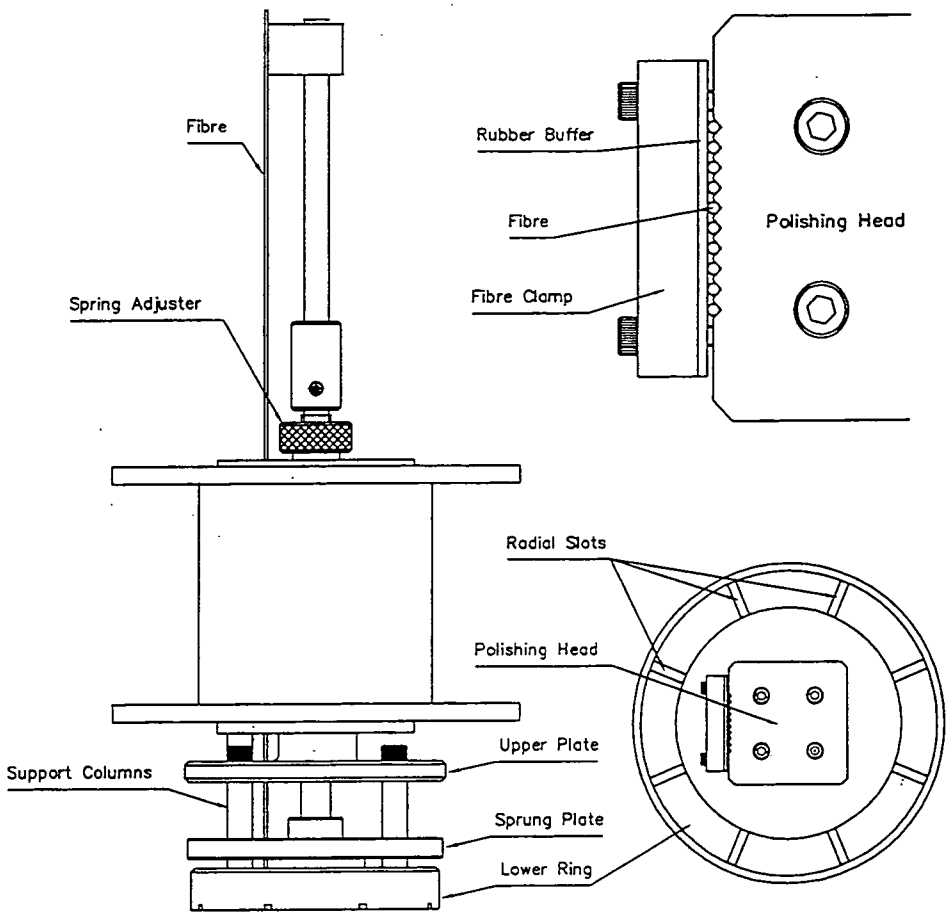

Figure 4.2 The fibre polishing jig (left). An underside view of the lower ring and polishing head (bottom right) and an expanded view of the polishing head showing the clamping of the fibres in the V-grooves (top right).

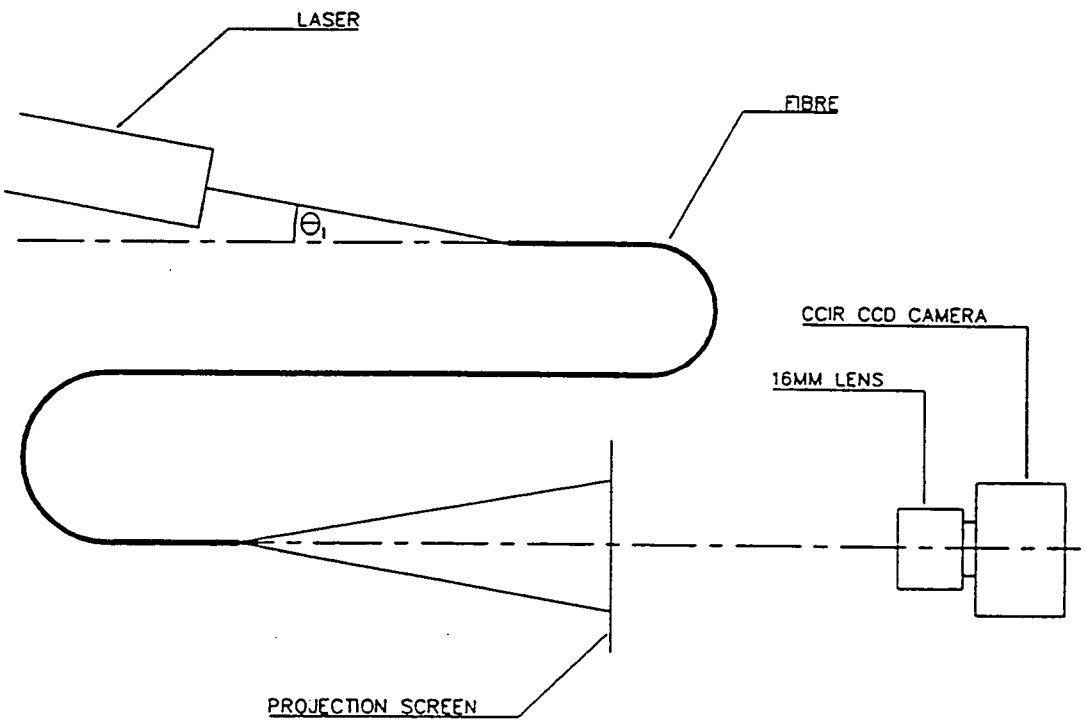

Figure 4.3 A schematic of the FRD laser experiment. The collimated laser beam is incident on the fibre input face at an angle of θ_I. The output pattern from the fibre is projected on a semi-transparent screen viewed by a CCD camera.

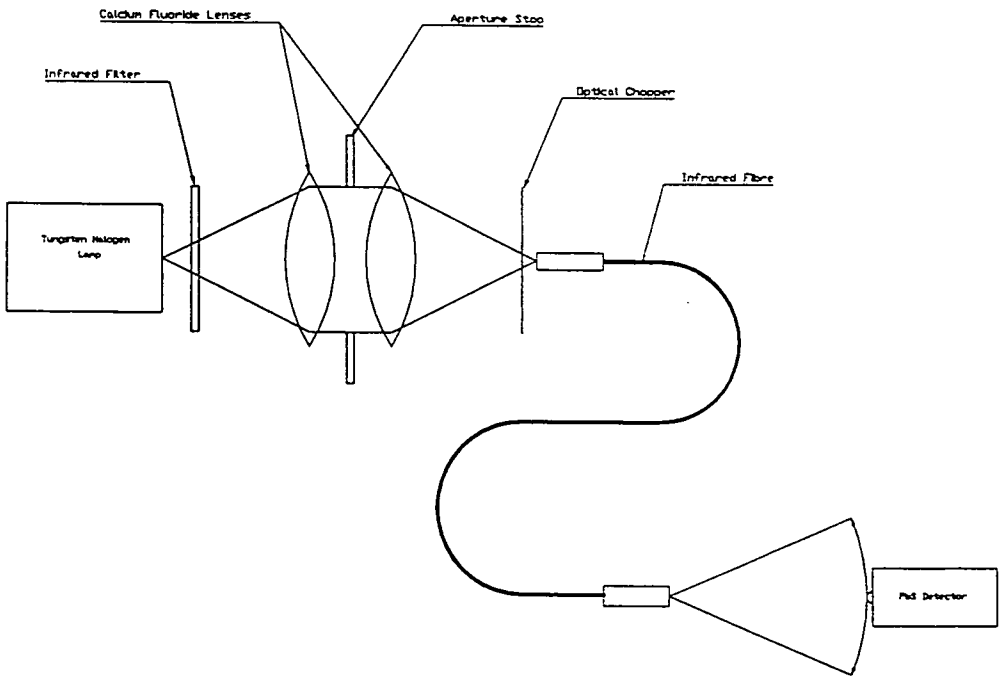

Figure 4.4 A schematic of the apparatus for infrared measurement of FRD in fibres.

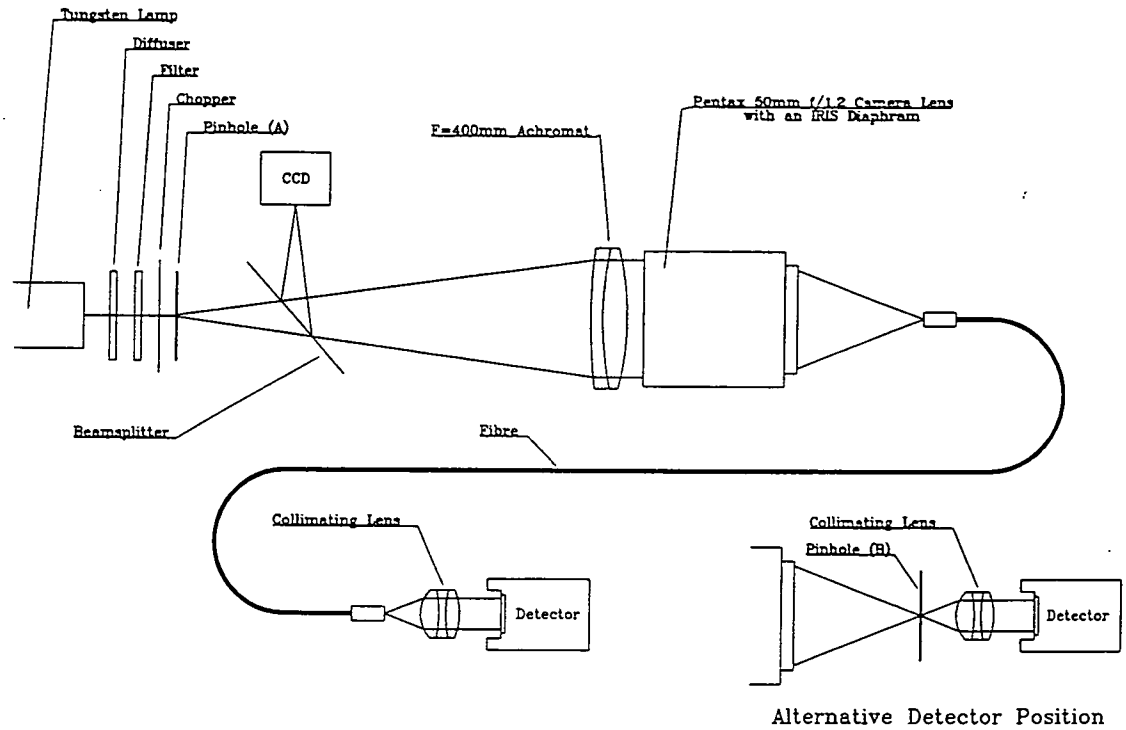

Figure 4.5 A schematic of the apparatus used for the throughput measurements of fibres.

Chapter 5: Microlenses and coupling with fibres.

5.1 Introduction

To ensure maximum throughput and resolution for a spectroscopic system that uses fibres it is important to have good coupling between the telescope beam, the fibres, and the spectrograph (Hill *et al.*, 1983). In this Chapter I will discuss the properties of the fibre that affect coupling, a number of methods of coupling including the use of microlenses and review the different types of microlenses that are available. A brief description of the microlenses used for SMIRFS is also included but this will be covered in greater detail in chapter 6.

5.2 Coupling telescope and spectrograph

It is often the case that either the telescope or the spectrograph are not suited to coupling with fibres. The spectrograph may have been designed to couple directly to the telescope in which case it should be well matched to the focal ratio and image scale of the telescope as is the case with SMIRFS. It could be an instrument designed for a different telescope in which case it may be poorly matched in both image scale and focal ratio. Or it could be an instrument designed specifically for fibre spectroscopy like WYFFOS (Bingham *et al.*, 1994) in which the spectrograph is well matched to the properties of the whole system but would not be well suited to direct coupling with the telescope as the telescope is f/2.8 and the spectrograph collimator f/8.2. In any case it is important to minimise throughput losses and maximise the resolution of the system. However, these two features are often in conflict with each other and a balance between the two is required.

Another consideration is the image scrambling properties of fibres. In chapter 2 it was noted that the FRD of the fibre affects the image scrambling properties of fibres. The more severe the FRD the more effectively the fibre scrambles the input image. As FRD is less severe at fast focal ratios the image scrambling is also less effective. Ideally the fibre output should be an evenly illuminated disk but there can be variations in illumination at focal ratios faster than ~ f/5 (Barden *et al*, 1993, Watson and Terry, 1993). Azimuthal scrambling still occurs but the spatial scrambling is incomplete so a

point source that hits the fibre face off axis can appear as a ring at the output face. This transference of spatial information reduces the wavelength stability obtainable with the spectrograph.

For an optically matched telescope and spectrograph, the most effective fibre coupling occurs when the product of effective image area (A) and solid angle of the cone (α) at the fibre input match that at fibre output, i.e. $A_{in}\alpha_{in} = A_{out}\alpha_{out}$. The minimum achievable $A\alpha$ of the fibre system is set by the effective collecting area of the telescope A_t and the solid angle on the sky accepted by the spectrograph α_s. So, when $A_{out}\alpha_{out} = A_t\alpha_s$ the best possible resolution/throughput combination is achieved (Hill *et al.*, 1983). The effective area of the image at the fibre output face affects the resolution of the spectrograph, the solid angle of the fibre output beam affects the amount of vignetting by the spectrograph collimator and consequently the throughput of the system. At the fibre input there are other considerations. The area of the fibre core is determined by the image scale of the telescope and the input focal ratio should be such that there will be efficient propagation down the fibre with minimal FRD.

5.2.1 Coupling at the fibre input

The simplest form of fibre coupling is a bare fibre with flat, polished input and output faces coupling the telescope focal plane to the entrance slit of the spectrograph. In this case the fibre core is effectively the field stop in the system and defines A_{core}. This should be larger than the area of the input image otherwise vignetting of the signal results ($A_{core} \geq A_{in}$). The area of the image at the fibre output is the same size as the area of the fibre core. This is a result of image scrambling within the fibre ($A_{out} = A_{core}$) which scrambles the light to evenly fill the whole core. The telescope beam focal ratio determines the angle of the fibre input cone (α_{in}), but the solid angle of the fibre output cone will have increased as a result of FRD within the fibre ($\alpha_{out} > \alpha_{in}$). Thus, $A_{out}\alpha_{out} > A_{in}\alpha_{in}$ and as a consequence there will be a drop in either, or both, the resolution or the throughput of the system. The loss of the spatial information means you cannot take advantage of good seeing conditions without introducing vignetting within the spectrograph, however this has the advantage of greater wavelength stability. With this simple form of fibre coupling, if there is a relatively fast input beam (f/2.5 - f/5), it is possible to achieve

reasonably efficient coupling between the telescope and the spectrograph. However, if the input beam to the fibre is relatively slow the increased FRD that results can lead to significant losses in either throughput or resolution.

One method to reduce the FRD problems of coupling fibres to slow foci telescopes is to speed up the telescope beam before it propagates down the fibre using de-magnification optics. This would increase the focal ratio of the fibre input beam (α_{in}) but would reduce the diameter of the fibre core (A_{core}) required to match the telescope image scale. This could be done using a large camera that reduces the whole field of view of the fibre system. However, it would be very difficult and expensive to design a system that produced a good image quality over a potentially very large field. Another approach would be to individually de-magnify the image for each fibre. Since the fibres need to be closely packed together for crowded field or area spectroscopy the optics would have to be small as is the case with microlenses.

5.2.1.1 Direct re-imaging

The simplest form of input microlensing is shown in Figure 5.1. In this case the image at the telescope focal plane is reduced in size and re-imaged onto the fibre input face. Reducing the image size consequently increases the total cone angle of the fibre input beam. However, the change in total cone angle at the fibre face is not simply the ratio of the image de-magnification introduced by the microlens. Those rays which were close to parallel at the telescope focal plane are now tilted towards the fibre axis, so there is an additional increase in total cone angle resulting from a change in the angle of the chief rays, i.e. the system is non-telecentric. This effect is similar to FRD in that it will increase the total cone angle of the fibre output beam. As a consequence there has been an increase in $A\alpha$ product, i.e. $A_{in}\alpha_{in} < A_{out}\alpha_{out}$. This non-telecentric effect is inversely proportional to the focal length of the lens and it can be reduced by using a longer focal length lens. However, as the rays beyond the telescope focal plane are diverging, an increase in the focal length of the lens requires a corresponding increase the diameter of the lens, which means the minimum possible fibre-fibre separation is increased. It is possible to correct the non-telecentricity by using a negative correcting lens between the

re-imaging lens and the fibre face. This straightens the chief rays but introduces additional surface reflection and transmission losses. Additionally, the fibre image scrambling affect the output image size in the same way as direct fibre coupling and the image fills the whole fibre core irrespective of input size, further increasing $A_{out}\alpha_{out}$.

5.2.1.2 Pupil imaging

A different method of coupling, known as pupil imaging, is possible with a single lens. In this case the telescope pupil is imaged onto the fibre face instead of the telescope focal plane image. Figure 5.2. shows the path of the rays from the telescope focal plane to the fibre face. The image size at the fibre face is the same as that for the direct re-imaging, shown in figure 5.1, but θ_{in} is smaller for pupil imaging. In this case, as it is a telecentric system, the $A\alpha$ product at the fibre input face is minimal, i.e. $A_{in}\alpha_{in} = A_t\alpha_s$. When direct re-imaging, the focal ratio and image size at the telescope focal plane affect, in turn, the focal ratio and image size at the fibre face. However, when pupil imaging, the focal ratio of the telescope affects the size of the image at the fibre input face and the image size at the focal plane affects the cone angle of the beam entering the fibre. With direct re-imaging the input image information is lost as a result of the image scrambling properties of the fibre, but with pupil imaging the image information is mostly conserved as the beam cone angle is only partially degraded by FRD. Therefore, the fibre output cone angle is sensitive to the telescope seeing conditions. The size of the image at the fibre input face is determined by the magnification of the microlens and the size of telescope pupil. If the fibre core is chosen to match the image size of the telescope pupil then image scrambling within the fibre will have no effect, as the images at the input and output will both be equal in size, i.e. the core size. If pupil imaging is used at the fibre output, the cone angle information is converted back into image size, consequently affecting the resolution of the spectrograph, and the spectrograph input cone angle is invariant, fixed by the fibre core size.

5.2.2 Lens coupling at the fibre output.

Irrespective of the input coupling method, the output cone will not have a sharp well defined edge to it as a result of FRD; the edge of the cone will have a gradual tailing off in intensity instead of a sharp drop to zero. It is possible to couple the fibre directly to

the spectrograph, but a faster spectrograph collimator would be required to compensate beam spreading introduced by FRD. However, it is often desirable to produce spectrograph collimators with slower focal ratios as this tends to reduce the aberrations, weight and cost of the system. This can be facilitated by the use of lens coupling at the fibre output.

In the case of direct re-imaging at the input, the intensity profile of the output cone will be fixed but with pupil imaging the intensity will vary with input image size. At the fibre output it is possible to simply reverse the coupling method used at the input. If direct re-imaging is used at the output, any increase in cone angle from the fibre, due to FRD, will correspondingly increase the cone angle at the spectrograph collimator. The FRD induced in a fibre can be highly variable with fibre orientation and from fibre to fibre. If pupil imaging is used any increase in output cone angle with be converted into an increase in the output image size. When pupil imaging has been used at the input, in most case it would be advantageous to use pupil imaging at the output. The resulting output cone angle is only dependent on the size of the fibre core and magnification of the lens. Consequently, it could be advantageous to use pupil imaging whatever the input coupling method, as it provides a well defined cone angle for the spectrograph collimator. The disadvantage is that the image size and therefore spectral resolution is poorly defined.

5.2.3 Summary of fibre coupling methods

a) Direct coupling without lenses:- Both the input and output apertures of the fibre are equal and well defined by the diameter of the fibre core, but $A_{out} \geq A_{in}$ resulting in a loss in maximum resolution when the size of input image is smaller than the fibre core. Also, fibre FRD increases the output cone angle ($\alpha_{out} > \alpha_{in}$) with potential signal loss from spectrograph vignetting. This can be substantial with slow input beams.

b) Direct re-imaging with microlenses:- Similarly A_{out} is well defined and $A_{out} \geq A_{in}$. However, the effects of FRD on the output cone angle can be reduced for slow input beams.

c) Pupil imaging with microlenses:- The output cone angle is invariant. However, the size of the output image, and hence the maximum resolution, is dependent on size of the input image.

The use of microlenses gives extra flexibility in spectrograph design. The use of fibres allows the spectrograph a considerable amount of flexibility as to where the spectrograph is positioned and by using differently paired input and output microlenses, the focal ratio of the spectrographs collimator can be altered to suit other design requirements. In addition, microlens arrays can be used with fibres in integral field spectroscopy providing a method of near continuous field coverage (~ 100% filling factor) which is not possible with a simple array of fibres due to the "dead" space between the fibre cores (Zhang & Allington-Smith, 1994). This is discussed further in chapter 9.

5.3 Types of microlenses

There are a number of devices available that can be used to change the input and output characteristics of fibres (Nicia, 1981). These can be divide in four types; fibre tapers, spherical lenses, rod lenses, and graded index (GRIN) lenses. The lens types are shown in figure 5.3. The first of these is not strictly a microlens but a modified form of fibre.

5.3.1 Fibre tapers

Fibre tapers consist of a length of conduit that changes core diameter along its length. Each time the propagating ray hits the core/cladding boundary the angle of internal reflection is slightly changed as a result of the taper and thus the cone angle of the beam and the diameter of the fibre core are gradually changed. It is possible to have tapers that have input to output ratios of 40:1 but ranges from 2:1 to 10:1 are more typical. It is important to ensure that the maximum internal reflection angle is not exceeded anywhere along the taper's length as this will result in light loss. Also there can be large losses through mis-alignment at the taper/fibre interface. The tapers can be integral with the fibre being manufactured from the same length of material but they are available in only very limited input/output ratios and usually only tapered at one end as they are usually the end section of a long fibre draw.

5.3.2 Spherical lenses

The first lens type to be discussed is the simple ball or spherical lens. These consist of a sphere of glass, the focal length is determined from the refractive index of the glass and the radius of the sphere. These types of lenses are available in a large variety of different diameters down to about 40μm. They are relatively cheap and come in a range of different glasses with a variety of refractive indices. These lenses by their nature tend to have relatively high power with short focal lengths and a focus close to the lens surface. When the refractive index n = 2 the focus occurs at the glass surface and the focal length is equal to the radius of the sphere. This type of lens was considered for the SMIRFS system but, even for a relatively low index material, the large diameter of the lens would not have been practical. Also there was the transmission of the glass in the infrared to consider.

For the paraxial rays:

$$r = \frac{2f(n-1)}{n} \quad \text{and} \quad s = \frac{r(2-n)}{2(n-1)}$$

where r = the sphere radius, n = refractive index of the glass, f = focal length of the lens and s = principle focus distance from the sphere surface. For a $CaFl_2$ (n ~ 1.43) spherical lens and f = 7.26 mm (focal length of the SMIRFS microlenses) , r = 4.37 mm giving a lens that is nearly 9 mm in diameter. The focal point s = 2.90mm

5.3.3 Rod lenses

The second type is the rod lens. This consists of a cylinder of glass with a spherical curve on either one or both of the ends. The length, refractive index and radius of curvature can all be adjusted to alter the focal length of the lens. These lenses also have the advantage that if a flat output face is used they can be fixed directly to the fibre face using an index-matching epoxy, cutting down on reflection losses. This type of lens provides much more flexibility in design and is well suited to the pupil imaging coupling employed with SMIRFS.

For the paraxial rays and a convex-plano rod lens:

$$r = F(n-1)d$$

$$D = h + \frac{r}{F(n-1)}$$

$$s = \frac{r}{n-1}$$

$$l = \frac{rn}{n-1}$$

where r = radius of curvature, F = focal ratio of the telescope, n = refractive index of the glass, d = diameter of the fibre core, D = Diameter of the lens, h = the size of the image to be accepted by the fibre, s = distance from telescope focal plane to front of the lens and l = the length of the lens. For the SMIRFS system F = 36.3, n_d ~ 1.43 ($CaFl_2$), d = 0.200mm, h ~ 1.31mm (2 arcsecs). So the lens parameters should be as follows: curvature r = 3.12mm, the diameter of the lens D = 1.51mm, the image distance s = 7.26mm and the lens length l = 10.38mm.

The SMIRFS microlens specifications were slightly different from the above as there were manufacturing difficulties in producing lenses to this specification. The final lenses had r = 3.00mm, D = 3.00mm, l = 3.00mm. The result was s ~ 6.98mm and the image size h ~ 2.8mm (~ 4.3 arcsecs). The large image size can be altered by using a field stop in the system. This is discussed further along with ray tracing of the SMIRFS lenses in Chapter 6.

5.3.4 Graded index (GRIN) lenses

A graded index lens consist of a glass rod that is polished flat at both ends and is rather like graded index fibre. It has a radial refractive index gradient and the power of the lens is determined by the length of the lens. The incident rays travel along the lens as a sine wave. The point at which the end of the lens is located relative to the period of the wave

will determine the angle of the output rays. For example if the rays are at the turn over point of the sine wave (towards the edge of the fibre) they will emerge parallel, whereas if they are at the cross over or focal point they will emerge with their maximum angle. There are also distributed index planar lenses that have a three dimensional index gradient.

5.3.5 Lens aberrations and reflection losses

Since the microlenses are simple and relatively small the most dominant aberrations are chromatic and spherical aberrations. The chromatic aberrations are dominated by longitudinal aberrations which are functions of the dispersion of the glass material used in the lenses and are not related to the type of lens used. Spherical aberrations are related to the maximum cone angle of the lens output beam. In slow lenses this is not a significant problem but for faster beams it can become severe. Ray tracing the lenses gives a clear idea of the effects the lens aberrations have on the image quality. This was done for the SMIRFS optics and is detailed in chapter 6.

The reflection losses can contribute significantly to the throughput losses of the system. Using microlenses introduces another four glass surfaces. If index matching materials or anti-reflection coatings are not used there will then be six air/glass surfaces each reflecting about 4% of the light (assuming n ~ 1.5), or a total reflection loss of ~23%. This will be even higher if high refractive index materials are used to produce high power lenses.

5.3.6 Choosing your microlens

Each of the different microlens types has its strengths and weaknesses:

a) Fibre tapers:- These tend to be very long and are only available in a relatively limited number of sizes and input/output ratios, but can provide very efficient coupling.

b) Spherical microlenses:- These lenses tend to have short focal lengths and relatively large aberrations. If long focal length lenses are required the diameter of the lens becomes unfeasibly large. However, being spheres, they are relatively easy to align.

c) Rod lenses:- These lenses provide much greater design flexibility than spherical lenses and can have either a short or long focal length. Also they can butt directly up against

the fibre face, which with index matching gels can reduce the reflection losses. However, they have a specific optical axis making alignment more difficult.

d) GRIN lenses:- Finding suitable material to provide the graded index and good transmission could prove difficult and the lenses may only available in a limit range of powers, but they can be relatively inexpensive and effective.

5.4 Summary

Direct fibre coupling is adequate if both the telescope and spectrograph have fast beams but if slow beams are involved some form of extra optical coupling is required. Large optical systems can be used to modify the whole field but these can be difficult to design and expensive to build. Another technique is to separately couple each fibre using microlenses. The microlenses can either be used to directly re-image the telescope focal plane on the fibre face or the telescope pupil can be imaged onto the fibre face using a pupil imaging technique. The latter has the advantage in that the output beam cone angle is well defined and one can take advantage of good seeing conditions because the output image size is dependent upon the image size at the telescope focal plane rather than on the diameter of the fibre. Several different types of microlenses are available; the microlenses chosen for SMIRFS were a form of rod lens. The characteristics of these lenses along with some of the alternative type of microlenses are discussed.

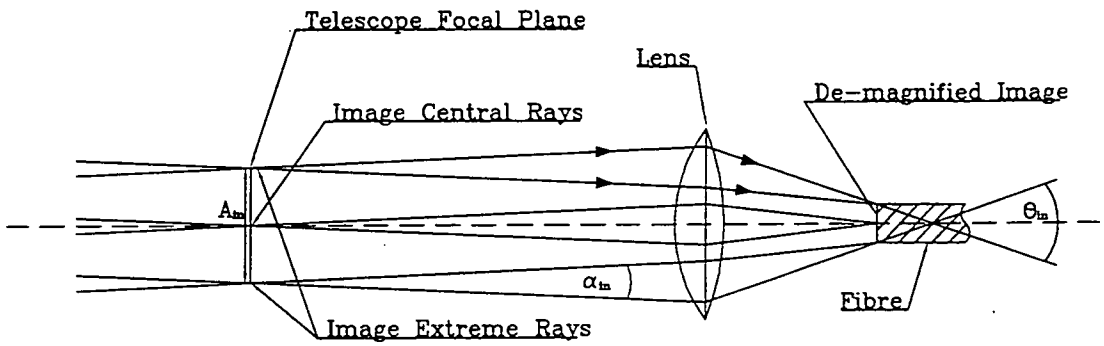

Figure 5.1 Direct re-imaging with a simple lens. The image at the telescope focal plane is re-imaged onto the fibre face. The input image is assumed to be circular with an area A_{in}. The cone angle of the telescope beam is α_{in}. The total cone angle incident on the fibre face is θ_{in}. For simplicity θ_{in} is labelled after the fibre face, but strictly speaking the angle will have changed as the result of refraction at the air/glass boundary.

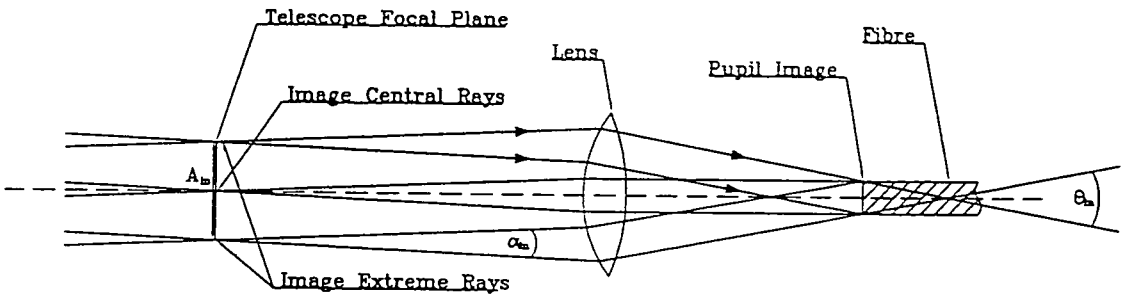

Figure 5.2 Pupil imaging with a simple lens. The telescope pupil is imaged onto the fibre face. The focal plane image has an area A_{in} and the cone angle of the telescope beam is α_{in}. The total cone angle incident on the fibre face is θ_{in} and is affected by the focal plane image size. For simplicity θ_{in} is labelled after the fibre face, but strictly speaking the angle will have changed as the result of refraction at the air/glass boundary.

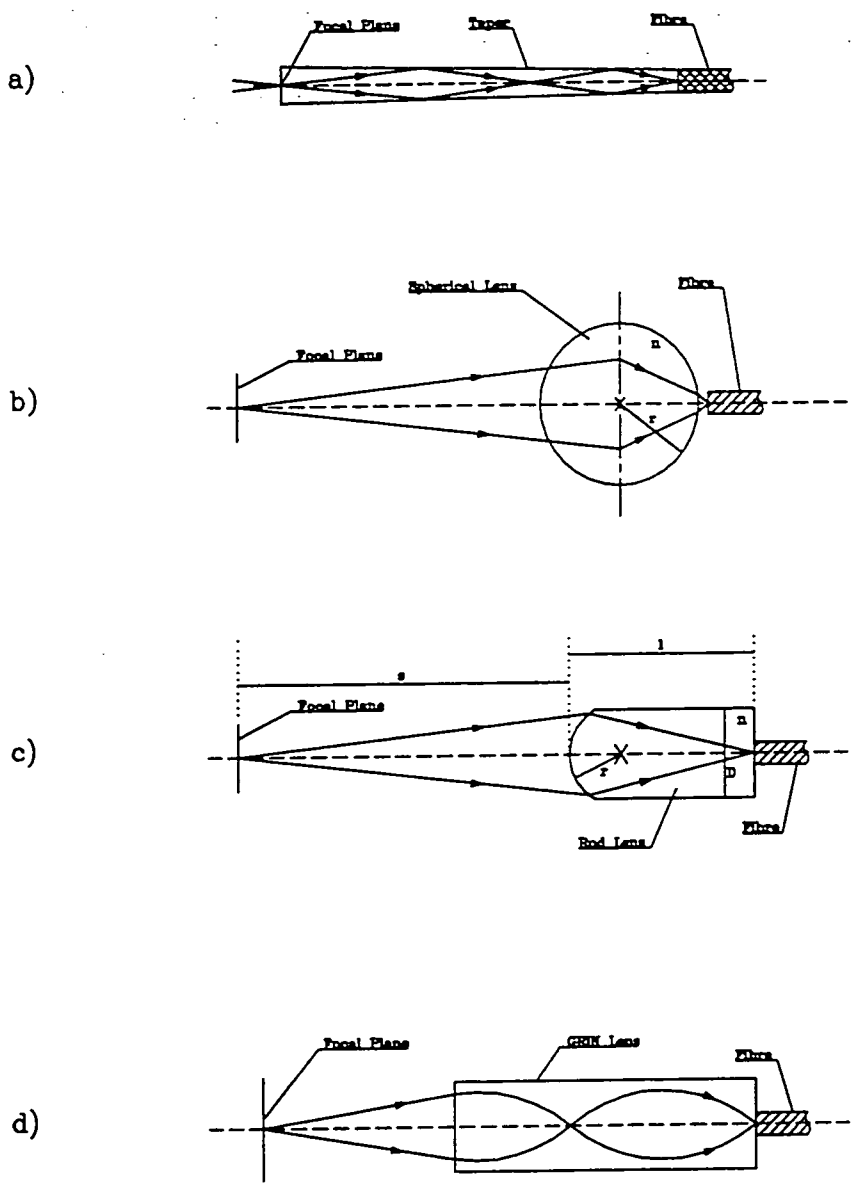

Figure 5.3 Four different types of microlenses. a) is a fibre taper. b) is a spherical microlens, where r is the radius of the lens and n is the refractive index of the glass. c) is a rod microlens, where r is the radius of curvature of the lens face, D is the diameter of the lens, n is the refractive index of the glass, l is the length of the lens and s is the distance from the focal plane to the front face of the lens. d) is a graded index (GRIN) lens.

Chapter 6: SMIRFS-an infrared multi-fibre system for UKIRT

6.1 Introduction

SMIRFS (Spectroscopic Multiple InfraRed Fibre System) is an infrared multi-fibre system that was designed and built at Durham (R. Haynes & I. R. Parry, 1994) for use at the 3.8m UK InfraRed Telescope (UKIRT) in Hawaii. It was designed as a prototype plug plate fibre system for the CGS4 spectrograph (Mountain *et. al.*, 1990) to work in the J (~1.25±0.05μm), H (~1.65±0.1μm) and K (~2.2±0.2μm) bands. There are two fibre bundles, each containing 14 target fibres. One bundle is made from a low OH^- silica fibre for use in J and H, the other is made from zirconium fluoride (ZrF_4) fibre for use in K. In this chapter I will discuss the aims of the project, the design considerations, specification and ray tracing of the optical components, and provide a technical description of the various components of the instrument.

6.2 Design considerations

In designing a fibre system for UKIRT to work in J, H and K bands which was also to interface to the cooled long slit spectrometer CGS4, there were several points to consider. First, it was necessary to consider the fibre material. Silica fibre is used for fibre spectroscopy in the optical, however this starts to severely attenuate the signal beyond ~ 2μm, so a suitable alternative was required for the K band. Secondly, fibres are not well suited to the propagation of a slow focal ratio beam such as at the UKIRT Cassegrain focus, thus a method of efficiently coupling the fibres to the f/36 beam was required. Also thermal emissions from SMIRFS needed to be keep to a minimum if the system was to perform well in the K band.

6.2.1 Aims

When this project began, very little astronomical work had been done with fibres in the infrared. Since then there have been publications by other groups working on infrared fibres (R. Dallier *et. al.*, 1993, Levin *et al.*, 1993 and Coude Du Foresto *et al.*, 1993). The aim of the SMIRFS project was to develop a fibre system for astronomical spectroscopy to work in the wavelength range 1 - 2.5 μm which includes the J, H and K

bands. It was to be a prototype system which would be used as a test bed for developing techniques and experience for future near-IR fibre systems. The system would interface between UKIRT and CGS4 providing it with a multi-object capability. Initially the system would be "warm" but if thermal emission from SMIRFS was found to be too high in the K band, the system would be capable of being cooled.

6.2.2 General considerations

SMIRFS was designed to couple UKIRT to the CGS4 spectrograph which accepts a slow f/36 beam. It is well known that the FRD losses produced by a fibre increase dramatically at slower focal ratios. With an input beam of f/36, even with a good fibre, typically less than 20% of the output beam falls within f/36 and this is clearly undesirable when feeding an f/36 spectrograph such as CGS4. One solution is to speed up the beam entering the fibre so it propagates down the fibre at a faster focal ratio where FRD losses are smaller. The beam can then be reconverted back to an f/36 beam at the fibre output to match the spectrograph. This can be done by microlensing both at the input and the output of the fibre (Hill *et al.*, 1983).

In the visible region it is possible to use silica fibres but in this case we needed to work beyond 2μm. Silica fibres attenuate heavily beyond 2μm and were therefore unsuitable for the K band. ZrF_4 fibres however have very little attenuation in the 2μm region and suitable lengths of fibre were available which displayed favourable transmission, mechanical and FRD characteristics.

Thermal emission from "warm" objects must be considered when working in the near-IR and every effort should to be made to keep it to a minimum. At the typical temperatures occurring inside the UKIRT dome the contribution to the background counts from thermal emissions from "warm" material in the optical path should be negligible in J and H, however in the K band these emissions can become significant. One solution is to "cool" the whole system to reduce thermal emissions, the other is to try and avoid "viewing" objects that produce high levels of thermal emissions. Thermal emissivity calculations were made for the fibre material (see chapter 4) which suggested that the contribution to background levels from the fibres themselves would be small but care

needed to be taken to ensure the system "viewed" a minimum about of blackbody sources, such as lens mountings or telescope structure.

SMIRFS, being an addition to an existing spectrograph, was to have minimal effects on the normal configuration of CGS4. It was therefore necessary to position the fibre slit into the focal plane position inside the spectrograph without dismantling it. This could be done by projecting the image of the fibre slit using 1:1 re-imaging optics. This required the removal of the existing calibration unit from CGS4, so an alternative method of calibration had to be derived.

When observing astronomical fields, the fibres needed to be accurately positioned in the telescope focal plane. There have been numerous fibre positioning systems developed, many of them are complicated automated systems involving robot positioners such as MX (Hill and Lesser, 1986), AUTOFIB2 (Parry *et al.*, 1994) and 2df (Taylor *et al.*, 1994). However, as SMIRFS was a development system it was simpler to use a plug plate system such as MEDUSA (Hill *et. al.*, 1982), FOCAP (Gray, 1983) and FLAIR (Watson, 1988). Also a system for acquiring the astronomical field and guiding would be required and it was felt a system using guide fibres would to be the best solution.

6.2.3 SMIRFS Infrared fibres

The transmission for a 1m length of infrared optimised silica fibre drops from 96% at 2.0μm down to 66% at 2.4μm. ZrF_4 fibres, however, have very good transmission in this region. For a 1m length the transmission is 98% at 2μm and >99% at 2.4μm (see chapter 2). The ZrF_4 fibre was a lot more expensive than the infrared optimised silica fibre, costing ~£100 per meter as opposed to ~£3 per meter. The fibres were to be relatively short, ~1.2m, so the attenuation using silica fibres would not be totally crippling, but as this was a development instrument ZrF_4 fibre was tried for the K band. However, silica fibres have better transmission shortward of 1.8μm and were preferred for the J and H bands. It was decided that there would be two fibre bundles: one of ZrF_4 optimised for the K band and one of silica optimised for the J and H band. It should be noted that ZrF_4 fibres tend to be far more fragile than silica fibres. It was very difficult to work a sample of 70μm core ZrF_4 fibre without breakages. It was therefore decided that

the minimum core size of the fibres should be at least 150μm if the optical configuration would allow this.

The silica fibre bundle used Polymicro FIP200/220/240 fibre, an Ultra Low OH^- all silica fibre with a polyimide buffer. This had good transmission characteristics out to 1.8μm and displayed favourable FRD characterises. Fibres from two manufacturers of ZrF_4 fibres were acquired and tested. The first was a length of IRGUIDE-1 200/250-2 from Le Verre Fluore (France) with a 200μm core, 250μm cladding, 380μm polyacrylate buffer and a numerical aperture of ~ 0.2. The second was a length of Type II GCA-1268, ZrF_4 fibre from Infra-Red Systems Inc. (USA) with a 200μm core, 240μm cladding and a 250μm buffer (material unknown but thickness suggested polyimide). The fibres were first ferruled and polished. To get a rough evaluation of their FRD characteristics a laser was shone down the fibres with an input angle of ~ 10° (equivalent to the extreme ray of an f/2.8 beam or N.A ~ 0.18) and the output profile viewed (see chapter 4). The IRGUIDE-1 fibre displayed a relatively thin well defined ring indicating little FRD, however the test length of the GCA-1268 fibre had severe FRD; the output ring was so thick it filled the entire numerical aperture. To ensure that this effect was not a result of local stressing or a damaged section of fibre, the test fibre was cut into three equal lengths, then re-ferruled and polished again. If it was unusual stressing from one of the steel ferrules or a damaged section of the fibre causing the FRD then this should have been confined to only one of the three fibres. However, the FRD did not noticeably improve for any of the lengths. It was therefore concluded that either the GCA-1268 fibre had inherently high FRD or that it was particularly susceptible to local stressing by the ferrules. In either case it was not suitable for our purposes, so the Le Verre Fluore IRGUIDE-1 was chosen as the fibre for the SMIRFS K-band bundle.

6.2.4 SMIRFS microlenses

UKIRT and CGS4 have a slow f/36.3 beam. If an input beam of f/36 was injected into a good fibre typically less than 20% of the output beam would fall within f/36 due to FRD. However, at faster input beams the FRD becomes much less severe. The ideal propagation condition in fibres is generally agreed to be f/4 - f/3 (Baudrand *et al.*, 1994). One solution to this problem is to speed up the beam entering the fibre so that it

propagates at a faster focal ratio with less FRD. The beam could then be reconverted back to f/36 at the fibre output to match the requirements of the spectrograph. This could be achieved by using microlenses at both the fibre input and output. Two methods of microlens coupling were considered. The first was direct re-imaging of the telescope focus and the second was pupil imaging in which the secondary mirror of the telescope (which is the pupil for UKIRT) was imaged onto the input fibre face. Pupil imaging was chosen as the coupling method for both the input and output of the fibres because the direct re-imaging method of coupling does not maintain the telecentricity and as a result introduces FRD effects which combine with the FRD produced by the fibre to increase the beam speed at the fibre output. The pupil imaging coupling method maintains the telecentricity and therefore does not introduce FRD over and above the FRD due to the fibre alone. The other benefit of using pupil imaging at the output was that FRD induced in the fibre increases the image size on the detector but does not affect the output beam speed. This reduces the resolution of the system but there would not be throughput losses due to beam mis-matching. It was felt that, for this application, a trade off in resolution was the better option. The principles of microlens coupling are explained in greater detail in chapter 5 and briefly summarised in Table 6.1 below.

Pupil Imaging with microlenses	**Direct re-imaging with microlenses**	**Direct coupling without microlenses**
Output image is poorly defined and proportional to the input image size. The maximum resolution is therefore dependent on input image size.	Output image is well defined being directly proportional to the fibre core size. This can result in loss of maximum resolution.	Output image size is well defined and related to the fibre core size. This can result in loss of maximum resolution.
The input beam has the same focal ratio as the output beam, i.e. the cone angle is invariant. This means minimal losses from spectrograph vignetting.	The output beam is faster than the input beam due to FRD in the fibre. This can result in throughput losses from vignetting.	The output beam is faster than the input beam. This is particularly noticeable when coupling slow beams and can result in large losses from vignetting.

Table 6.1 Summary of differences between the techniques for coupling with fibres.

6.2.5 The field plate and fibre pointing

The configuration of UKIRT only allows a small field of view ~ 4 arcminutes in diameter. This limits the type of science that can be achieved with SMIRFS as crowded fields are required to obtain a sufficient number of suitable objects in the field. Though there was little that could be done about the size of the field it was important to exploit as much of the available field as possible. This involved keeping the minimum fibre separation small as well as exploiting the maximum field area. Another very important consideration was the pointing of the fibres at the secondary mirror. For fibre systems designed for "fast" telescopes or prime focus systems this is not such an important criterion as the mirrors subtend a relatively large angle, but for SMIRFS it was vital that the fibre pointing was accurate. This is a consequence of the fact that the fibres are viewing a 313.4 mm diameter mirror nominally 11384 mm away.

Figure 6.1 demonstrates the effects of pointing on the amount of light from the secondary mirror that would be imaged onto the fibre core. This assumes that the secondary mirror is re-imaged to match perfectly the size of the fibre core. It shows that a pointing error of as little as 0.1° would mean ~ 8% of the light from the secondary mirror would miss the fibre core. Also since the size of the field plate is ~ 1/2 that of the mirror, if a flat field plate was used, a fibre at the edge of the plate would lose ~ 25% of the light from the mirror. To correct for this the field plate had to be curved on a radius equal to that of its distance to the mirror, so all the fibres in the field pointed at its centre. The whole field plate system also had to be very rigid so there were no pointing errors due to flexure as the telescope tracked across the sky. It would be necessary to align the field plates when the telescope was pointing at the zenith where the instrument support unit was accessible.

A point source image such as a star would appear to be typically 1-2 arcsecs across at the focal plane of UKIRT due to seeing and telescope tracking. At the UKIRT f/36 plate scale (1.525 arcsecs/mm) the image would be ~ 0.7-1.3mm in diameter. Field curvature effects over a 4 arcminute field for a field plate that was in focus at its centre, would only increase the spot size by ~ 130μmm which was smaller than the diffraction limited width of ~ 175μm at a wavelength of 2μm. This could be reduced further by fixing the field plate at the optimal focus position. It was therefore not necessary to correct for the

field curvature of the telescope. The ray tracing of UKIRT is detailed later in this chapter.

6.2.6 The slit projection unit.

SMIRFS was designed to feed light, via the fibre bundle, from the telescope focal plane to the normal telescope focal position inside CGS4. Because this is a cryogenically cooled spectrograph it was not practical to gain access to the inside of the instrument. It was therefore necessary to mount the fibre slit outside CGS4 and project an image of the fibre slit onto the normal focus inside CGS4. This could be done using either transmission optics or reflection optics.

After reviewing various transmissive optical designs, by far the simplest solution involved using mirrors. This method would not suffer from the difficulties of chromatic aberrations and choice of anti-reflection coatings associated with transmission optics systems. The possibility of combining the focal ratio conversion at the fibre output (~f/5 to f/36.3) with the re-imaging of the slit, instead of using individual output microlenses, was considered but the aberrations were found to be very difficult to control.

In the end a simple system involving individual microlenses at the fibre outputs for focal ratio conversion and a spherical mirror for the re-imaging of the fibre slit was chosen. This required a 1:1 re-image of the slit. Normally a parabolic mirror would be required if the image quality was to remain good but as this would be a spectroscopic application, and the fibre beams were ~f/36, the spherical aberrations associated with a spherical mirror were not significant. The reflectivity of the mirror coatings in the 1-2.5μm region was also reviewed. In this region gold and silver have a reflectivity of ~98% and aluminium ~96%. The different coatings would have relatively little effect on the throughput of the system, but the thermal emissivity (1 - reflectivity) of the aluminium mirror will be nearly twice that of silver or gold. Thus gold and silver mirrors were more suitable particularly in the K band. However, the thermal emissions from aluminium mirrors would still be relatively small compared to the brass of the fibre slit material (ε~0.6 at 2μm).

Thermal emissions from "warm" surfaces at the typical telescope dome temperatures at UKIRT (~0-10°C), though not a problem in the J and H bands, could significantly

increase the background signal from SMIRFS in the K band. At the input end of SMIRFS there will be contributions from the sky, the telescope mirrors and any telescope structure viewed by the fibre. There would also be the contribution from the fibres themselves. However, the thermal emission from a surface is proportional to 1-T, where T is the transmission, which for the optical components should be relatively high. The surfaces that contribute significantly to the thermal emission are those that have low reflectance, low transmission or those that are confined inside an enclosed area. Therefore every effort needed to be made to keep the amount of warm material, that would eventually be viewed by the CGS4 detector, to a minimum. The "cold" Lyot stop inside CGS4 would serve to mask out any emission from outside the optical path of the f/36.3 beam. To minimise the amount of emission from material on either side of the fibre slit it was necessary to image through the "cold" long slits inside CGS4. This masked off much of the "warm" material of the slit block but still left some material "visible" between the fibres, along the length of the slit.

6.2.7 The fibre slit

When designing the fibre slit one has to consider how it will appear at the detector; the fibre size and fibre to fibre spacing are both important considerations. Sampling theory suggests that ideally there should be at least 2.5 pixels per fibre. However, particularly with the current infrared arrays, the numbers of pixels available is limited. Also the fibres need to be separated sufficiently so there is no overlap of the spectra.

SMIRFS was originally intended to be used with the 58x62 InSb array. Due to delays in manufacture this array was upgraded to a 256x256 InSb device before SMIRFS was complete so the design was altered to suit. However, not all 256 pixels are available along the slit. The CGS4 slit length is ~90" long, and the pixel scale is 1.23" with the 150 mm camera and 0.62" with the 300 mm camera. Thus there are about 73 or 147 pixels along the slit. A typical fibre image would be about 2" across but could be up to 4" if the field stops were not employed. The diameter of the microlenses limits the fibre spacing at the slit to no closer than ~4.6". In addition there should be suitable separation of the spectra in order that the individual spectra can be extracted from the data frame.

Using the 150 mm camera, the fibre image could cover up to 4 pixels and allowing a 1 pixel separation of the spectra, the fibres should be spaced at 5 pixel centres. This allows up to 14 fibres per slit and gives a fibre slit length of ~82". The pixel coverage would double when the 300mm camera was employed.

6.2.8 Guide fibre unit

Field acquisition is usually done at UKIRT using a cross-head guide camera situated below the infrared reflecting dichroic. However, SMIRFS required a system for aligning the field with the fibres in the field plate. A simple way of achieving this is to place a number of guide fibres in the field. These are then used to correct for any offset or rotational discrepancies between the crosshead and the SMIRFS field plate unit. The guide fibres could either be coherent bundles or a hexagonal arrangement of 7 closely packed fibres with one in the centre and 6 surrounding it. The latter arrangement is shown in figure 6.11. It is possible to monitor the position and motion of the star image on a guide fibre input face by observing the illumination at the output of the fibres.

The infrared light falling on the field plate of SMIRFS has been reflected off the dichroic in the Instrument Support Unit of UKIRT. This splits the light so that most of the visible light is transmitted through the dichroic to the crosshead camera while most of the infrared light is reflected towards the field plate. Despite this the guide fibre system was designed to utilise the small amount of visible light that is reflected towards the field plate by the dichroic (~30%). This was necessary as there were insufficient resources to develop a guide system using the infrared light. With 70% of the visible light being lost before it reached the guide fibres it was important to ensure high throughput of the system, also the detector sensitivity needed to be sufficient so that suitable guide stars could be found in the field.

6.2.9 Reflection losses in the system

Reflection losses within the SMIRFS system were expected to be quite large as there are a number of air-glass surfaces in the system. Using anti-reflection coatings or index matching gels was not planned as this was a prototype system with a limited budget. For an air-glass surface and an incident angle of 0°

$$R = \frac{(n-1)^2}{(n+1)^2}$$

where R is the reflectivity and n is the refractive index of the medium. With a glass surface the reflectivity changes very little for small changes in incident angle and as the incidence angles for SMIRFS are relatively small this is a reasonable approximation.

Material	Refractive Index (2.5μm)	Reflection
Calcium Fluoride	~ 1.40	~ 2.8 %
Silica	~ 1.43	~ 3.1 %
Zirconium Fluoride	~ 1.50	~ 4.0 %
Gold Coated Mirror	-	~ 98 %
Silver Coated Mirror	-	~ 98 %

Table 6.2 Typical reflection losses for air-glass surfaces and mirror coatings at approximately 2.5μm.

As the SMIRFS system has 6 Air/Glass surfaces per fibre and two mirror surface in the SPU in addition to the those present when observing with CGS4 alone, the reflection loss are significant. Table 6.3 shows the estimated reflection losses from SMIRFS alone for each of the fibre bundles and are calculated from the values given in table 6.2.

	Including SPU Mirrors	Without SPU Mirrors
ZrF_4 Fibre Bundle	~ 22 %	~ 18 %
Silica Fibre Bundle	~ 20 %	~ 16 %

Table 6.3 Estimated reflection losses for the SMIRFS system.

These figures suggest that up to 22% of the throughput losses expected with the SMIRFS system will come from reflection losses. However, this figure could be significantly reduced if the microlenses were anti-reflection coated and index matching gel were used in the space between the fibre face and the back of the microlens. The total throughput estimates for SMIRFS, including material attenuation and optical alignment losses, are discussed in chapter 8.

6.3 Ray tracing the optical components of SMIRFS

The areas analysed using ray tracing included the telescope field curvature, the fibre microlenses and the optics in the slit projection unit. It was not felt to be necessary to analyse the guide fibre optics. The ray tracing was carried out using the ZeMax software package.

6.3.1 Field curvature of UKIRT

The optical layout of UKIRT was ray traced using data supplied by Royal Observatory Edinburgh and the resulting image quality was analysed. Figure 6.2 shows the tangential and sagittal components of the field curvature, also the distortion of a ~4 arcminute field. As the distortion was positive this indicated it was pincushion distortion however, it was so small (< 0.005%) as to be negligible. Figure 6.3 shows the spot diagram for a point source at the centre of the field (0.00°), and point sources 0.022° (~ 1.4 arcminutes) and 0.033° (~ 2 arcminutes) from the field centre. The solid circle represents the Airy disc. It can be seen from this diagram that the maximum spot size caused by incorrect focus due to field curvature was ~ 130μm in diameter. The diffraction limit of the telescope was ~ 150μm. The maximum spot size could be reduced if the telescope was optimally focused for the whole field. Figure 6.4 shows the spot diagram for UKIRT with the focal plane curved on a 814.5 mm radius to correct for the field curvature. The radius was calculated by the ray tracing program to give the optimal focal correction. The maximum spot size was reduced to ~ 30μm diameter.

The plate scale of UKIRT is 1.525 arcsecs/mm, so a 1" image would be ~0.66mm in diameter. Thus, though the field curvature of UKIRT was relatively large, even at the very edge of the SMIRFS field it would only have a small effect (20% increase for a 1" object) on the typical image size of a star at the focal plane. It was therefore decided that it was not necessary to curve the SMIRFS field plates to correct for field curvature.

6.3.2 Microlenses

The technique of pupil imaging was chosen as the method of coupling the fibres at the input and output of the SMIRFS fibres. Figure 6.5 shows the path of the rays from the

focal plane of the telescope through the plano-convex $CaFl_2$ microlens on to the 200μm core of the fibre.

There are three sets of 3 rays, the central group of 3 rays represents the axial and extreme rays of the telescope beam (f/36.3) for an image centred on the microlens and the two other sets of rays come from the edge of a 2 arcsec diameter image. It can be seen that the f/36.3 rays of the telescope are parallel when they emanate from the microlens and are therefore effectively focused at infinity. Also the sets of parallel rays completely fill the core of the fibre effectively imaging the pupil of the telescope (the secondary mirror) on the fibre face. This is not the case with direct re-imaging in which the rays from the telescope are focused onto the fibre face by the microlens.

Note that the cone angle of the beam entering the fibre is dependent on the size of the image at the telescope focal plane and not on the focal ratio of the telescope beam. Therefore the speed of the beam entering the fibre is dependent on the pointing and seeing conditions. If one now turns the system around to represent the fibre output, it can be seen that the image size at the focal plane inside CGS4 will be dependent on the beam angle coming out of the fibre, which will be a combination of the beam angles that entered the fibre and any increase caused by FRD. Thus the image size and hence resolution of the spectrograph will be dependent upon the seeing conditions and the FRD in the fibre. However, any increase in the cone angle due to FRD will not effect the focal ratio of the beam at the focal plane inside CGS4, thus preserving the throughput.

It can be seen that with direct imaging coupling (figure 5.1), the field position at the focal plane affects the focal position of the ray on the fibre face. The centre of the image is focused at the centre of the fibre face and the edge of the image is focused at the edge of the fibre face. This means that the fibre has a well defined aperture on the sky. This is not the case with the pupil imaging where, ignoring aberration effects, the only things limiting the image size at the focal plane are the diameter of the microlens and the maximum acceptance angle of the fibre. Thus unless the field stop is employed the fibre aperture on the sky would be ~ 4 arcsecs (3mm x 1.525 arcsecs/mm) and the fibre cone would be ~ f/2.5 which nearly fills the numerical aperture of the fibre. Using a field stop is acceptable in J and H but in K the introduction of a "warm" field stop would increase

the thermal background from the instrument. The "cold" slit inside CGS4 can be employed to reduce the background from the sky in good seeing conditions as there are ~1.2, ~2.5 and 4.9 arcsec slit widths available.

6.3.3 The slit projection unit (SPU)

Figure 6.6 shows the optical layout of the slit projection unit. This consists of the fibre slit, spherical mirror (focal length = 203.2 mm) and a flat folding mirror. The fibres in the slit point to the infinite focus of the spherical mirror. After reflecting off the spherical mirror all the fibre axial rays are parallel but the f/36.3 beams from the fibre converge on a focus. The flat folding mirror allows the image to be projected into CGS4. Figure 6.7 shows the through focus spot diagram for point sources corresponding to the fibre positions in the slit. The top 2 rows correspond to fibres at the middle of the slit and the bottom 2 rows to fibres at either end of the slit. The spot size for the extremes of the slit is ~ 50μm in diameter. This is comparatively small; a typical 1 arcsec image measures ~ 660μm. Also with the intended CGS4 configuration using the 150mm camera, the effective pixel size at this point would be 800μm across; this would be halved using the 300mm camera. Therefore the spot size produced by the SPU was negligible compared to the likely image sizes and the size of the detector pixels.

6.4 Technical description of SMIRFS

Figure 6.8 shows the overall layout of the SMIRFS system on UKIRT. There are essentially three separate elements which are linked by fibre bundles. The first is the field plate unit (FPU) which attaches to the West port of the instrument support unit (ISU). The second is the guide fibre unit (GFU) that is linked to the FPU via the guide fibre bundle. This is fitted to a mounting plate alongside IRCAM at the North port of the ISU. Thirdly, there is the slit projection unit (SPU) linked to the FPU via the infrared fibre bundle. The SPU is mounted onto the front of CGS4 in place of the CGS4 calibration unit at the South port of the ISU. The dichroic is positioned to direct the light from the telescope to the West port and onto the SMIRFS field plate.

6.4.1 The field plate unit (FPU)

Figure 6.9 shows the design of the SMIRFS FPU. The FPU acts as a support for the fibres so they can be aligned at the telescope focus. It consist of a large tube with a

flange at the top and bottom. The base of the FPU is square and mounts directly onto the West port of the ISU with 4 large bolts. The tube acts as a stand off that enables the field plate to be positioned near the telescope nominal focus. It is in fact a little beyond the nominal focus (~ 9 mm) as the telescope focus is in front of the fibre microlenses. The inner ring is welded to the tube and the second ring can be rotated relative to the inner ring by adjusting the micrometer. This allows for rotational adjustment of the field plates so that the plate orientation matches that of the crosshead camera. The rotation can then be clamped by tightening the six inner ring bolts. The third ring acts as a holder for the field plate. The field plate is attached to this ring which is then fixed into the second ring by a dowel and six bolts. Also attached to the third ring is the plate tensioner. As long as the field plates match each other it is not necessary to adjust the plate rotation each time a plate is changed. The field plates consist of 1.2mm thick disks of admiralty brass with 7mm holes drilled in them corresponding to the positions of the target objects in the field. Each plate is marked on the outward face to indicate North as seen in the field. There is a small hole at the centre of the plate to attach the plate tensioner. The tensioner rod has a fine thread at the top and a knurled nut that can be tightened to distort the plate. Tensioning the field plate was necessary to ensure that the fibres at the edge of the field pointed correctly at the secondary mirror of the telescope (see section 6.2.5).

6.4.2 The slit projection unit (SPU)

Figure 6.10 shows the layout of the SMIRFS SPU. It was designed to fit in place of the CGS4 calibration unit and employs the same locating and fixing mechanism as the calibration unit. It attaches to CGS4, sliding between the ISU and the front of CGS4 on two locating rails. It is then held in place by four bolts. The gap between the ISU and CGS4 is quite narrow which accounts for the offset slit. It would have been much simpler to manufacture the slit blocks if they had not been angled towards the spherical mirror, but there would not have been room for the flat folding mirror mount. Numerous fibre slit and mirror layouts were considered but this seemed to be the most effective.

The fibre slit is snugly located in a carefully machined slot that allowed accurate re-location of the slit. It is held in place with bolts at either end. The fibre slit block was machined so that it points at an angle of ~ 3.6° towards the centre of the spherical

mirror. Both the spherical and flat mirrors are mounted on kinematic mounts that allow fully independent tip, tilt and linear translation. It is important to have this independent adjustment to allow accurate alignment of the fibre slit image with the CGS4 optics (see chapters 7 & 8). The tip, tilt and translation mechanism can be accessed by removable plates at either end of the SPU. All the adjusters have locking mechanisms to prevent the unit shifting as the telescope orientation changed.

There is a hole in the side of the SPU (not shown) opposite the flat folding mirror which allows the light to be projected through the CGS4 window. The unit was designed so that the height of the centre of the fibre slit and both mirrors corresponds with the centre of the slit inside CGS4. It is possible to adjust the height of the fibre slit image using the mirrors but only by a small amount. Also, the CGS4 slit is longer than the fibre slit so there was some margin of leeway here.

6.4.3 The guide fibre unit (GFU)

Figure 6.11 shows the layout of the guide fibre unit, which consists of a pair of 35mm camera lens which re-image the output face of the guide fibre bundle onto the UKIRT spare SCANCO camera. The unit is fully enclosed to prevent stray light damaging the SCANCO during setting up when the dome lights are on. The whole unit attaches to a mounting plate on the North port of the ISU by 4 bolts through the base plate.

The SCANCO is attached to the endplate of the GFU by 8 bolts which screw into the camera face. The camera bolts are only accessible when the 50 mm lens mount is removed from the GFU. It is therefore necessary to attach the camera before installing the camera lenses. The SCANCO is an intensified TV with an extended S20 photocathode. Figure 6.12 shows the typical quantum efficiency of a S20 photocathode, however further losses in the detector reduce the overall response of the camera by a further 50%. It was originally intended to use a CCD as the detector but there was not a spare camera available. These typically have much higher QE, peaking about 50% at 700nm and tailing off at about 1μm.

The first lens is a x 2 teleconverter which attaches to a Pentax 135mm f/1.8 lens, giving the lens pair an effective focal length of 270 mm. The third lens is a Pentax 50 mm f/1.2 lens. This combination gives a de-magnification of the guide fibre image of ~ 5.4 in an

effort to increase the light intensity on the detector. With the 600μm fibres this gives a fibre image size of ~ 110μm at the detector which matches the minimum resolution reasonably well. Both the lenses have their focusing rings clamped at infinity but can be moved on a keyway to focus the system. The first two lenses collimate the beam and the third focuses it on the detector.

The guide fibre bundle slides into a machined block at the front face of the GFU and is located and fixed with a dowel and 3 bolts. It is important to remember to switch off the SCANCO camera before removing the guide fibre bundle to prevent damage from stray light.

The guide fibre bundle is ~ 3m long and consists of 3 groups of 7 fibres each with a 600μm core size. Each group of 7 fibres constitutes a guide fibre. The arrangement at the input end can be seen in figure 6.11. It consists of 7 fibres in a closely packed array. This arrangement is repeated at the output (figure 6.11) but the fibres are separated so they can be individually resolved by the camera. The orientation of these 7 fibres is the same at both the input and output so the movement of a light source at the input is imitated at the output. The input of the each of the 3 guide fibres is fixed in a brass ferrule similar in design to the input ferrule of the target fibres. The guide fibres were designed to fit in the same holes in the field plate as the target fibres, however due to a manufacturing error the ferrules are 0.5mm larger in diameter than the target fibre ferrules. This means that some flexibility in the positioning of the guide fibres was lost but we hope to correct this for future use. The 3 guide fibres are also encased in an armoured flexible tube secured to the fibre output assembly at one end and to the FPU at the other. This provides support and protection for the fibres from stretching and bending forces. Chapter 7 contains a description of the guide fibre manufacture and assembly.

6.4.4 The infrared fibre bundles and fibre slits

Chapter 7 contains details on the assembly of the fibre bundles, only the details of the design are discussed here. Each of the 2 fibre bundles contained 14 fibres with microlenses at both ends of every fibre.

6.4.4.1 The fibre input

The design at the input of the fibres can be seen in figures 6.13 and 6.14. Figure 6.13 shows an assembled unit and figure 6.14 the discrete components of the microlens holder. The fibre ferrule fits snugly into the back of the microlens holder and can be slid in and out to allow for the focusing of the microlens onto the fibre. A small gap was designed between the two components which was filled with epoxy to fix the ferrule and the holder once the microlens was aligned. The whole assembly was made of brass as this material is easier to drill without runout.

The fibre ferrules, which are identical to those at the output slit, consist of three concentric holes. The smallest is designed to fit the stainless steel tube that terminates the fibre. The tolerance on the concentricity of this hole was very tight as it was important to ensure that the fibre axis was parallel to that of the ferrule. The hole size is different in each of the bundles as the steel tubes were a different size depending on the fibre material. The silica fibre tubes have an outer diameter of 0.81 mm and the ZrF_4 0.71 mm. The holes sizes specified were slightly undersize as conventional drills often drill slightly oversize and it was important to have a tight fit. Low runout D-drills were eventually used to produce these holes as there were problems with runout using conventional drills. The medium sized hole was designed to fit the PVC core of the protective furcation tube and the largest hole to fit the outer sleeving of the furcation tube. The steel tube protrudes ~ 2mm beyond the end of the ferrule so any glue seeping through from the microlens holder when aligning and fixing the microlens would tend to collect around the end of the ferrule and not on the face of the fibre.

The microlens holder consists of a tubular section at the back, then a flange, a small neck section with 4 holes drilled into it at right angles to each other, and then a threaded portion. The tubular section is designed to be a tight fit on the fibre ferrule in order to aid the alignment procedure (see chapter 7). It is important that the flange section is perpendicular to the fibre and microlens holder axis. The flange keys up against the back of the field plate and as such determines the fibre pointing. The neck section has two functions. The 4 holes allow access to the microlens for alignment during the manufacture of the fibre bundles but the neck itself allows accurate location in the field plate holes. Along with the microlens alignment and field plate drilling accuracy, this

determines the final positional accuracy of the fibres in the field. To provide a suitable face for the microlens alignment holes, the neck is thicker than the brass plate so a washer fits between the field plate and the retaining nut to allow the holder to be securely clamped in place. The threaded portion is for the retaining nut at the optional field stop. The field stop can be screwed onto the holder to reduce the contribution from the sky in good seeing conditions. The 1.4mm hole corresponds to a stop of ~ 2.1 arcsecs in diameter. Note that the telescope focal plane is at the end of the microlens holder not at the field plate. The hole in the front of the holder is 3.2mm in diameter to allow for a small adjustment of the 3mm diameter microlens. Due to de-magnification effects the ±100μm available movement was sufficient since a movement of 10μm corresponds to moving the secondary mirror by ~ 15mm. The holes were finished off with an end mill to provide a flat seat for the microlens.

The minimum separation of the fibres in the field is set by the retaining nut. This is fractionally under 12mm across, which set a minimum fibre to fibre separation of 18.3 arcsecs.

6.4.4.2 The fibre slit

Figure 6.15 shows the fibre slit block. This fits into the end of the slit projection unit (see figure 6.10) and the image of the slit is then projected into CGS4. The 14 fibres in the bundle fit into the back of the block and the 14 microlenses are fixed to the front of the block. The fibres and microlenses are arranged so that the axial rays from each are directed at a point corresponding to the infinite focus of the spherical mirror in the SPU. This ensures that the fibre axial rays emanating from the spherical mirror are parallel (see section 6.3.3). Due to the confined space available for the SPU it was also necessary to angle the fibre slit at 3.57° so that the flat folding mirror could be included. Each of the fibres was separated so that there was no overlap in the fibre spectra on the CGS4 detector, yet the end fibres were not vignetted by the CGS4 slit (see section 6.2.7).

The fibre slit was made from a solid block of brass. The outside was carefully machined to be located snugly in the slot in the SPU where it is fixed by two bolts. The fibre ferrule holes were drilled to a high angular and size tolerance as both have a significant effect on the pointing accuracy and as a consequence the throughput of the system.

Small errors could be compensated for during the alignment of the microlenses. The fibre output ferrules are identical to the input fibre ferrules describe in the previous section (6.4.4.1), and fit into the holes at the back of the slit. The ferrules can be moved in and out to adjust the focus of the microlenses. The microlenses are positioned in counterbored recesses in the front of the slit. The recesses are oversize to allow movement of the microlens for alignment and are finished with an end mill to provide a flat seat for the microlenses. The radius of the curve at the front of the slit block matches the angle of the fibre pointing. This effects an improvement in image quality of the slit compensating to a great extent for the spherical aberrations of the spherical mirror even though it is not the ideal radius. It was a compromise that provided reasonable image quality with simple manufacturing of the slit block and was much better than using a flat slit.

6.5 Summary

SMIRFS is a infrared multi-fibre feed designed to couple UKIRT with the CGS4 spectrograph and work in the J, H and K bands. Two different fibre materials were used, silica for the J and H band bundle and zirconium fluoride for the K band bundle. Each bundle contains 14 fibres. To efficiently couple the f/36.3 telescope beam to that required by CGS4 (also f/36.3), it was necessary to use microlenses at the input and output of the each of the fibres. The input microlens converted the telescope beam from f/36.3 to approximately f/5 at the fibre input, for efficient propagation with relatively little FRD, and a second microlens was used at the fibre output converting the beam back to f/36.3 matching the requirements of the spectrograph. The technique of pupil imaging was used for these microlenses as it provides a well defined output focal ratio that does not degrade as the result of FRD.

Accurate pointing of the fibres is very important and the field plates were curved to ensure the fibres correctly viewed the telescope pupil. Access to the spectrograph's nominal focal plane was not possible, so an optical projection system was necessary. This imaged the fibre slit inside CGS4. Considerable effort ensured that as little "warm" material as possible was viewed by the spectrograph in order to minimise the thermal background in the K band. Some of the "warm" material of SMIRFS would be masked

out by the "cool" slit within CGS4 but the material that lay in between fibres remained visible. As SMIRFS was a development system little effort was made to reduce reflection losses in the system. These losses were estimated at ~ 22%. A guide fibre system was developed to utilise the small amount of visible light that was reflected onto the SMIRFS field plate by the infrared dichroic. This enabled accurate alignment of the field plates with the astronomical fields.

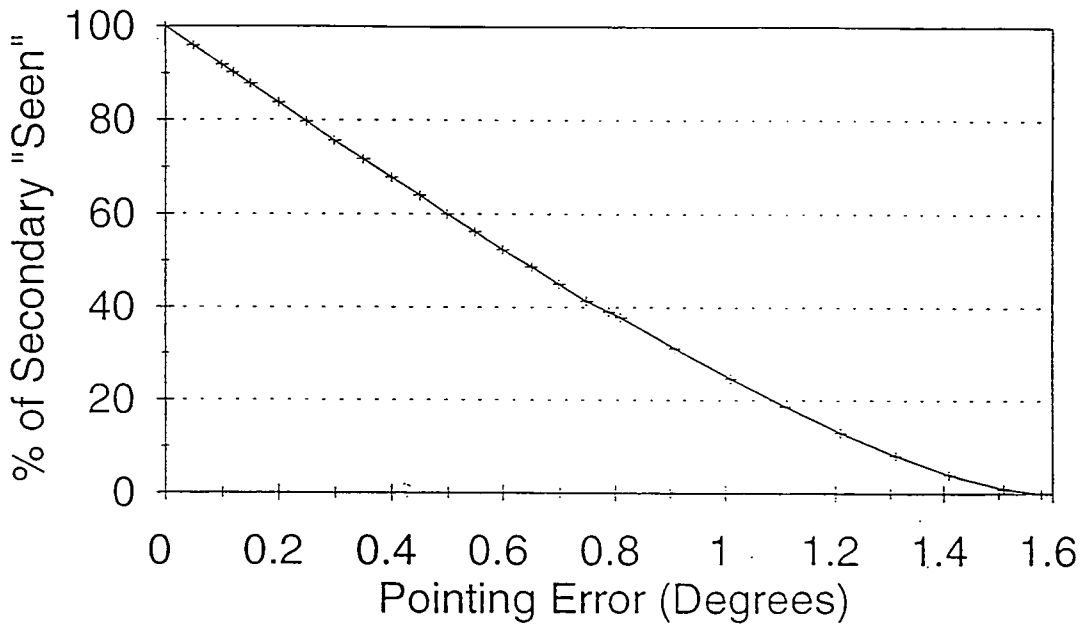

Figure 6.1 The effects of angular pointing on the amount of secondary mirror light viewed by the SMIRFS fibres. This assumes that the area viewed by fibres is exactly the same size as the secondary mirror of UKIRT.

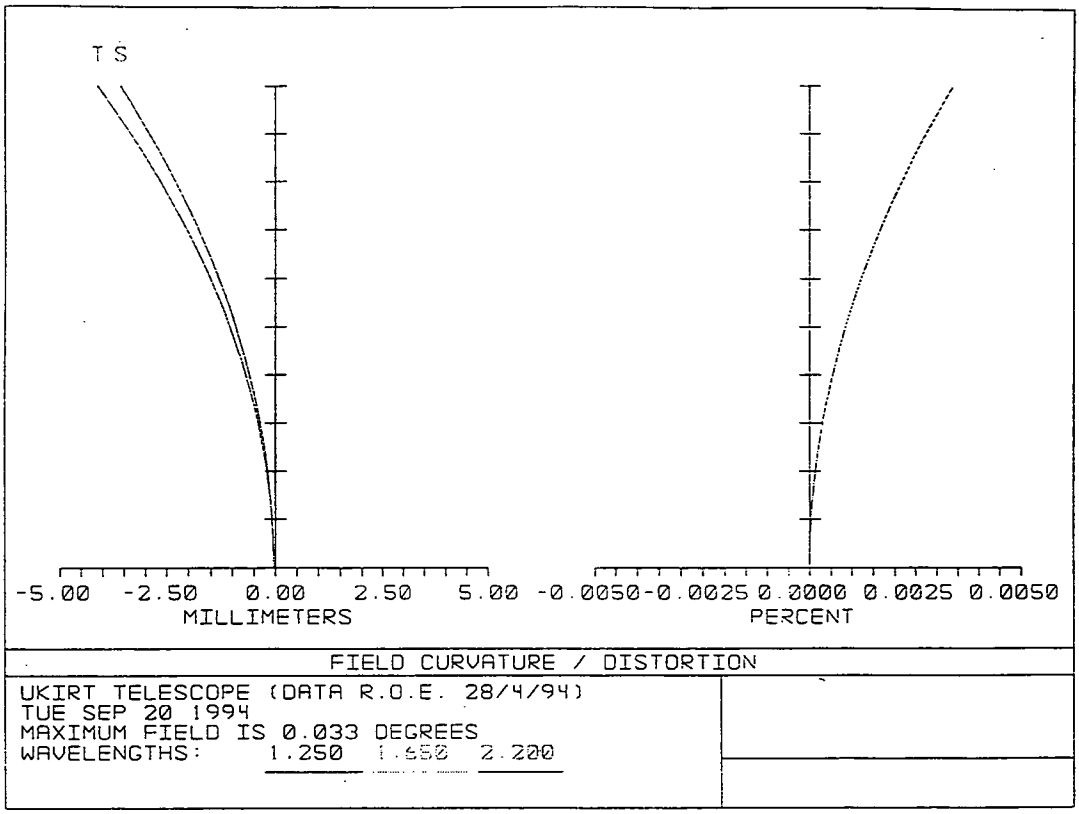

Figure 6.2 The field curvature and distortion at the focal plane of UKIRT with the f/36.3 secondary mirror. The field size was 4 arcmins across. The plot on the left shows the tangential (T) and Sagittal (S) component of the field curvature from the centre to the edge of the field (2 arcmins). The plot on the right shows the percentage distortion of the field. The distortion is positive indicating pincushion distortion. The vertical scales in both plots have 0.2 arcmin divisions.

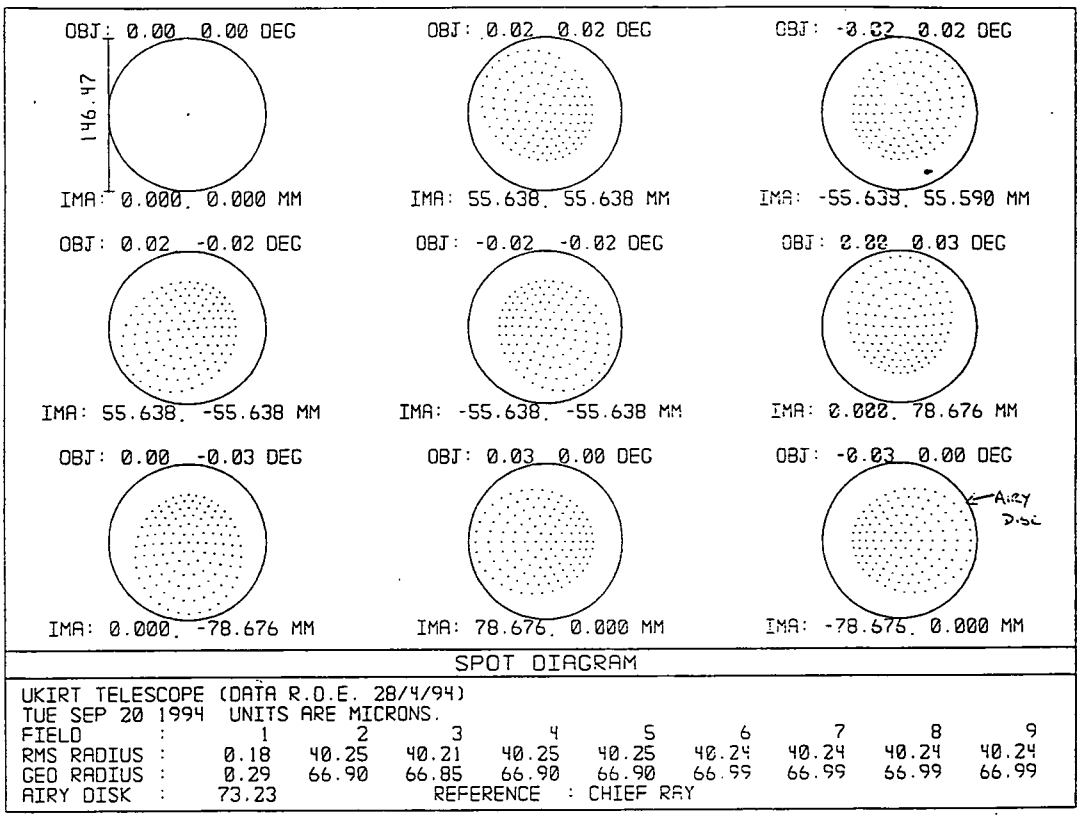

Figure 6.3 Spot diagrams showing the effects of field curvature at the focal plane of UKIRT (f/36.3 secondary mirror). The images of the point source are projected onto a flat plane with the optimum focus at the centre of the field. Moving from left to right and then top to bottom; the first diagram corresponds to the centre of the field, the next four diagrams to positions 1.4 arcmins from the centre, and the last four diagrams to positions 2 arcmins from the centre. The geometrical and rms radius of the images and the size of the Airy disc are given, in microns, at the bottom.

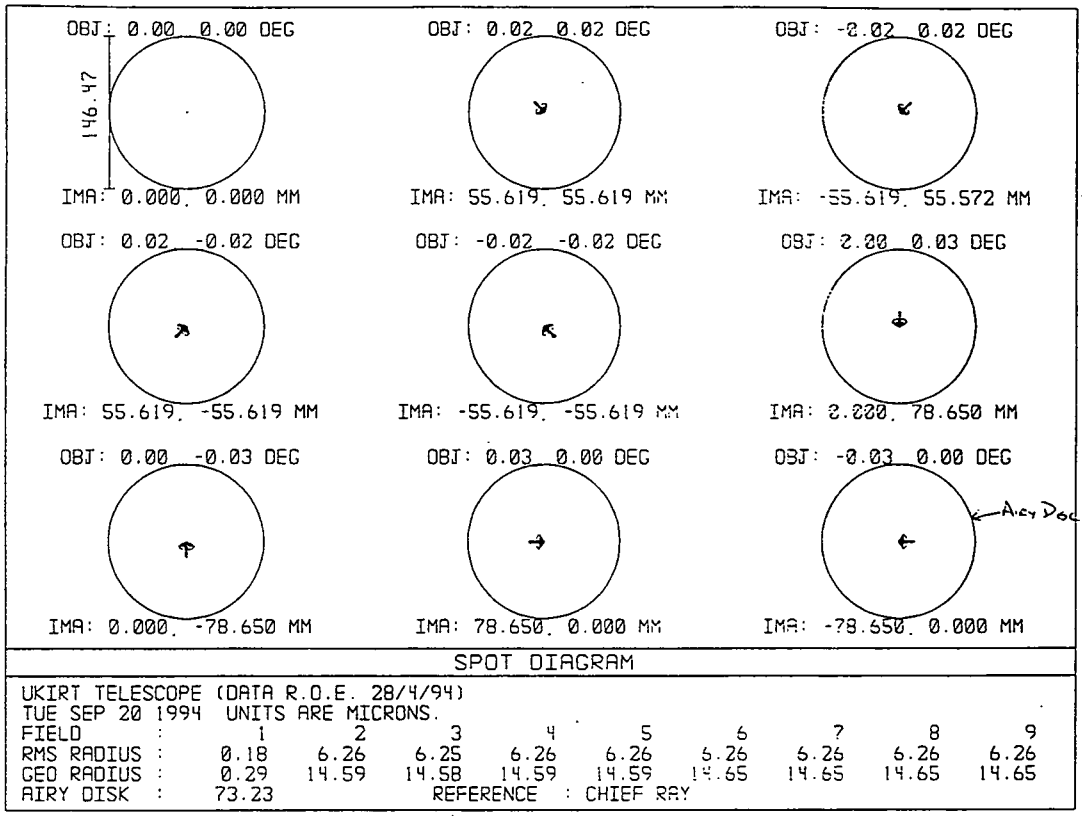

Figure 6.4 Spot diagrams showing the effects of field curvature at the focal plane of UKIRT (f/36.3 secondary mirror). This differs from figure 6.3 in that the images are projected onto a plane that is curved with a radius of 814.5mm. Moving from left to right and then top to bottom; the first diagram corresponds to the centre of the field, the next four diagrams to positions 1.4 arcmins from the centre, and the last four diagrams to positions 2 arcmins from the centre. The geometrical and rms radius of the images and the size of the Airy disc are given, in microns, at the bottom.

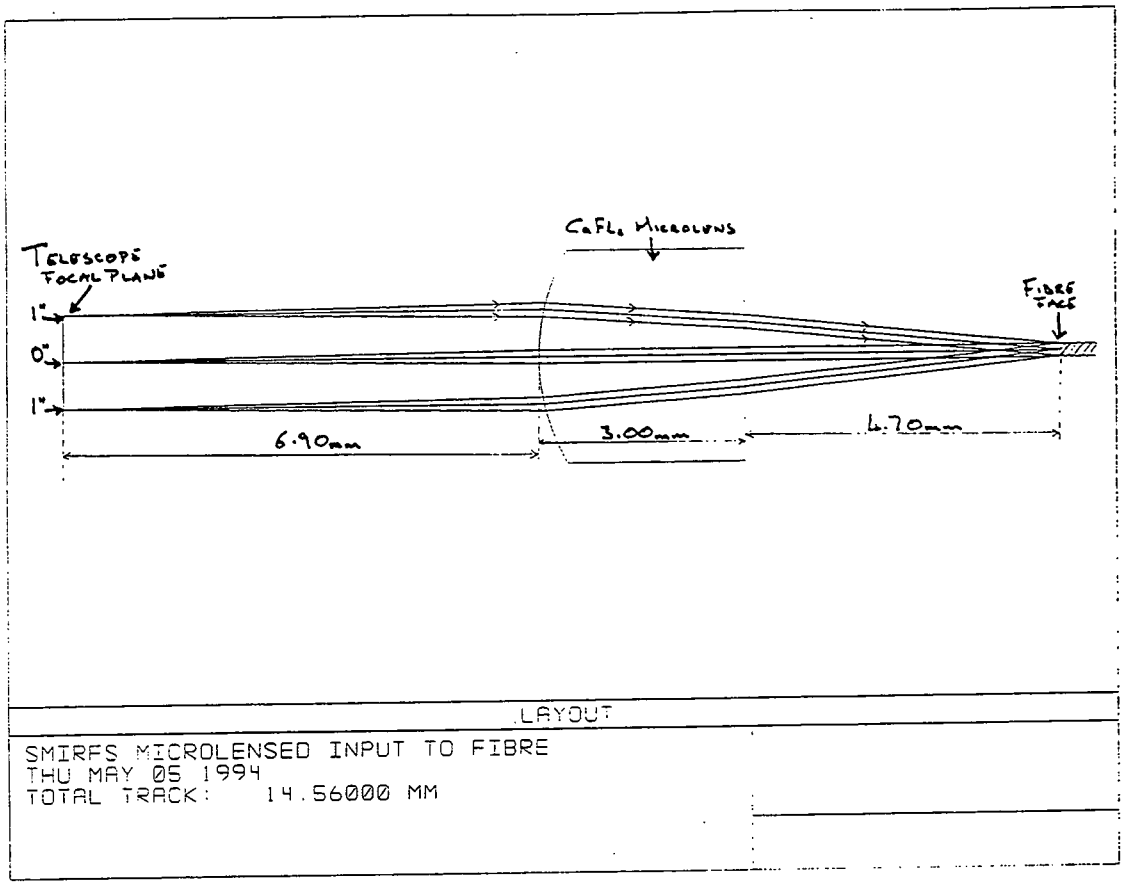

Figure 6.5 A ray trace of the pupil imaging used at the input of the SMIRFS fibre bundles. The rays correspond to central and extreme ray of an image which is 2 arcseconds (1.31mm) across at the telescope focal plane. The fibre core is 200±1μm in diameter. The radius of curvature of the front face of the microlens is 3.00mm. The distances have been chosen to minimise the size of the image at fibre face. The system is optimised for a wavelength of 2.2μm.

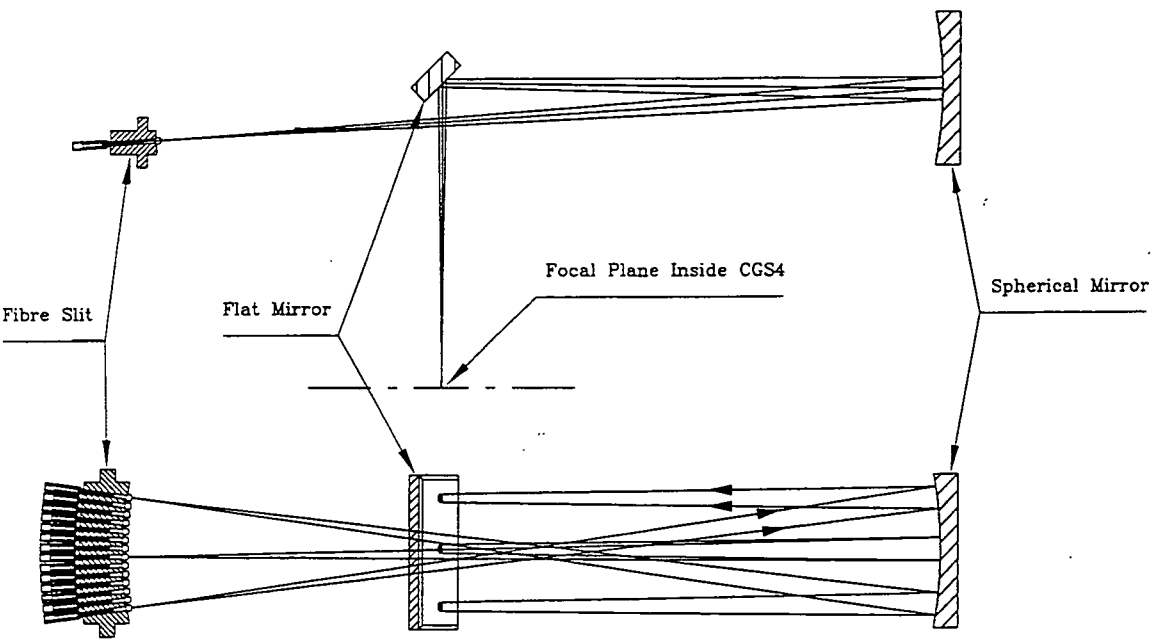

Figure 6.6 The optical layout of the slit projection unit (SPU). The top figure shows the plan view of the SPU. The bottom figure shows the side view, as seen from the focal plane of CGS4. For simplicity only three sets of rays are shown.

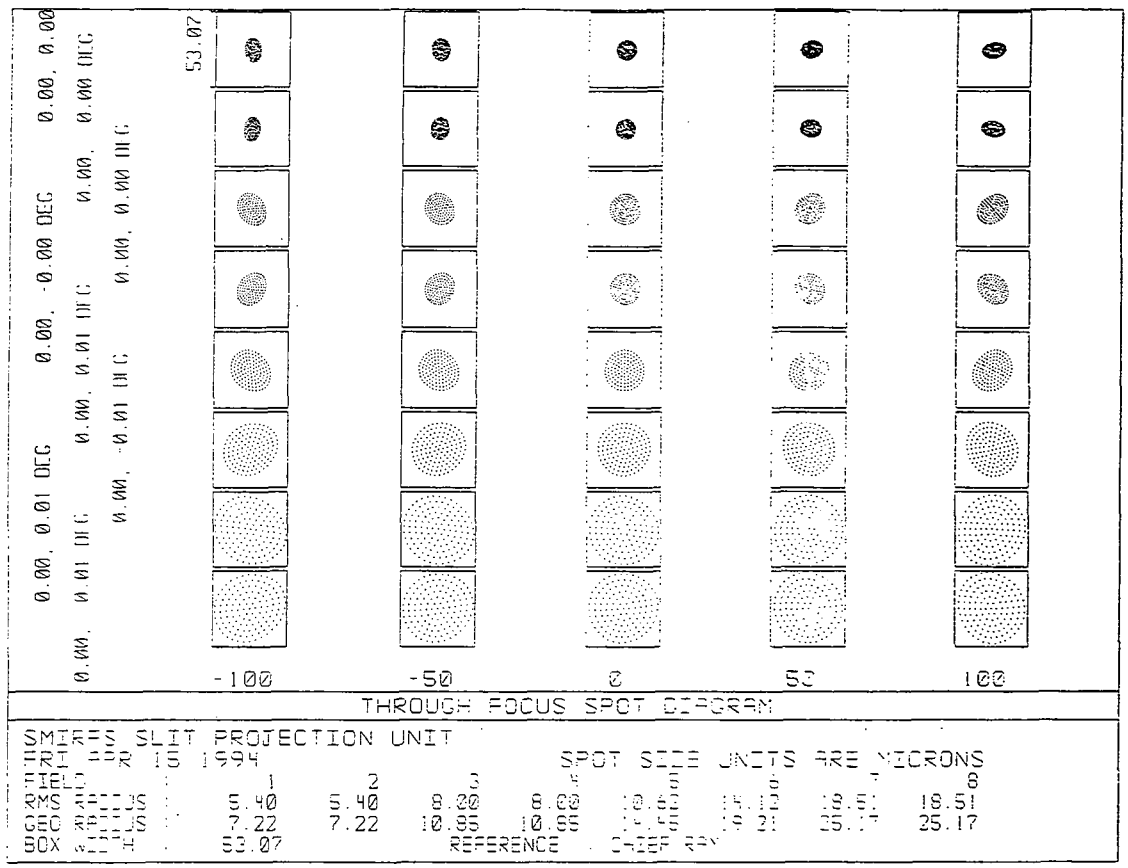

Figure 6.7 The through focus spot diagram for the slit projection unit (SPU). It shows the image sizes at the focal plane of CGS4, assuming the fibres to be point sources, and demonstrates the aberrations in the system. From left to right the focal position moves from -100μm, through the optimum focus, to +100μm. From top to bottom they are grouped into pairs. Each pair is an equal distance from the centre of the fibre slit. The pairs from the top are positioned at ± 3.1", ± 15.5", ± 27.9" and ±34.1".

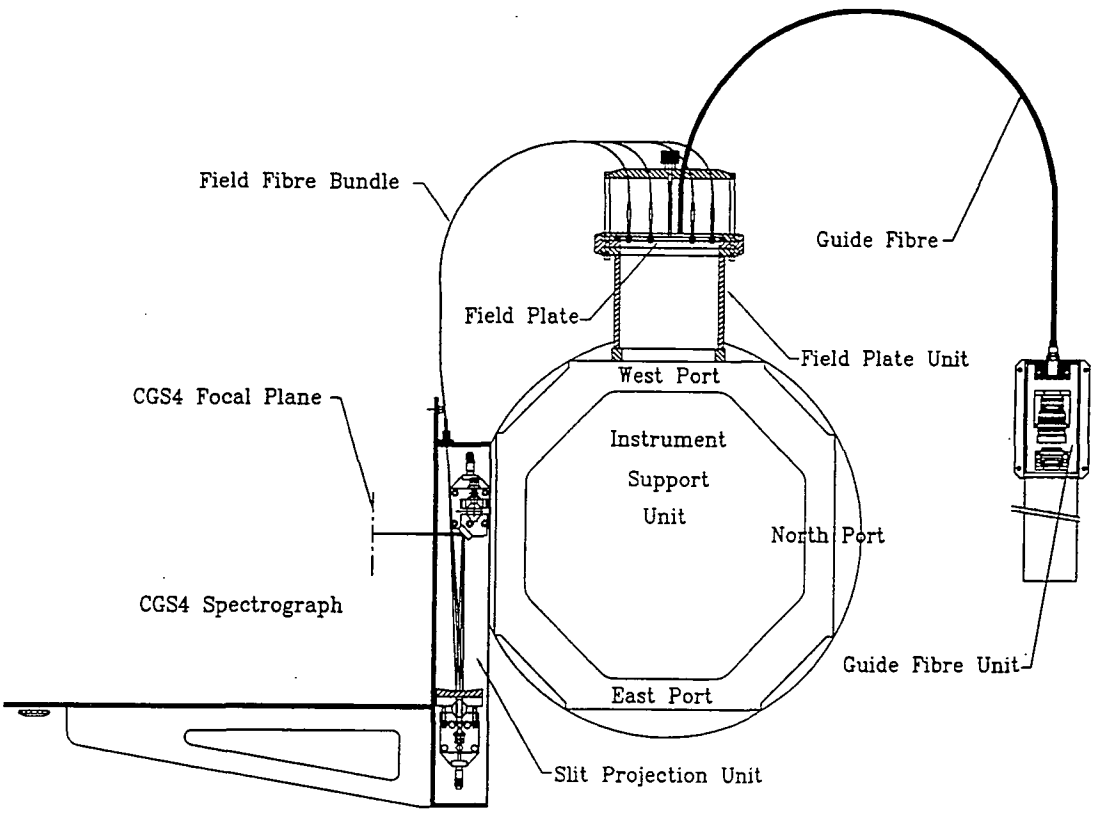

Figure 6.8 A plan view SMIRFS showing the layout around the instrument support unit (ISU) of UKIRT. The guide fibre unit attaches to the optical table for IRCAM (not shown) at the North port of the ISU.

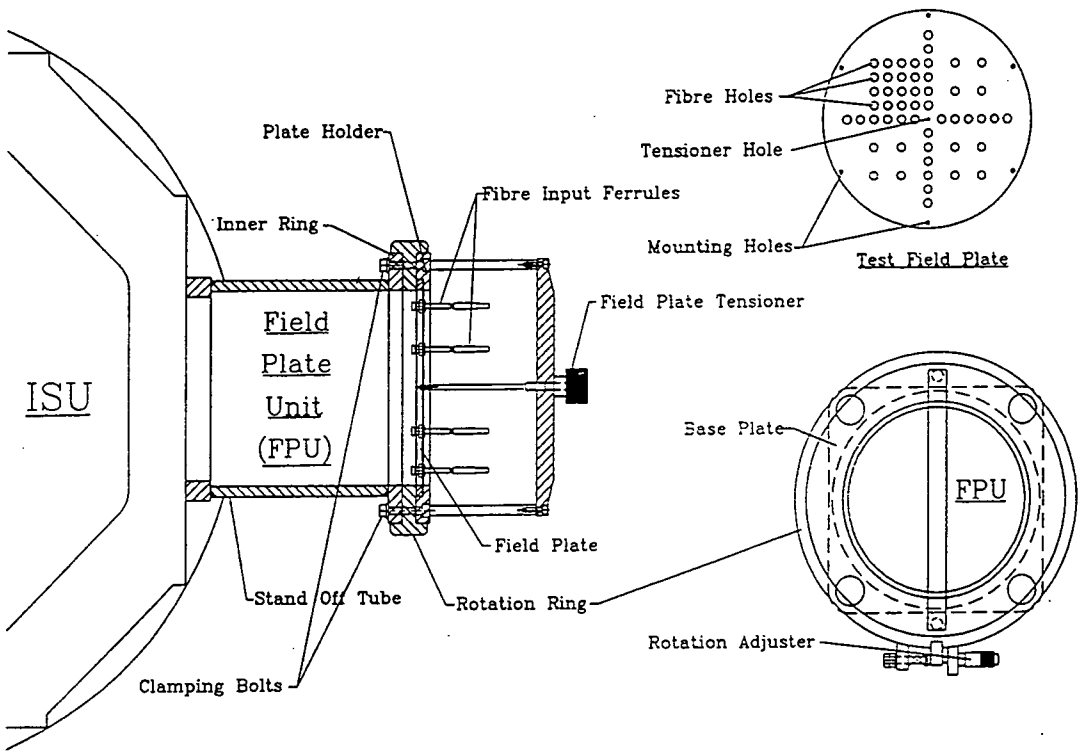

Figure 6.9 The layout of the field plate unit (FPU) shown in plan view (left) and end on looking toward the West port of the ISU (bottom right). One of the test field plates is shown in the top right corner.

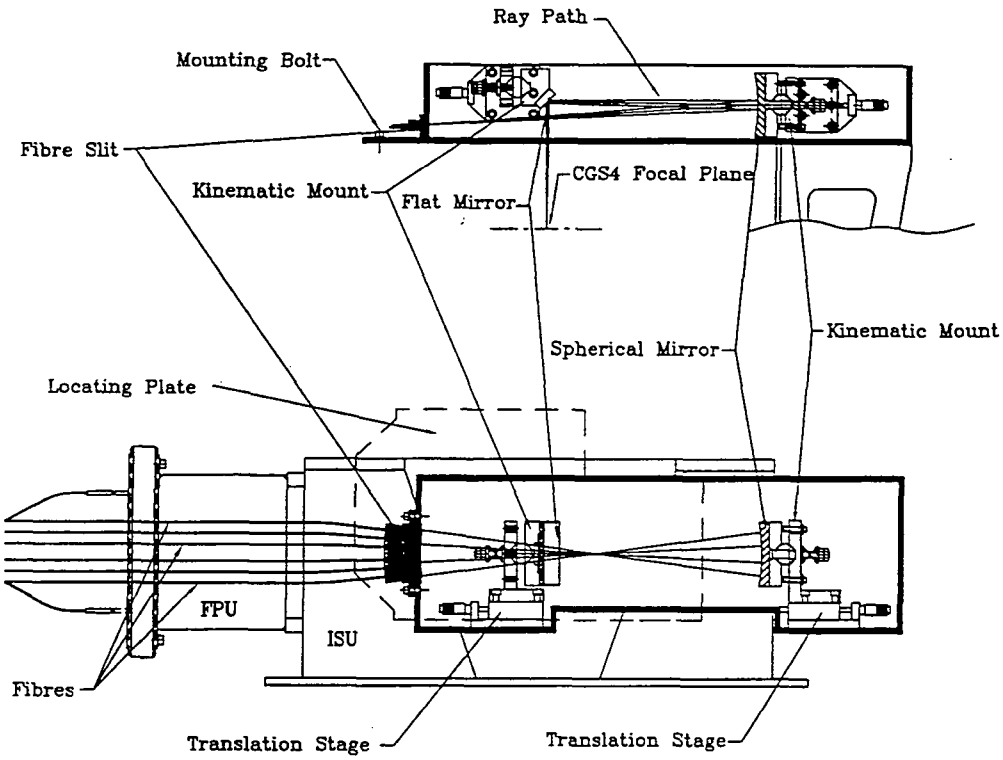

Figure 6.10 The layout of the slit projection unit (SPU). The top diagram shows a plan view of the SPU. The bottom diagram shows a side perspective as viewed from CGS4 at the South port of the instrument support unit.

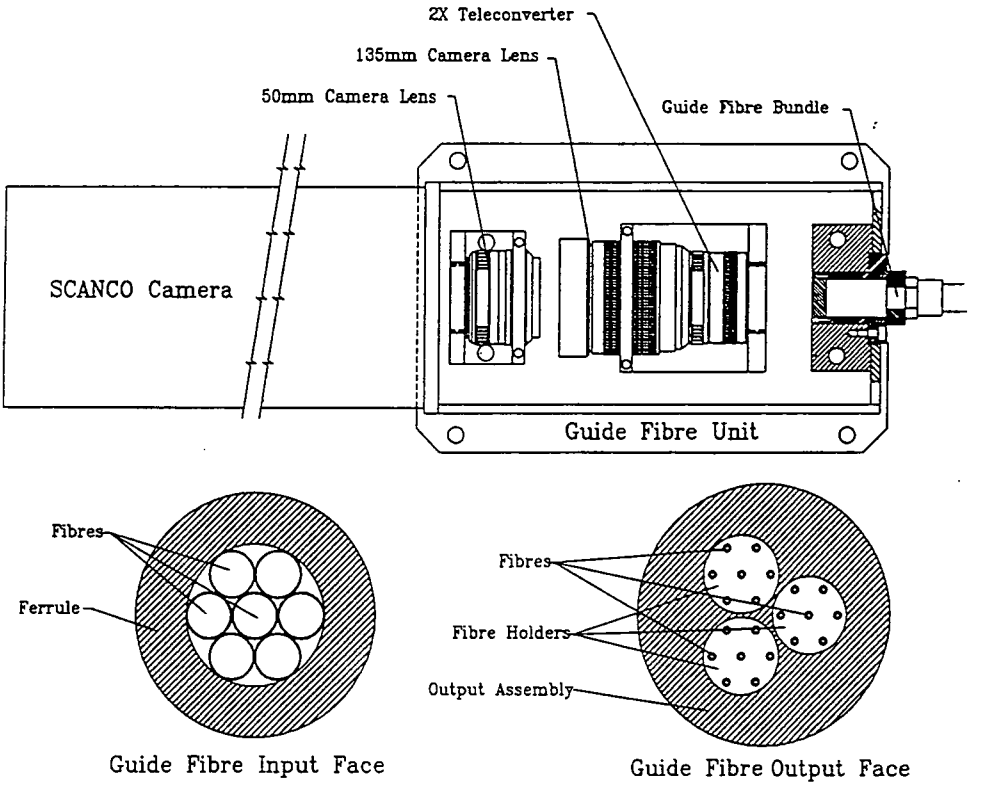

Figure 6.11 The layout of the guide fibre unit (GFU). The top diagram shows a plan view of the GFU with the output end of the guide fibre bundle protruding from the right and the SCANCO camera attached on the left. The diagram at the bottom left shows the arrangement of the individual fibres at the input of a guide fibre. The diagram at the bottom right shows the arrangement of the all fibres at the output end of the guide fibre bundle. Each group of seven fibres correspond to one guide fibre.

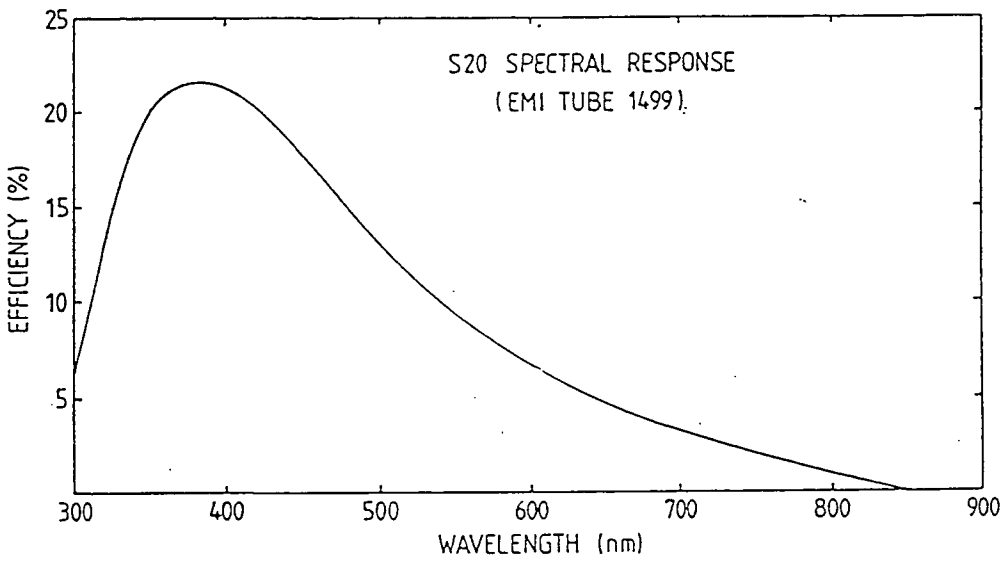

Figure 6.12 A plot of the photocathode efficiency of S20 versus wavelength. This material was used for the photocathode of the SCANCO camera.

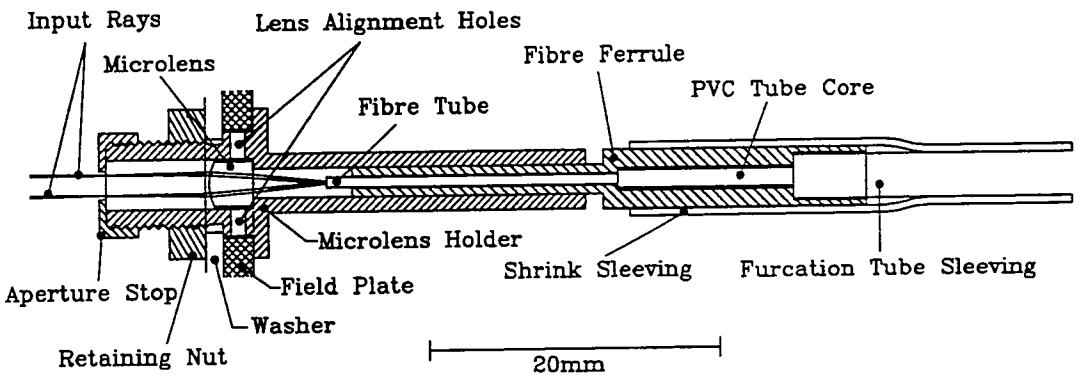

Figure 6.13 The layout of the input assembly for the SMIRFS fibres including the extreme rays from 2 arcsec image. The back of the aperture stop corresponds to the focal plane of the telescope.

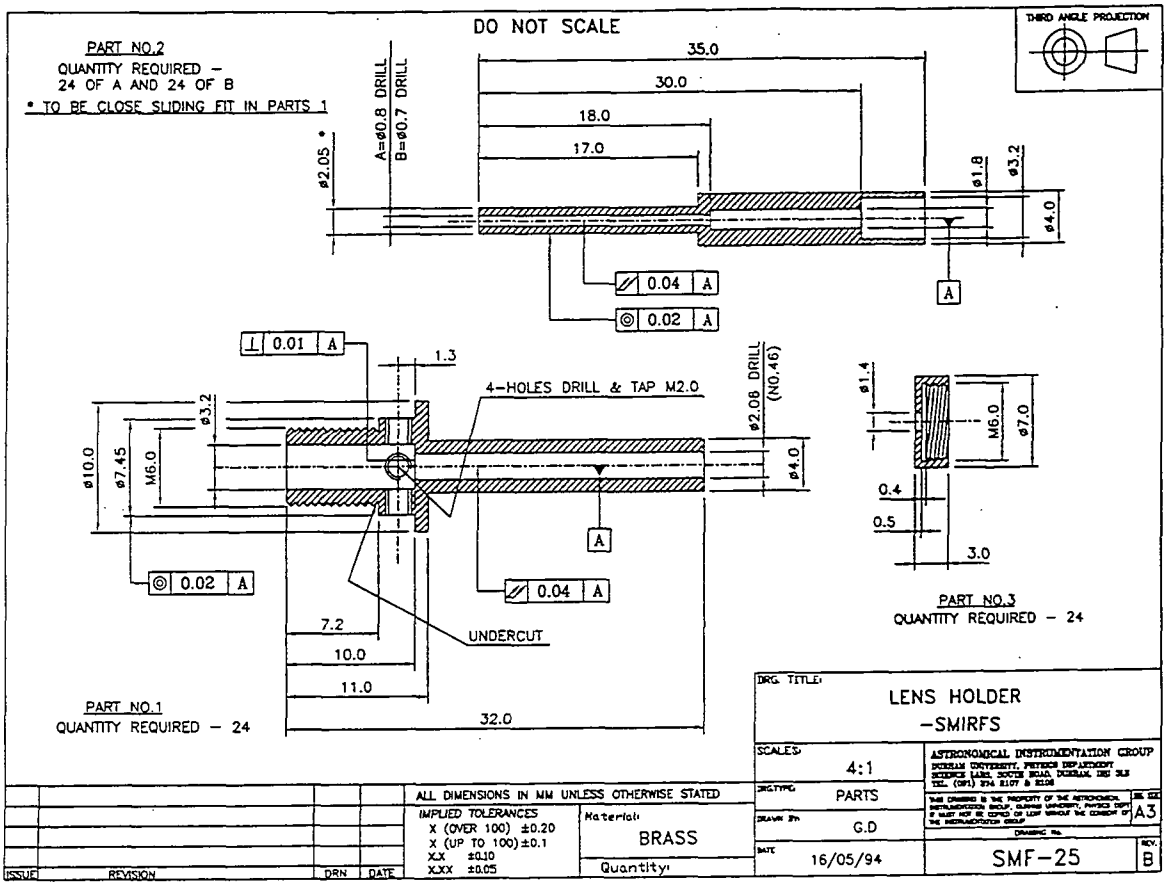

Figure 6.14 The dimensions and manufacturing tolerances of the microlens holders, fibre ferrules and the aperture stops for the SMIRFS fibres.

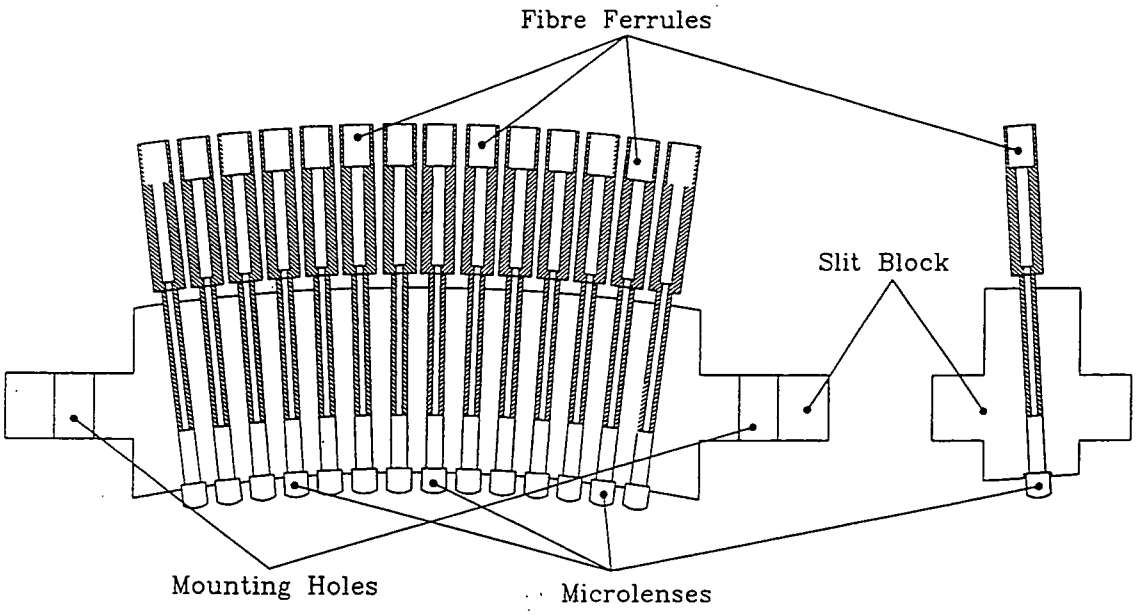

Figure 6.15 The layout of the SMIRFS fibre slit block viewed from the side and the edge. For simplicity the fibres are not shown.

Chapter 7: Manufacture and testing of SMIRFS

7.1 Introduction

The chapter contains details about the preparation of the SMIRFS fibre bundles, fibre polishing and alignment of the microlenses. Results from fibre throughput and FRD measurement of the fibres are presented. Also alignment procedures for the slit projection unit are discussed. All of these features can have a significant effect on the throughput of the whole system and therefore require careful attention.

7.2 The SMIRFS fibre bundles

As the whole project revolves around the performance of the fibre bundles, considerable attention and effort was spend in their preparation and assembly, from the selection of the fibre material right through to their packaging for transportation. The decision to manufacture two fibre bundles, one using a Ultra low OH silica fibre from Polymicro Technologies and the other zirconium fluoride fibre from Le Verre Fluore has been discussed previously in chapter 6. The following section contains a detailed description of how the fibres bundles were prepared.

7.2.1 Pre-polish preparation

Both fibre materials were supplied as single lengths, so it was necessary to cut them to the appropriate size. Great care was taken when handling the bare fibres particularly the ZrF_4 as it very susceptible to breakage, far more so than silica. The fibre was laid out on a bench, then cleaved into 1.2m lengths using a scalpel on a hard surface such as glass. A small amount of pressure with a sharp scalpel blade was sufficient to cleave the ZrF_4 fibre, however with the silica fibre it was sometimes necessary to bend the fibre after scouring the surface with the scalpel, much as one cuts panes of glass. If too much pressure is applied with the scalpel the fibre ends tend to shatter or crumble instead of producing a "clean" break. A sharp scalpel blade reduces the risk of the fibre crumbling and the hard glass surface lowers the probability of the fibre shattering. Commercial cutters are available for cleaving fibres, however we achieved reasonable results using a scalpel without the added expense of a cleaving tool. Good fibre cleaving was not

important in this application as we polished the fibre faces to achieve good flatness and surface finish at a later stage.

When polishing fibres that have a polyacrylate buffer material, it is often recommended that the buffer should be removed before the fibre is polished. This can be done by soaking the fibre tip in either a methylene chloride solution or acetone until the buffer becomes soft enough to remove. It is best to remove the buffer with something fairly soft such as your finger nails, so as to reduce the risk of damaging the fibre cladding. Failure to do so can cause round off of the fibre face as a result of the fibre flexing within this soft coating material during polishing. However, it was not found to be necessary to remove the polyacrylate buffer from the ZrF_4 fibres. This was because of the polishing technique employed and, more importantly, the fact that ZrF_4 is a softer material than fused silica, which is more frequently used.

The silica fibre used for SMIRFS had a polyimide buffer coating. This is a much harder, thinner material than polyacrylate and therefore does not require removal before polishing. It is also far more chemically resilient and therefore much hard to remove anyway.

After cutting the fibres to the right length, the fibres were inserted into a protective sleeving. This consisted of a hollow PVC core surrounded by a layer of re-enforcing Kevlar strands all encased in a thin PVC jacket. This provided good protection against nipping, stretching and sharp bending, however it was flexible enough to allow the fibres to be routed from the slit projection unit to the telescope focal plane. The lengths of fibre were terminated at both ends with a 30 mm length of stainless steel hypodermic tubing, 25 & 21 gauge for the silica fibres and 22 gauge for the ZrF_4 fibres. The second steel tube was required for the silica fibres to increase the outside diameter to a suitable size for the brass ferrules that eventually terminated the fibres. The steel tubes were fixed to the fibre with Araldite epoxy resin. The minimum amount of this relatively low expansion epoxy was used to reduce stress induce FRD. In my experience the inherent FRD, for most short lengths of fibre (1 or 2 meters), is small compared to FRD induced by localised stressing. The most common cause of this local stressing is the epoxy used to fix the steel tubes. Any excess or lumps of epoxy on the fibre can significantly

increase the FRD. Also, the slow curing time of the epoxy permits manipulation of the tubes before the adhesive becomes unworkable.

The Araldite epoxy for the steel tubes was left to cure for at least 24 hours after which the brass ferrules were epoxied in place. RS quick setting epoxy was used for the brass ferrules as it was thinner than the Araldite making it easier to slide the ferrules over the steel tubes and protective sleeving. Identical brass ferrules were fixed to both the input and output ends of the each of the fibres. This rigidly fixed the protective sleeving to the steel tubes, thus enclosing the fibres in a protective sheath that significantly reduced the risk of fibre damage during handling.

Once the fibres had been polished, adhesive shrink sleeving was used to further strengthen the area where the protective sleeving meets the brass ferrule at the input end of the fibres. This was added as protection against the extra mechanical stresses induced by the plugging and unplugging of the fibres from the field plate.

Considerable problems were encountered during the manufacturing of the brass fibre ferrules in producing the 0.81 mm and 0.71 mm holes to fit the steel tubes. These were both small in diameter and about 20 diameters in length. They proved to be very difficult to produce without runout. After attempting various conventional drilling techniques a satisfactory result was eventually achieved using a very high speed drilling machine and low runout D drills. Two other methods were suggested, spark erosion and a drilling technique that employs a specialised drilling head. This is a bit like drilling with a lathe. The piece to be drilled is mounted in the drilling head which rotates at very high speed ~10,000 revolutions per minute and the drill is centred and fixed in place. It differs from lathe drilling in that the piece is moved towards the drill as opposed to the drill moving towards the piece. These are both relatively specialised techniques which are more expensive than the conventional techniques and were beyond our relatively small budget. However, both these techniques are said to produce small diameter holes with very little runout. The design and tolerances of the brass ferrules are shown in figure 6.14.

7.2.2 Fibre polishing

The relative merits of the different fibre polishing techniques has been discussed previously (See chapter 4). The technique used for all the SMIRFS fibres, including the

guide fibres, was dry polishing using 3M aluminium oxide polishing papers. The fibres were loaded in the polishing jig which could be used to simultaneously polish both ends of up to four fibres at any one time. The pressure that the fibres exerted on the polishing medium could be varied by means an adjusting screw and loading spring. The design of the polishing jig is detailed in chapter 4 (see figure 4.2).

The polishing apparatus can be seen in figure 7.1. This photograph shows the polishing cloths at the front of the bench with the polishing jig on the interferometer which was used to check the surface flatness and finish quality. The polishing jig contains only one fibre in this picture which can be distinguished by its orange protective sleeving. The image on the monitor shows the face of the fibre. The fibre is the light grey area in the middle, the slightly dark area surrounding that is the epoxy and the surrounding bright material is the stainless steel hypodermic tubing. In this case there are two concentric tubes as the fibre material is silica.

The polishing papers were taped down onto ~ 6 mm thick plate glass providing a cheap, flat, blemish free surface. These had to be keep scrupulously clean as any dirt underneath or on top of the polishing papers was likely to cause scratches on the fibre face. One advantage of polishing by hand was that if the polishing paper surface became damaged it could be felt in the way the polishing jig moved, thus it was possible to reduce the amount of scratching that occurred. These damaged areas of the paper would then be avoided though it was important to remove any debris from both the polishing paper and the jig. The finer papers (1μm and 3μm) were particularly prone to surface tearing and had to be replaced regularly.

Figure 7.2 shows the interferograms from the face of one of the silica fibres, that made up the SMIRFS bundle, at various stages during the polishing process. Figure 7.3 shows the interferograms from one of the ZrF_4 fibres. The last picture is a straight-forward image without interference fringes to give a clearer idea of surface finish. It can be seen that as the polishing progressed the surface quality of both the silica and the ZrF_4 fibres improved. However, the silica fibres did exhibit a small amount of rounding off after the 1μm paper had been used. Table 7.1 lists the typical polishing times for the different grades of paper. At each stage the fibres and jig were meticulously cleaned, using cotton

wool buds and alcohol, to ensure that polishing material from the previous courser grade paper did not contaminate the next polishing paper.

Grade of Polishing paper	Silica fibres	ZrF_4 fibres
1000 grit Emery	5 minutes	5 minutes
9μm AlO_2	1 minute	1 minute
5μm AlO_2	45 seconds	45 seconds
3μm AlO_2	1 minute	1 minute
1μm AlO_2	4 minutes	2 minutes

Table 7.1 Typical polishing time for SMIRFS fibres.

First, the fibres were flattened and any chips in the fibre face removed using a 1000 grit emery paper. Then, at each stage, the fibre faces were inspected for both surface blemishes and flatness using an interferometer. It was not always apparent that the surface unevenness had been removed as the fibre image after the 1000 grit had been used was quite dark. If at a later stage it became apparent that the fibre face was chipped or pitted it was advisable to start the polishing again with the 1000 grit emery paper as removing the imperfection with a fine paper took a considerable amount of time.

Following the emery paper a 9μm AlO_2 paper was employed for about 1 minute. It was important to keep a slow fluid circular motion going with the polishing jig otherwise the fibre face could become chipped as the fibres snagged and vibrated across the paper surface. Also, it improved the surface finish if the jig was gently rotated while maintaining the fluid circular polishing motion. The surface of the fibre at this stage was still fairly dark, however the steel tubing had gained a fairly bright though still heavy scratched quality to it. It was, at this stage, usually possible to get a clear interference pattern on the fibre surface which could be used to properly assess the surface flatness. The fibres were then briefly polished with the 5μm and 3μm AlO_2 papers, the finish improving each time. Finally the polishing was finished off using a 1μm AlO_2 paper. The fibres at this stage were very carefully inspected for surface dullness and imperfections. It was also important that the surface should be reasonably flat as rounding off would

introduce FRD effects into the fibre system. This was not found to be a problem with the ZrF_4 fibres but with the harder silica fibres a small amount of rounding off was difficult to avoid. This became worse if the fibres were polished for too long using the 1μm paper. If the rounding off was serious, it was necessary to start the whole polishing process from scratch with the 1000 grit emery paper. A 0.3μm AlO_2 paper was experimented with but this only compounded the rounding off problem. The 0.3μm paper was also prone to surface tearing which led to scratching of the fibre face.

7.2.3 Fibre throughput measurements

The method of measuring fibre throughput has been detailed previously in chapter 4. Table 7.2 contains the throughput results for the non-microlensed fibres after polishing was completed. The throughput experiment was performed at a wavelength ~ 0.9 ± 0.1 μm, using a silicon diode detector.

Fibre Number	Throughput ±4%	Fibre Number	Throughput ±4%
Si1	92%	**ZF1**	87%
Si2	92%	**ZF2**	86%
Si3	92%	**ZF3**	87%
Si4	92%	**ZF4**	87%
Si5	93%	**ZF5**	86%
Si6	93%	**ZF6**	86%
Si7	93%	**ZF7**	86%
Si8	93%	**ZF8**	86%
Si9	93%	**ZF9**	86%
Si10	92%	**ZF10**	86%
Si11	92%	**ZF11**	86%
Si12	93%	**ZF12**	86%
Si13	92%	**ZF13**	87%
Si14	92%	**ZF14**	86%
Mean	92.4%	**Mean**	86.3%

Table 7.2 The throughput for the SMIRFS fibres after polishing (without microlenses).

The uncertainty in throughput was estimated from a combination of the measurement fluctuations that occurred as one changed the rotational orientation of the fibre face and the detector alignment which was very sensitive to positioning. The detector had to be moved for each measurement so the throughput of each fibre could be referenced to a pin hole of the same diameter. Sources of throughput losses include surface reflections from the air-glass boundaries, attenuation by the fibre material and scattering from a poorly finished surface. The silica fibres have a transmission that is better than 99% at these wavelengths and reflection losses of ~ 3.5% (refractive index ~ 1.43) per surface giving a theoretical throughput of ~93%. The ZrF_4 attenuation losses of ~ 8% and the reflection losses ~ 4% (refractive index ~ 1.52) per surface give a theoretical throughput of ~ 84%. The figures for the silica fibres were very close to the expected results. The ZrF_4 results are a little better than predicted but they agree within the uncertainty. Also, the transmission losses for the ZrF_4 might be less than quoted by the manufacture for a typical length of ZrF_4 fibre. In any case, the throughput figures suggest that the surface finish of the fibre faces is very good, which is also apparent from the interferograms. The scattering losses from the fibre face appear to be very small.

7.2.4 Focal ratio degradation measurements

The experimental technique for measuring FRD has been discussed previously in chapter 4. Table 7.3 shows the estimated output focal ratio, with an input beam of f/5, for each of the SMIRFS fibres.

The results indicate that the FRD is less in the silica fibres than the ZrF_4 fibres. The mean output focal ratio from the silica fibres for a f/5 input beam was ~ 4.4 and for the ZrF_4 fibres ~ 4.2. These values are good, suggesting that the fibres have low inherent FRD and that stress-induced FRD from gluing and assembling the fibres has been keep low. It should be noted that with the optical layout of the SMIRFS fibre bundles, a change in output focal ratio from the fibre translates into a change in the image size of the fibre within the spectrograph. This results from the use of pupil imaging at the fibre output (see chapter 5). Therefore FRD does not degrade the throughput of the system as it can with simple fibre coupling, but it can affect the resolution.

Fibre Number	Focal ratio of the output beam ± 0.2	Fibre Number	Focal ratio of the output beam ± 0.2
Si1	4.4	**ZF1**	3.9
Si2	4.4	**ZF2**	4.3
Si3	4.1	**ZF3**	4.4
Si4	4.3	**ZF4**	4.2
Si5	4.7	**ZF5**	4.0
Si6	4.4	**ZF6**	4.1
Si7	4.3	**ZF7**	4.3
Si8	4.4	**ZF8**	4.3
Si9	4.6	**ZF9**	3.9
Si10	4.3	**ZF10**	4.3
Si11	4.5	**ZF11**	3.9
Si12	4.6	**ZF12**	4.1
Si13	4.6	**ZF13**	4.2
Si14	4.6	**ZF14**	4.2
Mean	4.4 ± 0.3	**Mean**	4.2 ± 0.3

Table 7.3 The FRD results for the SMIRFS fibres.

7.2.5 Microlens alignment

Accurate alignment of the both the input and output microlenses of the SMIRFS fibre bundles is absolutely critical to the overall throughput of the system (see chapters 5 & 6). Shifting the input microlens laterally by as little as 10μm is equivalent to shifting the secondary mirror of UKIRT sideways by ~ 15 mm. There was a small amount of variability within the microlenses supplied, so they were grouped into input and output pairs of matching focal length. First, the setting up of the alignment jig is described. This is followed by a detailed description of the microlens alignment procedure.

7.2.5.1 Alignment jig set up

First, a target consisting of a series of concentric rings, 10 mm apart, was mounted on the ceiling of the optics lab with a thin plum line emanating from its centre. With the plum bob attached to the line, the alignment jig (figure 7.4) was shifted on the optical

table until it was centred directly below the ceiling target. A silica test fibre and microlens were then used to align the jig, so that light shone through the fibre was centred on the ceiling target. The plum bob tended to oscillate about, so the jig was fixed at the mid-point of the oscillations to within ± 5 mm, 6500 ± 5 mm below the target. The relatively large oscillations of the plum bob, and hence the large error in the positioning the mid-point, were most likely due to oscillation of the building itself. The optics lab is not a brick building. It is of steel framed construction with a large surface area more susceptible to wind buffeting and low frequency vibrations.

(Note: Ideally the target should have been placed ~ 11391 mm from the microlens face thus corresponding with the distance from the secondary mirror to the focal plane of UKIRT (11384 mm) plus the distance from the focal plane to the face of the microlens (~ 7 mm). The target distance of 6500 ± 5 mm eventually used was the maximum achievable given the height of the ceiling in the optics lab. However, the net defocus that resulted was very small, so the effect was neglected.)

The fibre and microlens holder were mounted in the jig. A microlens was dropped into the holder and was adjusted so that the fibre image was centred on the target. The microlens was fixed with a small amount of UV curing epoxy (Vitralit 7105). The fibre/microlens assemble was then rotated. When the microlens was correctly aligned, relative to the fibre axis, the image of the fibre would remain centred on the target independent of rotation. If the microlens was incorrectly aligned the image would precess around and if the jig was correctly aligned this precession would be around the centre of the target centre. If not, the image precession would be offset from centre. The alignment procedure was a slow iterative process of microlens alignment followed by jig alignment, until the image remained centred on the target independent of the fibre/microlens assembly's rotational orientation. Only a small amount of epoxy was used to fix the microlens as it was necessary to break the bond each time the microlens was re-aligned. The epoxy residue could be removed from the microlens and the holder using ethanol prior to re-assembly.

7.2.5.2 Aligning the input microlenses

First, the microlens holder, the fibre brass ferrule and the microlens were thoroughly cleaned using ethanol providing a grease free surface for the adhesives to key to. The microlens holder was then mounted in the alignment jig. The input end of the polished fibre was then inserted into the back of the microlens holder. The brass ferrules of the fibre, manufactured to give a fairly tight fit inside the microlens holder, held in place under gravity. The microlens was carefully held in a pair of tweezers while a thin layer of UV curing epoxy (Vitralit 7105) was applied to the microlens wall with a small spatula. Great care was taken to ensure that no epoxy spilled onto the optical surfaces. The epoxy was chosen to be quite thick in its non-cured state, so it was less likely to run. However, if some epoxy did get on the microlens surface, it could be cleaned using ethanol. Next, the microlens was dropped into the microlens holder with the convex surface pointing up and pushed home, onto its seat, with a cotton wool bud.

The other end of the fibre was illuminated at ~ 0° input angle, with a low powered helium-neon laser (~ 5 mW at 632.8 nm). This produced an image of the fibre on the ceiling target. The image was focused by moving the fibre ferrule up and down inside the microlens holder and the image was centred on the target by moving the microlens laterally. The microlens was moved by 4 micrometers mounted on the alignment jig. These accessed the lens via the 4 holes in the side of the holder. Once the lens was correctly aligned, the epoxy was cured by illuminating it with a high intensity UV lamp (~30 seconds). The alignment was rechecked, as any mis-alignment would be very difficult to correct at a later stage. The microlens was then securely fixed in place with Vitralit 4280 epoxy. This was thinner than the Vitralit 7105 and could be injected into the space between the microlens and the wall of the microlens holder using a hypodermic syringe. The UV lamp illuminated the epoxy from above the microlens, and then down each of the 4 alignment holes to ensure all the epoxy was properly cured. It was clear when any epoxy got onto the optical surface as the projected image would become severely degraded. Excess epoxy could be cleaned off with ethanol. If epoxy got onto the back surface of the microlens it was possible to remove the fibre ferrule from the microlens holder to gain access to the back of the microlens. However, the ferrule holders were first marked so they could be re-aligned. As the ferrules were a tight fit it

was possible to relocate the fibre without requiring the re-alignment of the microlens. This completed, it was now possible to fix the fibre ferrule to the microlens holder using the Vitralit 4280 epoxy. This bond was further re-enforced with RS quick set epoxy and allowed to cure overnight.

7.2.5.3 Aligning the output microlenses

The alignment of the output microlenses was essentially the same as the input microlenses. However, the output images were aligned to form a pupil on a target set at the focal point of the spherical mirror inside the slit projection unit. The distance from the fibre slit face to the focal point of the mirror was ~ 210 mm. The slit projection unit was mounted vertically on the bench so the fibre slit face pointed upwards. The fibre slit was fixed in position at the end of the SPU. The fibre was inserted into the back of the slit block. Vitralit 7105 epoxy was applied to the microlens, which was then placed onto the front face of the slit block. The input end of the fibre was illuminated with the laser and the fibre image focused by moving the fibre ferrule. The image was aligned by manipulating the microlens with a pair of tweezers. When the lens was correctly aligned the epoxy was cured with the UV lamp. The circular recess in the slit block face, or microlens seat, was then filled with Vitralit 4280 UV epoxy to securely fix the microlens. The fibre ferrule at the back of the slit block was fixed with UV epoxy and re-enforced with RS quick set epoxy.

(Note: It was very important that the image formed on the target was both well aligned and correctly focused. If the image was mis-aligned or defocuses it would decrease the amount of light from the fibre core "seen" by the spectrograph and increase the amount of light from material surround the fibre core. This would not only decrease the signal throughput of SMIRFS, but as the non-core material is effectively black body it would act to increase the thermal background in the K band.)

7.3 The guide fibre bundle

The design of the guide fibre bundle has been discussed previously in chapter 6. This section contains a description of how the guide fibre bundle was assembled. It consists of 3 guide bundles each containing 7 individual fibres (see figures 6.11).

7.3.1 Fibre preparation

The fibre used for the guide fibre bundle was Ensign & Bickford HCN-M0600T-14 fibre, which has a 600 μm silica core, a bonded polymer cladding and a Tefzel® buffer. First, the individual fibres were cut into 3m lengths using a sharp scalpel. The buffer was striped back ~ 100 mm from the input and ~ 40 mm from the output end of the fibre. The buffer removal was necessary as the fibres needed to be closely packed together at the input end. At the output end it was to allow the fibres to be inserted into 19 gauge steel tubes for polishing. Tefzel® is extremely chemically resistant, so the only way to remove the buffer was to cut it off. Using a very sharp scalpel a thin strip of the buffer was "shaved" off. Considerable care was need to avoid scratching or "nicking" the fibre cladding. The buffer could then be un-peeled from around the fibre and the excess cut away. It was vital to maintain a sharp scalpel blade as it tended to snag if the blade lost its edge. The fibre was checked for cladding damage by shining a laser down it. Any damage areas were visible due to their excessive light leakage. If the fibre was damaged it was likely to break at a later stage, so the fibre had to be rejected.

The fibres were then sorted into groups of 7 fibres, inserted into the input brass ferrule and fixed into place with RS quick set epoxy, which was left to cure for over 24 hours. At the output end, the steel tubes were slid over the fibres until the fibres protruded from the end. Then the epoxy was applied to each fibre and the steel tube slid back until the fibre face was flush with the face of the tube. Great care was taken to ensure all the fibres were the same length as they were to be packaged together.

7.3.2 Fibre polishing

The guide fibres were polished in much the same way as the other SMIRFS fibres, using AlO_2 polishing papers. The output ends were polished first. If there was any breakage less time was wasted as this end took considerably less time to polish than the input face. Table 7.4 lists the typical polishing times for the SMIRFS guide fibres. Great care was taken when flattening off the input face of the fibres with the emery paper as they were prone to shattering. The input end of the fibre was more susceptible to snagging than the output end, which was rigidly held inside the steel tube. The rigidity of the input end relied on the epoxy and tight packing of the fibres.

Grade of polishing paper	Polishing time output face	Polishing time input face
1000 Grit emery	~ 10 minutes	~ 15 minutes
9μm AlO_2	~ 2 minutes	~ 2 minutes
3μm AlO_2	~ 2 minutes	~ 2 minutes
1μm AlO_2	~ 20 minutes	~ 3 hours

Table 7.4 Approximate polishing time for the input and output faces of the guide fibres.

The surface area of the SMIRFS guide fibres was much greater than that of the field fibres and they therefore took longer to polish, particularly the input ends. The input end of each guide fibre bundle consisted of 7 separate fibres mounted together in a brass ferrule with a total surface area of ~ 28 mm^2 of which ~ 2.2 mm^2 was fibre material. At the output end of each guide fibre bundle each of the seven fibres were separately mounted in steel tubes with an area of ~ 1 mm^2 of which 0.31 mm^2 was the fibre material. After polishing, these steel tubes were then glued into a brass mount, each fibre well separated from the other. This enabled light from each fibre in the bundle to be clearly resolved from that of its neighbour. The field fibres, however, had an area of ~ 0.52 mm^2 of which ~ 0.04 mm^2 was fibre material. All fibre faces were inspected for flatness and finish quality using the interferometer.

7.3.3 Final assembly of the guide fibre bundle

To ensure that image movement at the input of the bundle was imitated at the output, each of the 7 fibres was illuminated in turn. The output ferrule was then inserted into the appropriate hole in the output ferrule holder. The steel tubes were slid into place and adhered at the point where the tubes protruded out of the back of the brass holder, using Vitralit 4280 UV curing epoxy. The joint was re-enforced with RS quick set epoxy. Great care was taken to ensure all 7 fibres were flush with the face of the holder and clear of epoxy. All three bundles of fibres were inserted into steel re-enforced tubing which protected them from stretching, crushing and sharp bending forces. The steel re-enforced tubing is shown in figure 7.5 along with the guide fibre unit. The tubing attaches to the brass output assembly by a stainless steel lock nut. The complete guide fibre bundle locates into the guide fibre unit with a dowel and three retaining bolts, thus allowing the bundle to be removed for transportation.

7.4 The slit projection unit (SPU) alignment

Figure 6.10 shows the layout of the SPU. It consists of three components: the fibre slit, the spherical mirror and the folding flat mirror. Both of the mirrors are mounted on tip, tilt and translation stages. However, the position of the fibre slit is fixed. The spherical mirror acts to re-image the fibre slit at the correct distance in CGS4 and the flat mirror simply acts as a fold in the system. The sequence in which the mirrors are aligned is very important. Initially alignment is carried out on the bench prior to mounting the unit on the telescope. The unit can then be mounted on the telescope and the alignment fine tuned.

7.4.1 Bench alignment procedure

The cover plate is removed to allow visible access to the SPU mirrors and the alignment target. The fibre slit is mounted into position at the end of the SPU. Then the target is mounted 102 ± 3 mm from the outer face of the SPU. This is equivalent to the telescope focal position inside CGS4. The target is marked with the nominal position for each of the fibre images. To roughly align the system, the flat mirror is moved horizontally, until the centre of the mirror is approximately opposite the target marks. Next, a He/Ne laser is used to illuminated, in turn, each fibre input. The spherical mirror is aligned so the image from the illuminated fibre is projected back onto the fibre slit block. The spherical mirror inverts the image of the fibre slit, so the image from fibre 14 corresponded to the physical position of fibre 1, fibre image 13 to fibre 2, and so on. The adjustment provisionally sets the 1:1 magnification ratio of the system and ensures the axial rays from the fibres are parallel after hitting the spherical mirror. This closely approximates the normal optical layout, in which the axial rays from the different field positions of UKIRT enter CGS4 roughly parallel. The position of the spherical mirror also affects the focus of the fibre image, but the focal ratio is ~ f/36, so the focal position is not critical. The tip and tilt of the spherical mirror adjust the fibre beams so that they are co-axial with the input optics of CGS4. However, by initially re-imaging the fibres onto the slit block, we are assuming that the plane of the fibre slit is exactly perpendicular to the optical path of CGS4. Thus, a small adjustment might be necessary when the SPU is mounted on the telescope.

The spherical mirror is fixed in tip and translation, then adjusted in tilt so the fibre beams hit the middle of the flat mirror. The spherical mirror is then fixed in tilt. The flat mirror is adjusted in tip and tilt so the fibre images are aligned on the target marks. The flat mirror is then fixed in tip. To ensure that the fibre beam axial rays are perpendicular to the face of the SPU, the target is moved, in the focal direction, to a position as close to the flat mirror as possible (i.e. flat against the outside face of the SPU). The fibre images are then re-centred on the target using the translation and tilt adjusters. The target is moved back to CGS4 focal position and alignment corrections made. It is then moved flush to the SPU face again and alignment re-checked. This iterative process continues until the fibre images are centred on the marks at both target positions. The fibre beams are then perpendicular to the face of the SPU and will, hopefully, be co-axial with the CGS4 optics when the unit is mounted on the telescope. The flat mirror can now be fixed in translation and tilt, and the SPU cover plate replaced.

7.4.2 SPU adjustments when mounted to CGS4

This section describes the final alignment of the SPU mirrors when the unit is mounted onto CGS4. Note, that at this stage, it is imperative to follow the alignment procedure carefully as any erroneous, or out of turn adjustments are likely to propagate errors. These errors will most likely require the whole procedure to be re-started from the bench alignment stage.

The adjustment most likely required is a lateral shift of fibre slit image to align it with the cooled slit within CGS4. CGS4 does not have a direct imaging mode so any adjustments are made by peaking up the dispersed image signal.

The fibre slit image can be moved laterally in one of two ways: by a translation of the flat mirror (however, this affects the focus of the image), or by tilting the spherical mirror which changes the incident angle and position of fibre rays at the flat mirror. This requires that the flat mirror be tilted to compensate for the change in incident angle in order to maintain fibre beams co-axial with the CGS4 optics. The latter technique does not affect the focus but alignment is difficult to gauge; a change in signal intensity could be due to vignetting, either by the Lyot stop (fibre beams not co-axial with the CGS4 optics) or by the CGS4 slit (lateral mis-alignment of slit image). The first method of

translating the flat mirrors is much simpler, even though it does affect the image focus. However, the fibre beams are ~f/36, so there can be relatively large changes in focal position without significantly affecting the image size.

Any rotational mis-alignment between the image of the fibre slit and the cooled slit inside CGS4 can be removed using the image rotator mechanism inside CGS4 which is adjusted remotely from the telescope control room. It should not be necessary to adjust the vertical alignment of the fibre slit image as it is effectively shorter than the CGS4 slit, so a small amount of mis-alignment is allowable (see chapter 6). Yet, if any of the fibre slit image is vignetted by the top or the bottom of the CGS4 slit, the spherical mirror can be tipped slightly to shift the image position up or down on the flat mirror. However, as the incident angle has also changed, the flat mirror should then be tipped the opposite direction ensure the fibre beams remain co-axial to the CGS4 optics. Unfortunately, due to the limited time available before the commissioning run, there was not time the calibrate tip, tilt and translations required to align the mirrors. The alignment at the telescope was therefore very much trial and error, for which no accurate records were made.

Focusing the system is complicated as it involves making three adjustments, but, as mentioned earlier, the beams are f/36.3, thus the image size changed slowly with focal position. Since both the image size of the fibres and pixel scale of the spectrograph detector are large compared to likely effects of poor focusing, adjustment should not be necessary. However, to focus the system, first piston the flat mirror, then tilt the spherical mirror and the flat mirror to bring the image back into line with the CGS4 slit. This adjustment is limited because, if the spherical mirror is tilted too far the rays will eventually miss the flat mirror. The spherical mirror should not be moved in translation to adjust the focus as this will affect the divergence of the axial rays from the fibre beams. These must remain parallel to the optical axis of CGS4 or there will be vignetting by the Lyot stop.

7.5 Summary

The finish quality of the fibre faces, the alignment of the microlenses and the alignment of the slit projection optics can all have a significant effect on the throughput of

SMIRFS. The fibre preparation can affect the FRD within the fibres and care should be taken to avoid stressing the fibre. Things such as choice of epoxy and protective sleeving can have an effect. The finish quality of the fibre faces can affect fibre throughput and focal ratio. A poor finish leads to surface scattering and round off leads to lensing and focal ratio changes. It is helpful to monitor the finish during polishing with an interferometer that gives an indication of both surface flatness and finish quality. Cleanliness and polishing times were both highly influential on the final result.

The throughput and FRD of the fibres can be checked when the polishing is complete. The mean throughput for the silica fibres was 92.4% and 86.2% for the ZrF_4. These were very close to the predicted losses from fibre attenuation and surface reflection suggesting there was very little scattering loss from the fibre faces. The mean output focal ratio, for an input beam of f/5, was 4.4±0.3 for the silica fibres and 4.2±0.3 for the ZrF_4 fibres. However, because of the use of pupil imaging this translates into potential loss in resolution, not throughput. Both the FRD and the throughput measurements suggest that the fibre preparation and polishing was very successful. The alignment of both the input and output microlenses was critical and was carried out using an optical alignment system. UV curing epoxies were used to rapidly fix the microlenses in place, once they had been correctly aligned. There is a complicated alignment procedure for the slit projection unit which must be carefully adhered to or significant throughput losses can result. The first stage is carried out on the bench and the second, fine tuning stage, is carried out once the SPU is fixed to the telescope. If sufficient care is taken with preparation of the fibre bundle and alignment of the SPU the alignment losses should be negligible compared to the reflection losses in the system.

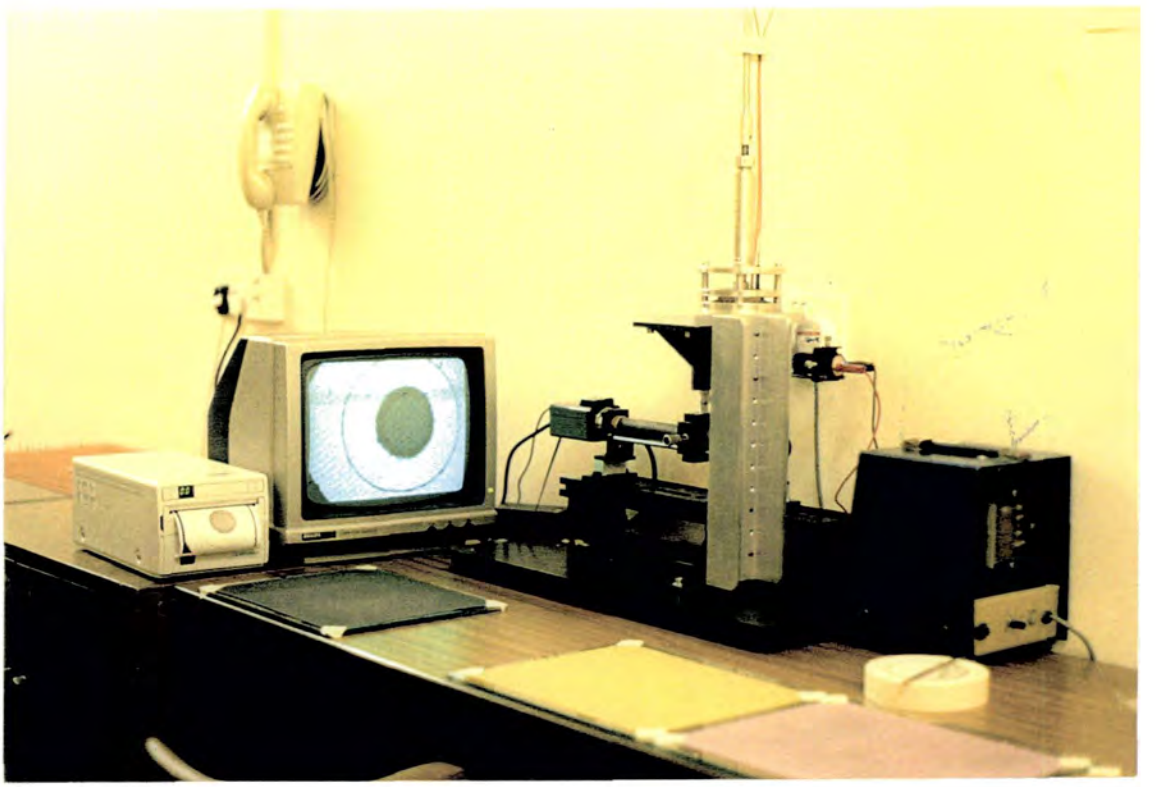

Figure 7.1 A photograph of the polishing apparatus. The polishing cloths are at the front of the bench. The television monitor is showing the interferogram of the fibre face. The black instrument with a silver tower is the interferometer, with the polishing jig on top of it.

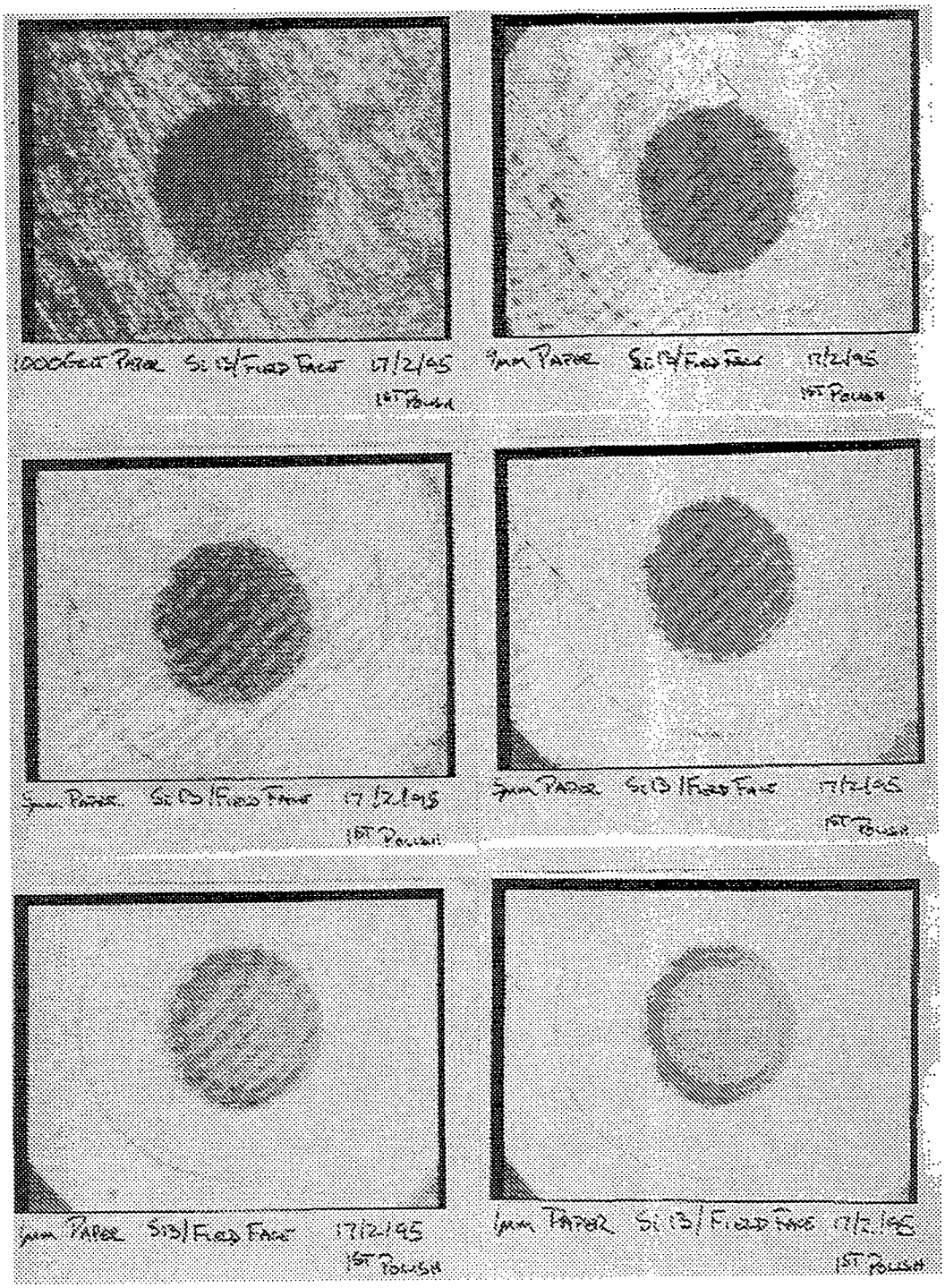

Figure 7.2 A photograph showing the interferograms of one of the silica fibres for SMIRFS. A frame was taken after each polishing stage; 1000 Grit paper (top left), 9μm AlO_2 paper (top right), 5μm AlO_2 paper (middle left), 3μm AlO_2 paper (middle right), 1μm AlO_2 paper (bottom left) and 1μm AlO_2 paper without the interference pattern (bottom right).

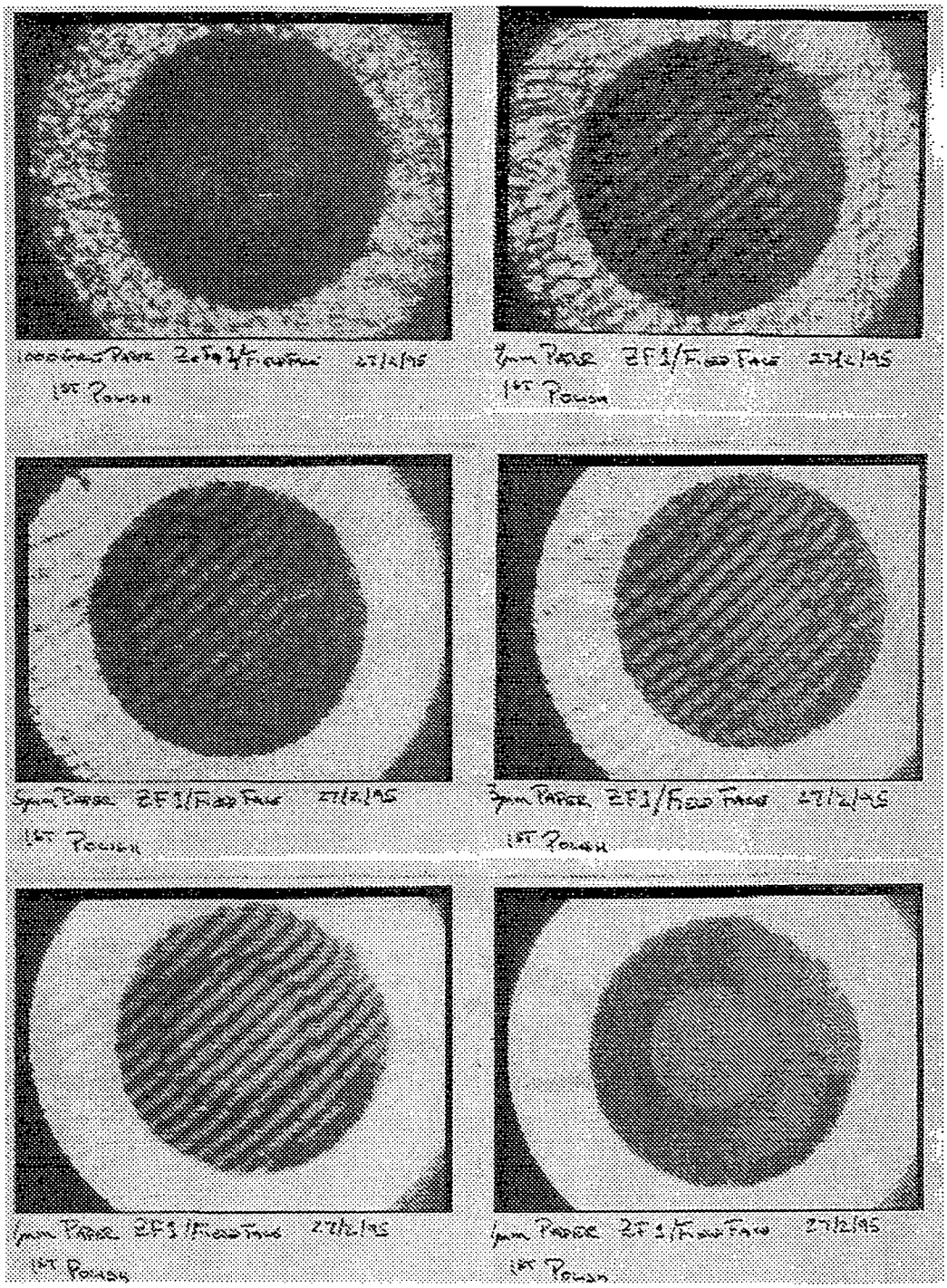

Figure 7.3 A photograph showing the interferograms of one of the zirconium fluoride fibres for SMIRFS. A frame was taken after each polishing stage; 1000 Grit paper (top left), 9μm AlO_2 paper (top right), 5μm AlO_2 paper (middle left), 3μm AlO_2 paper (middle right), 1μm AlO_2 paper (bottom left) and 1μm AlO_2 paper without the interference pattern (bottom right).

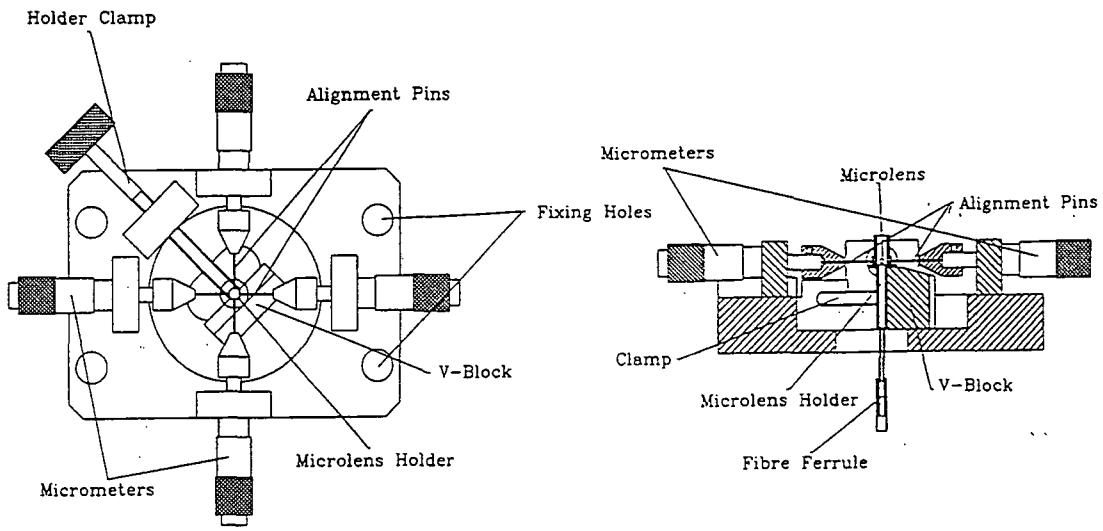

Figure 7.4 The alignment jig for the input microlenses of the SMIRFS fibre bundles. The diagram on the left shows a plan view and the one on the right a section across the middle of the jig.

Figure 7.5 A photograph of the guide fibre unit, with one side and the top removed, showing the camera lenses and the guide fibre bundle located at the left had end of the unit.

Chapter 8: Commissioning of SMIRFS

8.1 Introduction

The commissioning of SMIRFS was carried out at UKIRT in June 95 (Haynes *et al.*, 1995). PATT allocated two engineering nights and one science night. The first two nights were for setting up, aligning and performance assessment, while the third night was for the science programme. This involved obtaining medium resolution K band spectra of bright giants in a number of Galactic globular clusters and the Galactic Bulge. This chapter contains discussion on the set up and alignment procedures of the commissioning run and presents performance figures for SMIRFS, as well as an example spectrum from a Galactic Bulge giant.

8.2 Set up and alignment

The initial mounting and alignment of SMIRFS was carried out during the daytime when the telescope engineers were available to assist with the removal of the CGS4 calibration unit and the interfacing of SMIRFS with UKIRT. The fine tuning of the system was carried out during the two engineering nights.

8.2.1 The field plate unit (FPU)

The field plate unit was mounted directly onto the empty West port of the UKIRT instrument support unit (ISU). A circular test plate, containing 14 holes equally spaced equivalent to a 60 arcsec radius, was plugged with one of the fibre bundles and mounted in the field plate holder. The plate tensioner was rotated up by half a turn and the fibre slit was mounted in the alignment jig. A laser was then shone back down each fibre in turn projecting an image of the fibre up onto the secondary mirror of UKIRT. In the normal SMIRFS configuration the fibres view an area very slightly larger than the secondary mirror, which provides a little flexibility in the fibre pointing. As a result of this the laser induced fibre image produces a silhouette of the secondary mirror on the UKIRT dome. The shape of this silhouette indicates how well the fibre is pointing at the secondary mirror. If there is an even thin ring around the secondary dome shadow, the fibre is well aligned, however, a crescent shape indicates mis-alignment. The alignment of each fibre is individually checked; any bulk mis-alignment can be corrected by offsetting the UKIRT dichroic. Note that the dichroic is set to datum every time the

telescope is run up, so any offset in RA and DEC should be re-set at the beginning of the night. During the initial set-up of SMIRFS there had been problems with the dichroic sticking and it was not consistently finding the correct offset position. We therefore briefly checked the pointing at the beginning of each night to ensure the dichroic was correctly offset. The offset required during the commissioning run was -40 in RA and -100 in DEC, however, if the FPU is moved on the ISU then the offset is likely to change.

It was noted, during the fibre alignment, that any burring or dirt on either the fibre ferrule flange or around the hole in the field plate would cause severe pointing errors with up to 50% of the light missing the secondary mirror. The rotation of some of the fibres also slightly affected the pointing, so when a fibre was satisfactorily aligned the ferrule was marked to indicate North, as seen by the field plate. With the telescope pointing at the zenith, North was to the right when viewing the back of the field plate. The procedure was repeated for the second fibre bundle. It was found that if care was taken to remove any dirt or burrs and all the ferrule marks pointed North, for any one fibre less than 10% of the light would miss the secondary mirror. Optimal pointing over the whole fibre field was achieved when the field plate tensioner was rotated by approximately one half turn from the slack position. This was checked using a field plate that evenly spaced the fibres in a straight line crossing the whole field.

To align the field plate co-ordinates with that of UKIRT's cross head camera we mounted a field plate with guide fibres plugged in the following positions (0,-18), (0,-108) and (-108,0), relative to the (0,0) the field plate centre. The X co-ordinate corresponds to East, the Y co-ordinate to North and the units are arcsecs. A bright star was centred on the guide fibre at (0,-18) and the cross head camera (Autoguider camera) was moved until the star was centred in the camera. The telescope was then nodded to the North by 90', which moved the star image South to (0,-108). The rotation of the field plate was then adjusted, using the micrometer on the FPU, so the star was centred in the guide fibre at (0,-108). Next the star was centred in the guide fibre at (-108,0). The process was repeated until satisfactory alignment between the field plate and the telescope co-ordinates was achieved. The plate rotation was then locked in

place by tightening the six slotted bolts at the back of the FPU flange. The alignment process also provided a final check of the plate scale used for the field plates.

8.2.2 Slit projection unit (SPU)

The SPU was initially aligned on the bench using the alignment target. This procedure is described in chapter 7. The CGS4 calibration unit was removed and the SMIRFS slit projection unit slid into place. A field plate was plugged with one of the fibre bundles and mounted in the FPU. The fibre slit was carefully fitted into the SPU. This is a relatively delicate operation as the SPU is in a fairly tight space and the microlenses of the fibre slit are vulnerable at this point. The dome was then observed in the H-band with the dome lights on. This provided a reasonably stable source by which the signal, from each of the fibres along the slit, could be peaked up. CGS4 does not have a direct imaging mode so the alignment was performed using 75 l/mm grating and the 150mm camera; this gives a pixel scale of 1.23 arcsecs/pixel. The CGS4 slit was set to the maximum width of 4 pixels. There was a fault with the CGS4 slit rotation mechanism which left the slit aligned at 11.77° from the vertical, thus producing a sloping image of the fibre slit on the detector.

8.2.2.1 Alignment steps

When aligning the SPU it is important that the alignment steps are followed very carefully as deviation from this would probably require the removal of the SPU and re-alignment on the bench. The projection mirrors should be fixed in tip and tilt and should not be adjusted unless absolutely necessary. The only adjustments that should be necessary are slit rotation and the lateral alignment of the fibre slit with the cooled slit inside CGS4 (see chapter 7).

The SPU final alignment was carried out as follows: first, the flat mirror was translated perpendicularly to the optical path of CGS4 until fibres 7 and 8, the central fibres, were visible on the detector. The CGS4 image rotator was then used to align the fibre slit with the CGS4 slit so that all 14 fibres were visible. Once this was completed the CGS4 slit was changed to a 2 pixel slit (2.44 arcsecs) to allow fine tuning. The flat mirror and image rotator were then fixed in position. It should not be necessary to adjust the focus of the system (see chapter 7). Ideally the SPU should be aligned every time the fibre slit

is changed over as there is a small difference between the two, but this is not too serious as the throughput results discussed latter in this chapter confirm. However, there was a negligible effect on alignment caused by the removal and subsequent replacement of the same fibre slit.

When plugging the fibres into the field plate, the task was made considerably easier if the fibre slit was first removed from the SPU. Also, to speed up the process of changing fields, the new field plate was pre-plugged with one fibre bundle, while observing continued with the other. However, there was some extra loss in throughput with one of the bundles, as the SPU was not re-aligning for that particular fibre slit.

8.2.3 Guide fibre unit (GFU)

The guide fibres were predominately used for alignment of the FPU and acquisition of fields. Guiding was done using the cross head camera.

When setting up and using the GFU it was important to avoid saturating the SCANCO camera, as this could damage the unit. Under low lighting conditions, i.e. scattered torch light, the SCANCO camera was mounted onto the GFU. The 135 mm lens and 2× teleconverter were fixed at the mid-point along the slide. The 50 mm lens was mounted at its mid-point and the guide fibre bundle slotted into place. With the dome light off and the SCANCO switched on, the input faces of the guide fibres were illuminated with reflected light from a torch. Viewing the SCANCO TV monitor, the 50 mm lens was moved to focus the fibre images and then clamped in place.

(Note: it is vital that the manual gain control for the SCANCO is turned down to minimum when the dome lights are on, otherwise the camera will saturate.)

It was intended that the field acquisition would be carried out using guide stars but it soon became apparent that the most of the guide stars we had chosen were too faint to detect with the GFU. This was due to a number of reasons: first, we never had good transparency during the run, due mainly to high cirrus cloud. This caused a typical loss of a couple of magnitudes in brightness but at times this was significantly worse. Secondly, the system was designed to work at visible wavelengths (see chapter 6) and there was insufficient light reflected by the dichroic. Initially the camera system had been

designed around an ST-6 peltier cooled astronomical CCD but this had to be dropped because of the cost. This system would have provided the ability to integrate the guide star signal. It is also possible to integrate using the SCANCO but the electronics were not available to do this at the time of the commission run. The quantum efficiency of a CCD can be around 60% at 600nm and still be above 20% at 900nm. However, with S20 photocathode devices, such as the SCANCO camera, the quantum efficiency peaks at about 10% at 400nm, by 600nm it is down to about 3% and it has tailed of completely by 900nm (figure 6.12). In addition, the amount of optical light reflected by the dichroic falls off as you shift towards blue, so a CCD would be more suitable than the SCANCO as it is more red sensitive.

In the end, the field acquisition was carried out using a combination of the guide fibres and the cross head camera. Most of the field plates not only had holes for the guide fibre that corresponded to bright stars in the field, they also had guide holes at (0,10) and (0,100). These were originally included to provide a check of the field plate orientation. To acquire the field, a bright star, with accurate astrometry, was located in the vicinity of the field. This star was centred on the guide fibre at (0,10) and then centred on the cross head camera. The telescope was then moved to the guide fibre at (0,100) to check the field plate orientation. It was then possible to offset the telescope onto the star field with an accuracy of better than 1 arcsec.

With the SCANCO's gain set at about 3/4 it was possible to detect $m_v \sim 8$ guide stars and $m_v \sim 11$ guide stars with the gain set to full. Using the cross head camera it is usually possible to guide on stars down to $m_v \sim 15$-16. In dark time $m_v \sim 17$ is possible. By integrating for 2-3 seconds one further magnitude could be gained but two magnitudes were lost due to moonlight. It is apparent that the GFU will have to be redesigned for future use, perhaps based on the CCD system originally proposed. However, UKIRT is due to be upgraded with a more efficient dichroic. This will have much lower visible reflectivity, reduced from ~ 30% for the present dichroic, down to ~ 10%. This may require a completely new design for the GFU, possibly based on an infrared detector or a highly efficient visible light system.

A number of the separate fibres that made up the guide fibre bundles broke. This was probably due to the vulnerability of the input fibre ends to sharp bending stress. The input ferrules will need to be modified or completely redesigned as part of the development and upgrading of SMIRFS.

8.3 Throughput of the SMIRFS system

Initially the throughput of SMIRFS was to be determined by comparing the flux from a standard star with SMIRFS and then CGS4 alone. However, as the conditions were not photometric, dome flats were used. A number of dome flats were taken using SMIRFS with both the silica and the ZrF_4 fibre bundles, covering the J, H & K bands. SMIRFS was then removed and dome flats taken with CGS4 alone. These provided a reference flux for the relative throughput calculations. This method is not ideal as, strictly, the source should be at infinity. However, it provides a reasonable estimate of throughput.

8.3.1 Fibre collecting area

To provide a meaningful comparison it was important to normalise the frames to the same integration time and effective collecting area.

Conventional unlensed fibre systems present a well defined aperture on the sky which is simply a function of the fibre core size and the plate scale. In the case of SMIRFS the effective collecting area of the fibres is not well defined and the size of the output image from the fibre can be affected by the seeing conditions. This is a consequence of using pupil imaging and is discussed in chapters 5 & 6. When taking a dome flat with SMIRFS, to a first approximation, the fibre image size at the detector is the same effective size as that viewed by the fibre. This ignores FRD within the fibre which will have the effect of increasing the size of the image on the detector, but this should be relatively small. Thus, if the fibre image is 3 arcsecs across at the detector then the fibre aperture on the dome is $\leq$ 3 arcsecs across. Ignoring the effects of FRD will result in a small underestimate of the fibre throughput as the effective area of dome sampled by CGS4 alone will be slightly larger that that sampled by the fibre.

To make a valid comparison between the SMIRFS signal and the signal with CGS4 alone is was necessary to account for the different collecting area of the two systems.

Figure 8.1 shows a slice across an H-band dome flat taken in the non-dispersive direction. The fourteen peaks correspond to the fourteen fibres and are spaced at ~ 5 pixel centres. From this, it can be seen that most of the energy from each fibre falls within ~ 3 pixels and 2/3 falls within 2 pixels. The J and K band dome flats had similar profiles. Most of the dome exposures were taken using a 2 pixels slit width which means that approximately 1/3 of the fibre signal was vignetted by the CGS4 cooled slit. The extracted spectra consisted of a slice taken in the dispersive direction (i.e. horizontally), that was 4 pixels wide in the non-dispersive direction (i.e. vertically). Thus, the effective collecting area of the CGS4 spectra was 8 pixels, the product of the 2 pixel wide slit and 4 pixel deep extraction. Accounting for the smaller collecting area of the fibre and the 1/3 lost by the CGS4 slit, there should be approximately twice as much signal in the CGS4 spectra as there would be in the fibre spectra, assuming no throughput looses. These factors were taken into account when fibre throughput was calculated.

8.3.2 Deriving throughput of the fibre bundles

From initial estimates it was hoped that the total throughput of the SMIRFS system would be 60% or better over the J, H & K bands (see chapter 6)

To derive the J and H band throughput, extracted dome spectra were taken with SMIRFS and compared to the spectra taken with CGS4 alone. The dome lights were switched on for these exposures. First, the frames were all normalised to the same integration time. The spectra were then extracted and the mean signal calculated over a 0.2μm region centred on the middle of the band. The J-band was averaged from 1.1 - 1.3μm and the H-band from 1.55-1.75μm. The figures for the fibres were then corrected to account for the difference in collecting area. In most cases this meant multiplying the results by 2, but some of the J-band frames were taken using a 4 pixel wide slit so the slit vignetting was ignored. The resulting signal was then compared to the signal from the same set of pixels in the CGS4 frame. Comparing the same set of pixels each time reduced the effects of detector non-uniformity.

Deriving the K-band throughput was more difficult as the signal tended to be dominated by "instrument" thermal background beyond 2.2μm. As there was an additional contribution to the thermal background from the fibres and slit projection unit (see

chapter 6), it was necessary to subtract this contribution from the SMIRFS dome spectra before they were compared to the CGS4 spectra.

To determine the instrument background, which was derived separately for both of the fibre bundles, it was necessary to take a series of sky frames viewing different airmasses. An single sky frame was taken at the following 3 airmasses: 1, 1.5 and 2. Ideally, a number of frames should be taken at each airmass so that short term temporal changes in the sky lines could be averaged, but this was overlooked at the time.

Each frame contains contributions from various sources. There is the signal from the sky (thermal and non thermal, see chapter 3), the thermal background from the telescope, the thermal background from the various components of SMIRFS and the thermal background from the spectrograph. The "non sky" components are collectively referred to as the instrument background. As CGS4 is cooled, the thermal background from the spectrograph should be negligible. At different airmasses the only variable should be the signal from the sky. Thus, subtracting the 1 airmass frame from the 2 airmass frame, gives the signal from 1 airmass of sky with the instrument background removed. Subtracting this from the original 1 airmass frame gives the signal from the instrument background. This instrument background can then be subtracted from the SMIRFS dome frames leaving only the signal from the dome itself.

In summary;

(2 airmasses + instrument) - (1 airmass + instrument) = 1 airmass

and

(1 airmass + instrument) - 1 airmass = instrument

then,

(dome + instrument) - instrument = dome.

8.3.3. Throughput results.

The throughput results for the individual fibres of the ZrF_4 bundle and silica bundle are shown in figures 8.2 and 8.3 respectively. The error is estimated from uncertainties in

deriving the fibre collecting area and the mean signal count. The mean throughput and the maximum variation figures for the two bundles are shown in Table 8.1.

	Mean Throughput ZrF_4	Variation within ZrF_4 bundle	Mean Throughput SiO_2	Variation within silica bundle
J-Band	55%	+10 /-13	40%	+5 /-8
H-Band	62%	+13 /-19	48%	+8 /-7
K-Band	69%	+14 /-14	40%	+7 /-18
Mean	62%	+13 /-16	43%	+7 /-11

Table 8.1 Average throughput of fibre bundles.

The first noticeable feature is that the ZrF_4 fibres have, on average, 19% better throughput than the silica fibres. This is, most likely, due to a fibre slit alignment problem. When SMIRFS was set up for the final night's observing, the alignment of the slit projection unit was carried out using the ZrF_4 slit. Therefore, when the silica fibre slit was used, there was no guarantee the silica slit was optimally aligned with the CGS4 cooled slit. However, the ZrF_4 fibres, with an average throughput of 62%, demonstrate that significant multiplex gains can be achieved with multi-object fibre systems in the near-IR.

The fibre to fibre variations, which are more significant in the ZrF_4 bundle, are quite large in some cases and will need to be reduced. It is worth noting that the throughput figures for individual fibres are reasonably self consistent. This suggests that the fibre to fibre variation is a real one and not a feature of the measurement technique. Also, the ZrF_4 fibres consistently perform better in the K band than in H and better in H than in J, which is consistent with the transmission characteristics of the fibre material. The silica fibres perform best in the H band and marginally better in K than in J with one notable exception, fibre 14. A drop in transmission from the H to K band is consistent with the characteristics of the fibre, but the reason for the drop in throughput for the J band is less clear and does not follow the theoretical throughput predictions. However, the dome exposures taken with the silica fibre bundle, were taken just before sunrise and the "CGS4 alone" dome exposures were taken up to an hour later. The dome exposures were taken close to the dome opening and light leaking into the dome may have

significantly increased between the two sets of exposures. This would have a more significant effect on the J band flux than either the H or K band fluxes. The result would artificially reduce the relative throughput figures for the fibre bundle and this reduction would be more pronounced in the J band. Another explanation may be that stray light leaked into the system when SMIRFS was removed. The removal of the SMIRFS SPU left a fairly large gap between the ISU and the window of CGS4 and stray light could have increased the signal for the J band "CGS4 only" exposure. However, without further testing it is difficult to state categorically the reason for this anomaly.

8.3.4 Relative fibre throughput using sky frames

To provide a check of the throughput figures measured using the dome flats, a method for measuring the relative fibre to fibre throughput using sky frames was employed. The results were then compared with fibre to fibre throughput figures derived from the dome flat data. As we were employing beam switching as a sky subtracting technique, each object frame had a corresponding sky frame in which all the fibres pointed at sky. A number of suitable sky frames were taken in the J, H and K band using the silica fibre bundle, however only K band sky frames were taken with the ZrF_4 fibre bundle. As the field of view of SMIRFS is only 4 arcminutes it was felt that the spatial variation in the sky would be small over the field, hence the flux entering each fibre should be similar. The sky spectra was extracted from each of the 14 fibres in the bundle. The mean counts from each fibre were then compared to the fibre with the largest counts to derive the relative throughput. Two sky frames were analysed for each of the three wavelength bands (J , H & K) using the silica fibre bundle and two K band frames were analysed for the ZrF_4 fibre bundle. The results are shown in figure 8.3a. The results from the two sky frames are plotted (circles and triangles) along with the relative throughput figures derived from the dome flat throughput measurements (five pointed stars).

8.3.4.1 Relative throughput results

From figure 8.3a it can be seen that the relative throughput results are very consistent for both the J and H band with the silica fibre bundle. In the J band fibres 14 & 2 have relatively poor throughput and fibres 3, 5 & 9 have better than average throughput. The correlation between the sky frame data and that derived from the dome flats is good

with fibres 8, 12 & 13 being the worst. In the H band the picture is very similar. Fibres 3, 5 & 9 are better than average and fibres 2 & 14 are bad. The correlation between the sky frame data and that from the dome flats is very good. There is also good correlation between the J and H band results.

The K band results for both the silica and ZrF_4 fibre bundles show poor correlation between the sky frame data and the dome flat results. One of the problems encountered in extracting the K band spectra was the high thermal background in between the fibre spectra generated from the warm material of the fibre slit. Beyond about 2μm this dominates the sky signal from the fibres as the sky is cooler than the slit material. The thermal background signal should be fairly flat across the slit material, it having a uniform temperature. If during the extraction of the spectra a significant signal from the slit material contaminated the fibre signal this would have the effect of reducing the fluctuations from fibre to fibre as seems to occur. The dome flat signal would have been much larger than the sky signal and comparable with that of the slit material as they would have been at a similar temperature. Therefore contamination of the fibre signal with that from the slit material would have a less significant effect. The fibre to fibre fluctuations that are seen in J and H band results are also seen in the dome flat data for the K band. Given this similarity and the more dominant dome signal it seems likely that the dome flat throughput figures are more reliable than those derived from the sky frames.

Consistent poor performance of fibre 14 was seen in all the results. This was not present in the throughput results measured relative to CGS4 (figures 8.2 & 8.3). However, when looking at the original flux intensities it was noticed that not only was the signal significantly smaller for fibre 14 spectrum, but it was also significantly smaller for the comparable spectrum extracted from the "CGS4 alone" frame. This suggests that CGS4 is less efficient at that part of the slit than elsewhere. This has little effect on the value for the throughput derived with the dome flats when compared to CGS4 alone, but produces an artificially low result for the relative fibre to fibre throughput figures in figure 8.3a which compared the total flux in each fibre.

8.3.5 Sources of throughput loss

8.3.5.1 Fibre pointing

As discussed earlier, pointing errors at the fibre input can have a significant effect on the overall throughput. A small burr or piece of dirt on the fibre can create quite severe loss. In the worst cases up to 50% of the light from the secondary mirror can be lost by the fibre. This can, with care, be keep down to less than 10%, however pointing could feature significantly in the fibre to fibre throughput variations.

8.3.5.2 Transmission losses

Many of the following points have been discussed previously in chapter 6, but their effect on the fibre throughput will now be discussed further. The spectral transmission characteristics of the fibre and microlens materials will contribute somewhat to the overall throughput of the system. Table 8.2 contains the typical transmission for the lenses and fibres at different wavelengths. The values were derived from those quoted by the manufactures.

Wavelength (μm)	ZrF_4 transmission for 1m of fibre	SiO_2 transmission for 1m of fibre	CaF_2 transmission for a 3mm thickness
1.0	92%	>99%	99%
1.5	95%	>99%	99%
2.0	98%	96%	99%
2.2	99%	87%	99%
2.3	>99%	79%	99%
2.4	>99%	66%	99%
2.5	>99%	47%	99%

Table 8.2. Transmission as a function of wavelength.

The ZrF_4 fibre transmission improves with increased wavelength, losing roughly 8% in the J band, 5% in H and 2% in K for a 1.2m fibre. The transmission losses for the silica fibres are roughly 1% in the J and H band, but in the K they can be quite severe, from 5-41%. Over 2.1-2.3μm, the range used in the throughput measurement for the fibres, the mean transmission loss is ~18%. The transmission losses due to the $CaFl_2$ lenses would be about 2% losing 1% for each microlens.

There are also reflection losses to consider. There are 6 air/glass surfaces for each fibre as well as two mirrors in the SPU. This adds a contribution of ~22% for the ZrF_4 bundle and ~20% for the silica bundle, due to reflection losses (see chapter 6). In future versions of the system this could be reduced with the use of anti-reflection coatings and index matching gels.

8.3.5.3 Fibre output beam alignment

Another source of throughput loss is through small variations in the alignment of individual fibres beams along the fibre slit. As a result of the tolerances in the manufacturing of the fibre slit block, there will be small variations in the lateral positions of the individual fibres and microlenses. There could also be losses introduced as a result of slight differences in the focal length of the input and output microlenses which would affect the focal ratio of the output beam. Both these features could lead to vignetting of the fibre beams by Lyot stop inside CGS4, which confines the beam to f/36.3. However, considerable care was taken when manufacturing the slit blocks, pairing input and output microlenses, and aligning the microlenses, so the resulting losses should be less than 5%.

8.3.5.4 Slit vignetting

In addition, the FRD within the fibre, the position of the object, and the size of the object image at the fibre input, all have an effect on the size of the output image (see chapters 5 & 6). Thus, an individual fibre's FRD, the seeing conditions, astrometry and the CGS4 slit width can, have a significant effect on the amount of vignetting by the CGS4 slit. The losses can vary from almost nothing up to ~66%, if a 1 pixel wide slit were used with a 3 pixel wide image. However, with the throughput calculations made previously this has been taken into account.

8.3.6 Summary of throughput

	J-band	H-band	K-band
ZrF_4 fibre bundle (Estimated)	> 58%	> 60%	> 62%
ZrF_4 fibre bundle (**Measured mean**)	**55%**	**62%**	**69%**
Silica fibre bundle (Estimated)	> 65%	> 65%	> 53%
Silica fibre bundle (**Measured mean**)	**40%**	**43%**	**40%**

Table 8.3 Throughput results for the SMIRFS system.

The throughput estimates for SMIRFS shown in Table 8.3 include pointing, throughput, reflection, and beam alignment losses, but do not include SPU mis-alignment or slit vignetting losses. The mean throughput of ZrF_4 fibre bundle was similar to the estimates, though the fibre to fibre variations were worse than expected. The throughput of the silica bundle is lower than hoped; this may have been due to mis-alignment between the fibre slit and the cooled slit inside CGS4. Though many different features contribute to the throughput of SMIRFS, it is alignment errors and reflection losses which have the most significant effect on the overall throughput. It is also alignment error that is the most likely cause of the significant fibre to fibre variations.

8.4. Instrument thermal background

The thermal background is not really noticeable below about 2μm but beyond this thermal emissions from the telescope and instruments can make up a significant proportion of the detected counts. Figure 8.4 shows a 4 second exposure of a Baade window star field, without any sky subtraction, taken using SMIRFS. Those detector rows which show continuum or spectral features below 2.2μm are those illuminated by the SMIRFS fibres. Some are difficult to discern as the fibres were observing relatively faint sources such as faint stars or, for background subtraction purposes, sky. The brightest star in this frame was $m_k \sim 9.5$. Beyond 2.3μm the dominant signal was from those rows that correspond to the slit block material, not the fibres.

8.4.1 Thermal background estimates from observations

Originally it was proposed that a series of sky frames be taken at different airmasses. From these the background contribution from one airmass of sky could be compared to

the thermal background from the instrument. This was to provide a rough estimate of the thermal emissions from the SMIRFS compared to the sky thermal emissions. However, during the data reduction it became apparent that this was unfeasible, due to cloud and short term variation in the sky emission lines.

8.4.1.1 Data reduction

The results presented in figure 8.5 shows the ratio of total background using SMIRFS, with the ZrF_4 bundle, relative to that using CGS4 only over the wavelength region 1.9 to 2.5μm. This was calculated by comparing the signal in figure 8.6 with that in figure 8.7. The errors were estimated from the variability in the signal intensity measurement and represent the peak fluctuation in the ratio calculation. Figure 8.6 shows the signal using CGS4 only. It has been normalised to a 10 second exposure. The signal is composed of the non-thermal background from the sky and thermal background from the sky + telescope + spectrograph (CGS4 alone) Figure 8.7 shows the normalised signal using SMIRFS. This is composed of the non-thermal sky and the thermal sky + telescope + SMIRFS + spectrograph (with SMIRFS).

It should be noted however, that the two frames were taken a month apart as no CGS4 sky frames were taken during the SMIRFS commissioning run. Hence, the temperature of the dome may have changed significantly between the exposures. Also the sky frames were taken at different airmasses, the SMIRFS frame was observed at 1.475 airmasses and the CGS4 frame at 1.118 airmasses, thus the contribution from the sky in the CGS4 frame should be about 75% of that in the SMIRFS frame. However, there can be significant variations in sky background depending on the time of the exposure both during the night and from day to day (see chapter 3). This said, the results do offer a very rough indication of the thermal background contribution from SMIRFS in the K band.

8.4.1.2 The thermal background from SMIRFS vs CGS4 alone

In figure 5, it can be seen that below 2μm there is no significant difference between the two sky signals. I believe this is just a coincidence that may originate from two independent sources. Since, in the 2μm region the sky background dominates the signal and the thermal contribution from the instrument is negligible, the SMIRFS frame should

contain ~ 24% more sky emission than the CGS4 frame as they were taken at different airmasses. However, the SMIRFS data was taken using the ZrF_4 bundle which had a mean K-band throughput of ~ 69%. Thus, the fibre throughput roughly compensates for the extra signal expected from the large airmass. But, as previously mentioned the non thermal emissions can be vary considerably, so the argument does not necessarily hold.

Beyond 2μm the instrument thermal background becomes increasingly significant and by 2.14μm it is clearly dominating the signal (figure 8.7). The difference between the two signals reaches a peak at about 2.32μm, where there is 4 times the signal in the SMIRFS frame (a factor of 2 in signal/noise), after which the difference starts to fall off. This turn over is not due to a falling off in emission from SMIRFS but is due to a rapid increase of the signal in the CGS4 frame and can be seen in figure 8.6. The cause of this is discussed later.

8.4.2 Origins of the thermal background

Figure 8.8 shows curves for a blackbody at various temperatures from 0 to 15°C. They have been plotted so that the 5°C curve is scaled to the SMIRFS frame at 2.5μm. Comparing the curves in figure 8.8 with the instrument background curve in figure 8.7, it can be seen that the shape of the 5°C blackbody curve is reasonably well matched to that of the SMIRFS spectra. This correlates with the temperature in the dome during the exposure. The primary mirror temperature was nominally about 4°C, though there were some hot spots near some of the electronics crates. The increase in the counts for the CGS4 spectra beyond 2.3μm is also apparent. This may be due to the thermal emission from the telescope which has a typical emissivity of ~15% (see chapter 3). It is possible to develop a function that has a fairly similar shape to the data using a very simplistic model, in so much as it has similar intensity ratio levels and turnover as the data does. The dashed line in figure 8.5 is a best fit using this simple model. The CGS4 thermal emission is represented by a blackbody of temperature -10°C with an emissivity (ε) of 1, the SMIRFS thermal background as two blackbodies, one at 0°C with ε=0.9 and the other at 10°C with ε=0.4. The two different blackbodies for SMIRFS were required to produce the turnover in the curve beyond 2.35μm. A small flat continuum level was added to the SMIRFS and CGS4 functions before they were subtracted to produce the

curve before the turnover point, which otherwise looked like a decaying exponential. This continuum was a simplified representation of sky emission, which is fairly flat in this region. In a more complex model with more blackbody sources at different temperatures and different emissivities, also with a better model of the sky emission, it may be possible to improve on the fit. As the original data was taken over a month apart it does not warrant the effort. Better data taken under the same temperature, airmass and telescope conditions would give a more accurate guide of the contribution of SMIRFS to the thermal background signal.

The thermal background from SMIRFS is likely to be a result of contamination of the fibre spectra by thermal emissions from the brass of the fibre slit. Because of the way the fibre slit is viewed by CGS4 there is certain to be some thermal contamination from the material between the fibres. Brass has an emissivity of ε~0.6, also the fibre slit is in an warm enclosed space. Thus, the thermal emission from the slit material will approximate that of a perfect blackbody with emissivity relatively close to unity. However, the fibres are highly transparent and will therefore have an effective emissivity of one minus their transmission. The ZrF_4 fibres transmit better than 98%, thus the thermal emissions would only contribute 2% (ε~0.02) of the energy one would get from a blackbody at the equivalent temperature (see chapter 4). Therefore the thermal background from the fibres will be dominated by that from the telescope (ε~0.15).

The instrument background could be reduced by introducing a cool mask in place of the CGS4 cooled slit that effectively masked out thermal emission from the fibre slit. Alternatively the slit projection unit along with the fibre slit could be cooled to reduce the thermal background. By reducing the temperature by 10°C the thermal background can be reduced by a factor of ~2. Further tests should be carried out on the fibres, using a detector with a much finer sampling than the 3 pixels per fibre which was used for SMIRFS commissioning run. This would allow the fibre signal to be well differentiated from the fibre slit material.

8.5 Spectral resolution

Table 8.4 shows the maximum spectral resolution ($R = \lambda/d\lambda$) of SMIRFS and CGS4 without SMIRFS. The SMIRFS resolutions were calculated from the mean FWHM of a

number of emission lines. In the H and K bands the sky OH^- emission lines were used. However, in the J-band it was necessary to use emission lines from the dome light as non of the J band sky frames had skylines of a suitable intensity. The CGS4 resolutions were taken from the CGS4 users guide. The spectrograph was configured with the short focal length camera (150mm), the 75 l/mm grating and the grating set to 1st order.

Central Wavelength	R_{max} with CGS4 Alone	CGS4 slit width	R_{max} with SMIRFS	CGS4 slit width
1.2μm	~ 235	2 pixels	220±40	4 pixels
1.7μm	~ 330	2 pixels	300±35	4 pixels
2.2μm	~ 430	2 pixels	470±45	2 pixels

Table 8.4. Spectral resolution using the 150mm camera and 75 l/mm grating.

The resolution with SMIRFS is similar to that with CGS4 alone. Both the J and H band resolutions, for SMIRFS, are slightly lower which is to be expected as the fibre image size is larger than 2 pixels. The K band resolution is higher for SMIRFS but the circular fibre image is vignetted by the CGS4 slit. Thus the average width of the fibre image will be slightly less than 2 pixels.

8.6 Effectiveness of sky subtraction

During the SMIRFS commissioning the sky subtraction technique used was beam switching. In order to assess the effectiveness of this technique spectroscopic standard star frames were used. The data for the standard star had two object frames, one taken at the start of the sequence and one at the end (i.e. the forth frame). The second and third frames were sky frames in which all the fibres pointed at sky. The object frames contained one fibre that sampled the standard star, while the other 13 fibres viewed sky. The sky field was typically 10 arcminutes from the standard star field. A spectrum was extracted from one of the 13 fibres in the object frame that monitored sky. This spectrum was then compared with the spectrum extracted from the same fibre in the beam switched sky frame, showing how the sky varied between the two spatially and temporally separate regions. First, the beam switch sky spectrum was subtracted from the object frame sky spectrum. Then the rms. residuals that resulted were compared to the expected Poisson noise derived from the original mean sky counts. The photon noise

represents the absolute theoretical minimum sky residuals you could expect in an ideal system and thus provides a good comparison point for the effectiveness of the sky subtraction.

The counts were given in ADU's and in the J and H bands each frame was a combination of 20 x 2.0 secs exposures. This was to prevent the detector saturating and also has the effect of increasing the signal to Poisson noise by a factor of $\sqrt{20}$. To convert the ADU's into counts they were multiplied by the detector gain. The Poisson noise from N counts would normally be $\sqrt{N}$, but two frames were subtracted to get the sky residuals so the noise would increase to $\sqrt{2N}$. However each frame was composed of 20 co-added exposures so the Poisson noise would therefore be $\sqrt{2N \div 20}$. The ratio of mean sky residuals to the expected Poisson noise for the J, H and K bands are shown in Table 8.5 below.

Wave band	**Wavelength range**	**Ratio of sky residuals to expected Poisson noise**
J	1.15 - 1.35 μm	12.27 : 1
H	1.50 - 1.80 μm	4.91 : 1
K	2.00 - 2.20 μm	1.45 : 1

Table 8.5. Sky subtraction efficiency for SMIRFS using beam switching.

It is important to mention that the observations used to calculate the effectiveness of the sky subtraction were taken close to sunrise and with scattered high cloud; no other suitable data were available for the calculation. The sequence of frames was taken in the K band then H and finally J. The K band frames were taken about 35 minutes before sunrise, the H band ~ 25 minutes and the J band ~ 10 minutes before sunrise. The final frame in the J band started only 3 minutes before expected time for sunrise in Hawaii.

The K band residuals compare well with the Poisson noise limit being only 1.45 times larger. The region 2.0 - 2.2 μm was chosen instead of the region around the centre of the K band as this contained some sky emission features and was not completely dominated by the thermal background as it is longward of 2.2 μm.

The sky subtraction in the H band is not as good as that in the K band, however the H band region is full of strong sky emission line features that can vary significantly over short time scales. You would not expect the sky subtraction in this region to be as good as the thermally dominated K band and changes in sky brightness due to the approaching sunrise are more likely to effect the H band. An increase in the mean sky counts of 14% was noted between the first and last H band frames. This would contribute to the increase in sky subtraction residuals as well as the temporal changes in the emission line strengths and the inherent problems of effectively subtracting emission line features. Unfortunately the poor quality of the original data makes an accurate assessment of the sky subtraction very difficult and the figures would likely improve in better observing conditions (i.e. less cloud and sunlight).

The J band sky subtraction results are very poor when compared to H and K, however the mean sky counts increased by nearly 70% during the course of the exposures so these results are not surprising. This increase in counts is most likely a result of the imminent sunrise and a more realistic result could be obtained with better data.

It is difficult to draw a strong conclusion as to the effectiveness of beam switching for sky subtraction for SMIRFS as the data was so poor, however the H and K band results suggest that good sky subtraction could be obtained with this method. Further data taken in better observing conditions and with a larger number of observations should provide improved estimates of the sky subtraction accuracy obtainable with SMIRFS.

8.7 K-band spectra of bright K & M Giants

As part of the SMIRFS commissioning we planned to obtain K band spectra of bright K & M giants in a number of metal rich Galactic globular clusters and in the Galactic Bulge. The aim was to obtain metallicity estimates for these old populations in order to establish the evolutionary state of the Galactic Bulge. One major advantage of studying these stars in the K band is that there are a number of neutral metal lines that are relatively free from molecular absorption, such as TiO absorption which dominates the visible spectra. Relatively little reduction of the stellar spectra has been done, but figure 8.9 shows a SMIRFS spectrum of a K ~ 9.5 giant in NCG6553. The NaI and CaI metal features are visible as well as the CO bands beyond 2.3μm.

Sky subtraction for this spectra was performed using offset sky exposures. However, a number of fibres in each field were dedicated sky fibres providing accurate monitoring of any temporal variations. Originally it was planned to investigate optimal sky subtraction techniques (see chapter 3) but the adverse observing conditions prevented a meaningful study.

8.8 Data reduction

The initial data reduction was performed using the CGS4 data reduction software "CGS4DR". The detector was dithered by 1/2 a pixel and the two frames were then interleaved to produce two data points per pixel. A pixel mask was applied that contained most of the bad pixels, however, as the array is relatively new there are some bad pixels that are not present in the mask. These are usually clearly evident when the frame are displayed but they were ignored when reducing the data presented in this chapter. The software carried out first order wavelength calibration based on the central wavelength requested by the operator and the dispersion. In the middle of the array this should be accurate to about 2 pixels. However, as the CGS4 slit rotation mechanism was faulty, the fibre spectra were angled across the detector introducing a shift wavelength along the length of the slit.

The interleaved, pixel masked and roughly wavelength calibrated frames were further reduced using "FIGARO" as it is proved a more flexible system for dealing with multiple spectra than CGS4DR. The wavelength shift along the fibre slit was corrected as the spectra were extracted. Fibre 7 was assumed to be at nominally the right wavelength and the other spectra shifted to match. The amount of shift was gauged using the sky lines. The shift was measured on a few sky frames to get a good gauge of the shift for each fibre. The shift was found to be 0.05μm along the length of the slit. Once the shift for a set of rows was estimated the same shift was applied every time spectra were extracted. For the results presented it was not necessary to perform a more rigorous wavelength calibration.

8.9 Summary

The alignment of the various components of SMIRFS can have a significant effect on the throughput of the system. The throughput results give an indication of how

successfully the system has been aligned. Though the observing conditions were never ideal we were able to obtain some valuable data from the commissioning of SMIRFS at UKIRT. The mean throughput was ~ 62% using the zirconium fluoride fibre bundle and ~ 41% using the silica. The ZrF_4 compared well with the minimum throughput estimates. The low value for silica was most likely the result of the mis-alignment of the fibre slit. It was concluded that alignment errors and reflection losses were the major contributors to the throughput losses. A comparison of thermal background from the system was made, with and without SMIRFS. This peaked at ~2.3μm where the background signal was about 4 times larger with SMIRFS installed, than without. The spatial resolution estimates were made for SMIRFS using the FWHM of emission lines. The resolution with SMIRFS was close to the resolution expected of CGS4 and a 2 pixel slit width. The beam switching sky subtraction technique was assessed for SMIRFS and the residuals varied between 1.45 (K band) to 12.27 (J band) times the expected Poisson noise for the sky counts. However, the observing conditions were far from ideal being close to sunrise and slightly cloudy. It is likely that the results can be improved with better data, particularly in the J and H bands. An example spectra is presented showing NaI and CaI neutral metal lines. However, the guide fibres system developed for SMIRFS was not very successful. A number of the fibre broke close to the input ferrule, which will require re-designing for future use. Also, the whole system was photon starved and was unable to detect most of the guide stars. The detection system will need to be redesigned, particularly with the dichroic upgrade planned for UKIRT.

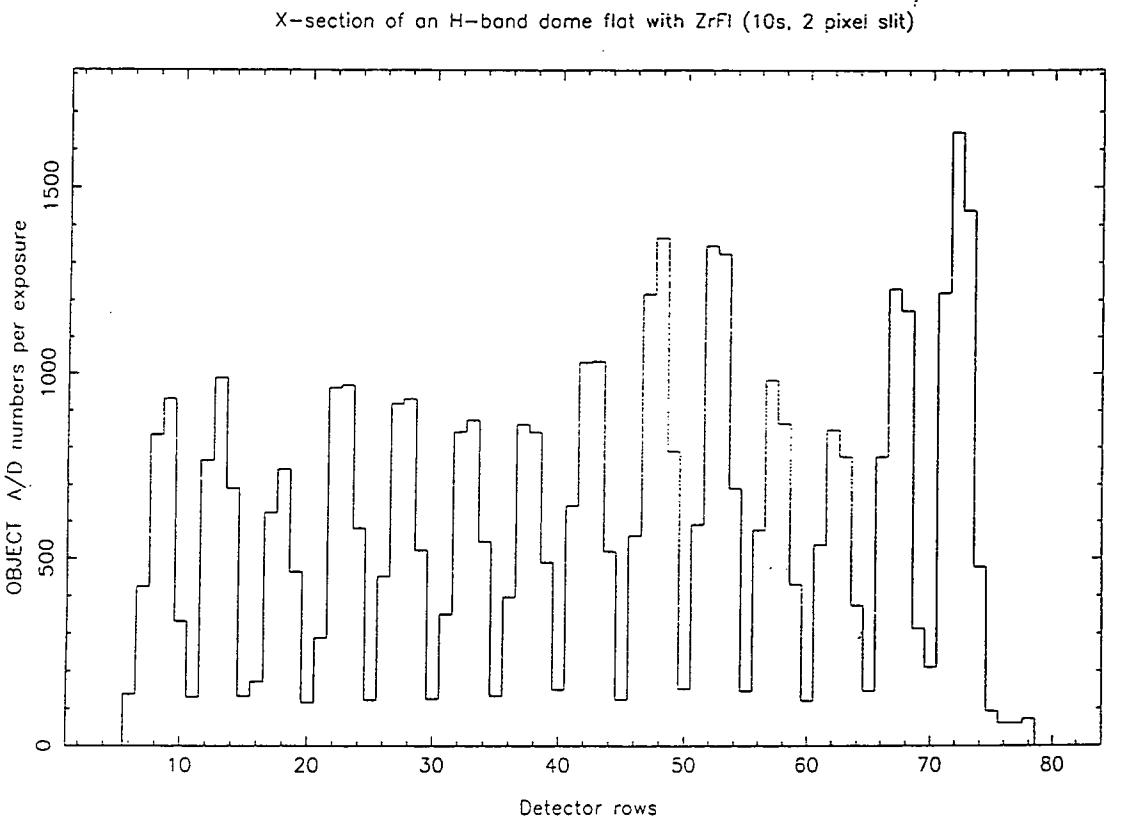

Figure 8.1 A vertical slice from an H band dome flat taken with the SMIRFS zirconium fluoride fibre bundle. The slice is one pixel wide and in the non-dispersive direction. The peaks correspond to the different fibres, starting with fibre 14 on the far left, through to number 1 on the far right. However, as the CGS4 slit was tilted relative to the elements of the spectrograph array, there is a shift to longer wavelengths as the detector row number increases.

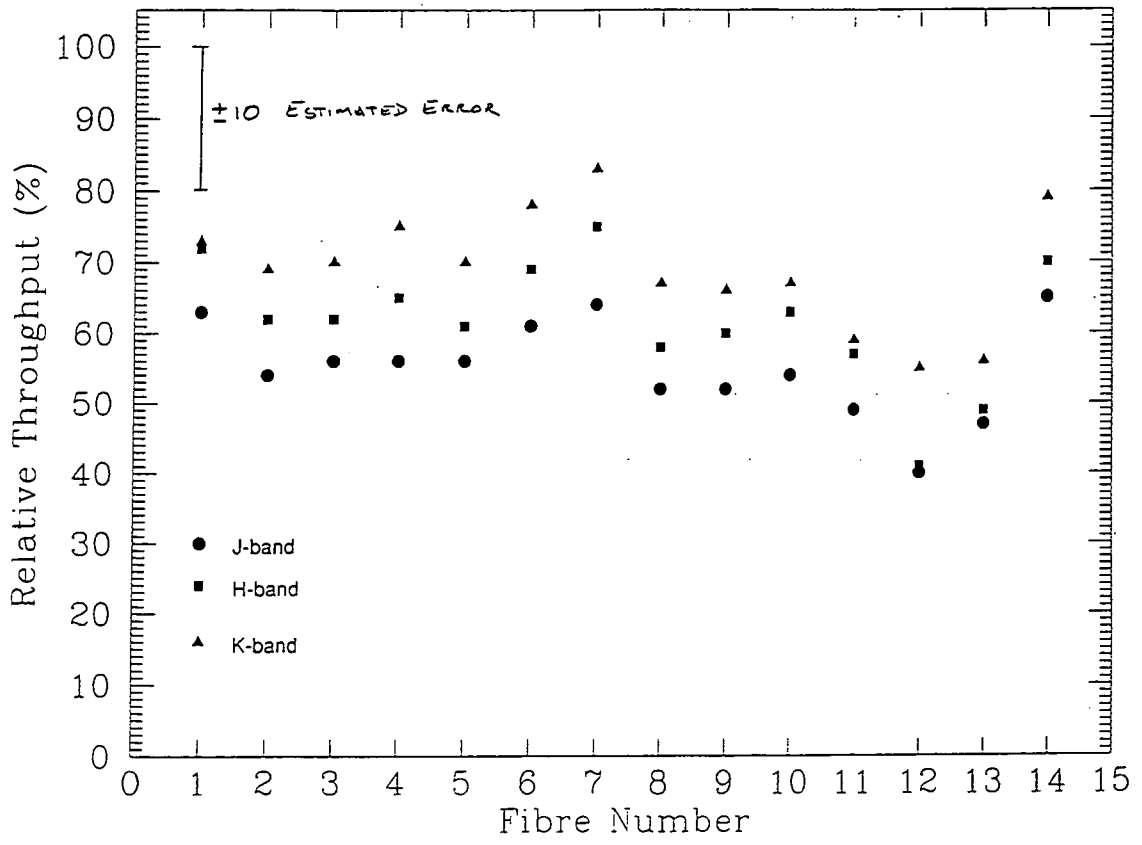

Figure 8.2 The relative throughput for SMIRFS with the zirconium fluoride fibre bundle. The throughput was calculated from dome flat data taken in the J, H and K bands and compared to the throughput of the system without SMIRFS.

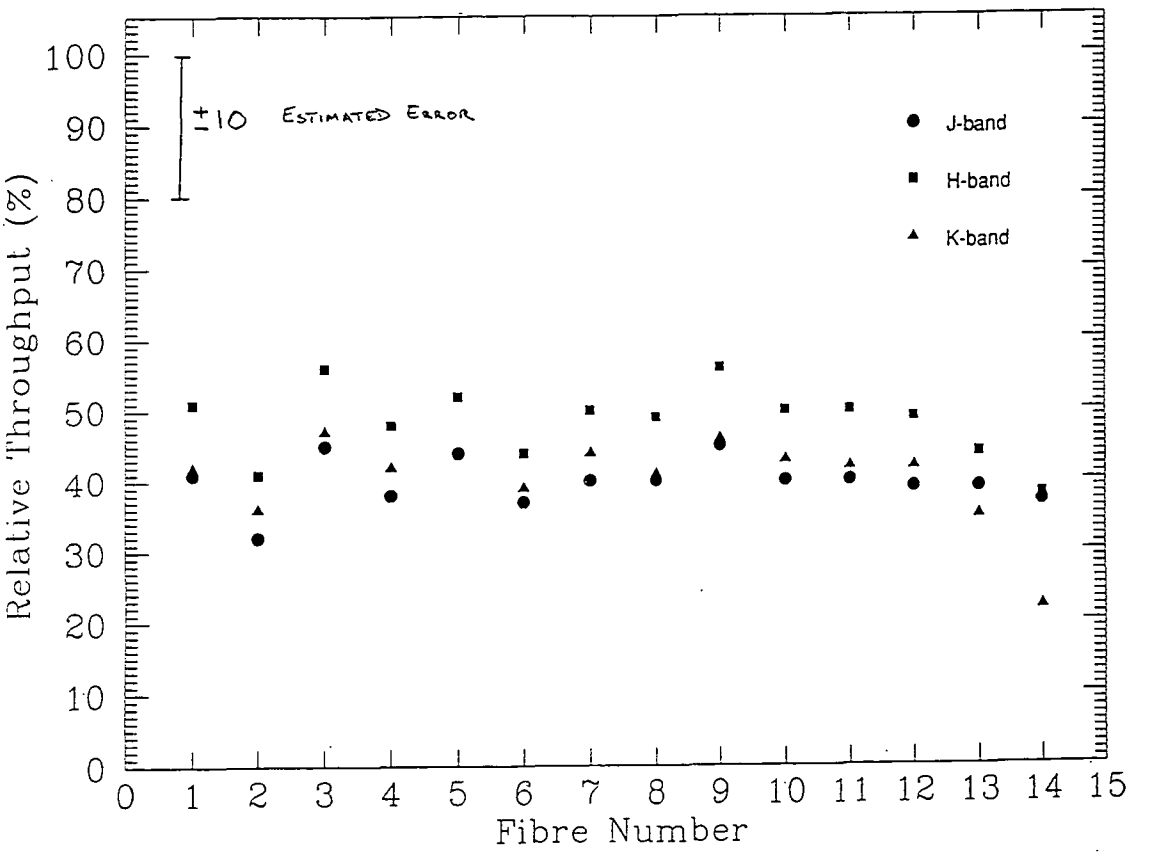

Figure 8.3 The relative throughput for SMIRFS with the silica fibre bundle. The throughput was calculated from dome flat data taken in the J, H and K bands and compared to the throughput of the system without SMIRFS.

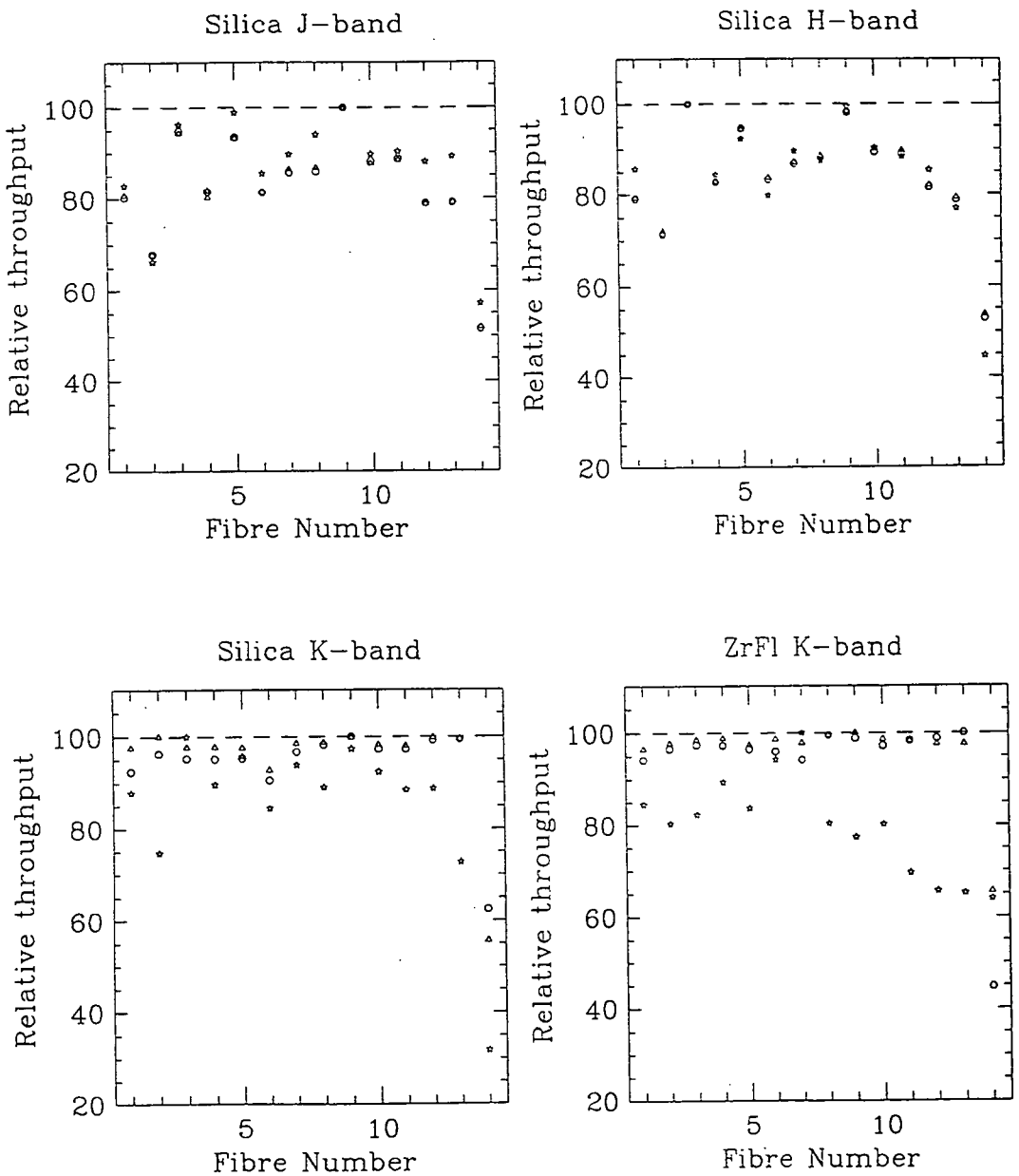

Figure 8.3a The relative fibre throughput figures for SMIRFS. The open circles and triangles are sky frame data. The stars are the dome flat data. The top left plot contains the J band results using the silica fibre bundle. Top right is the H band with the silica bundle. Bottom left is the K band with the silica bundle. Bottom right is the K band results using the ZrF_4 fibre bundle.

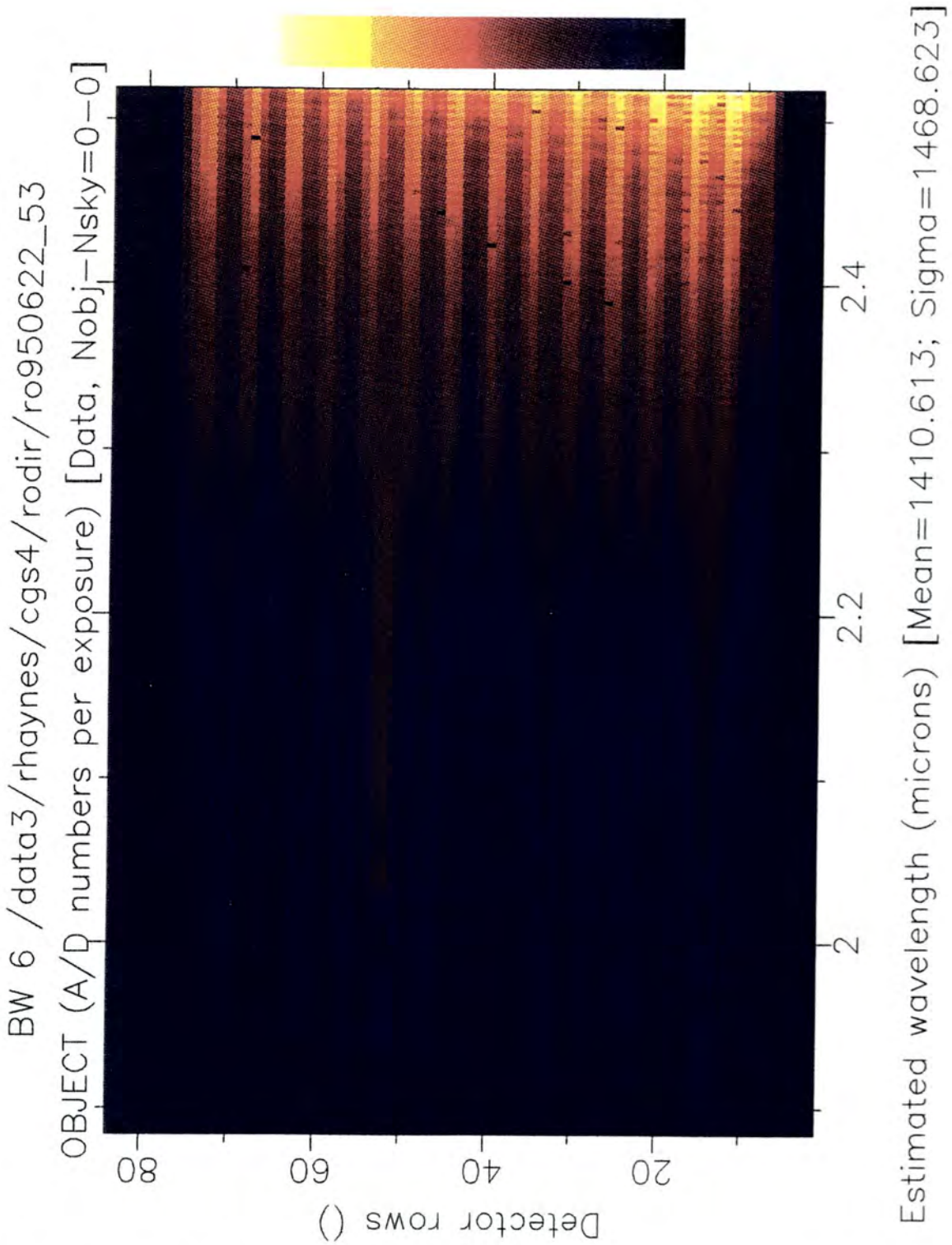

Figure 8.4 A K-band frame of giant stars in the globular cluster NGC6553 taken using SMIRFS. There has been no sky subtraction. The brightest star in the field is K ~ 9.5, in rows 51-53. The thermal background from the fibre slit material can be clearly seen beyond about 2.3μm.

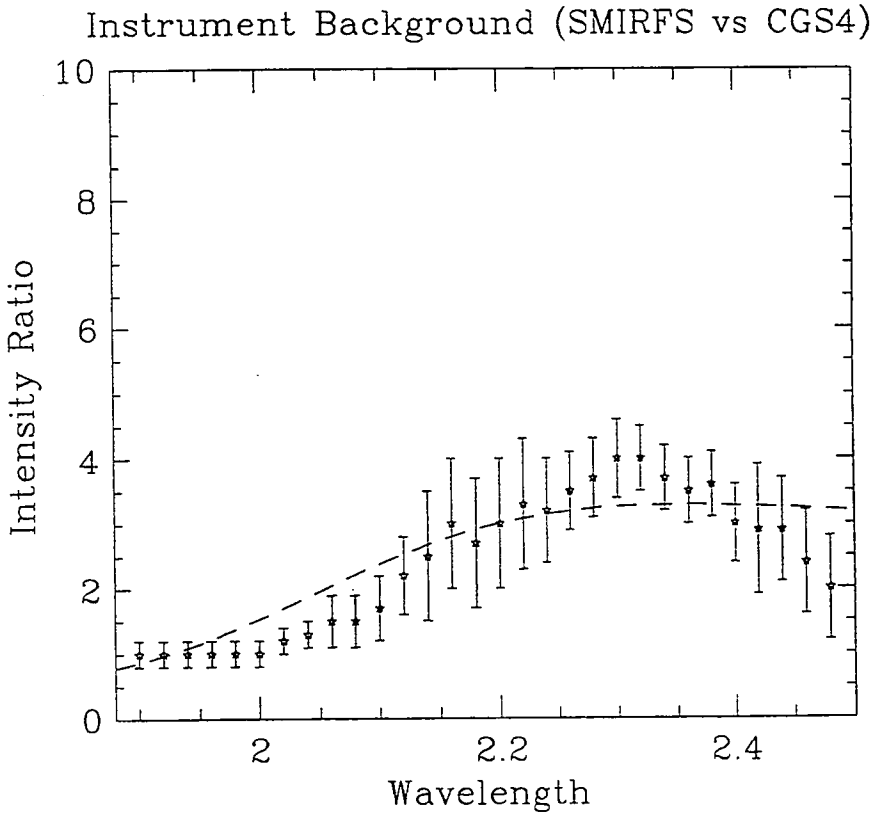

Figure 8.5 The ratio of instrument background with and without SMIRFS, for the K band. The results compare the signal of a sky exposure taken with SMIRFS to a sky exposure taken with CGS4 only.

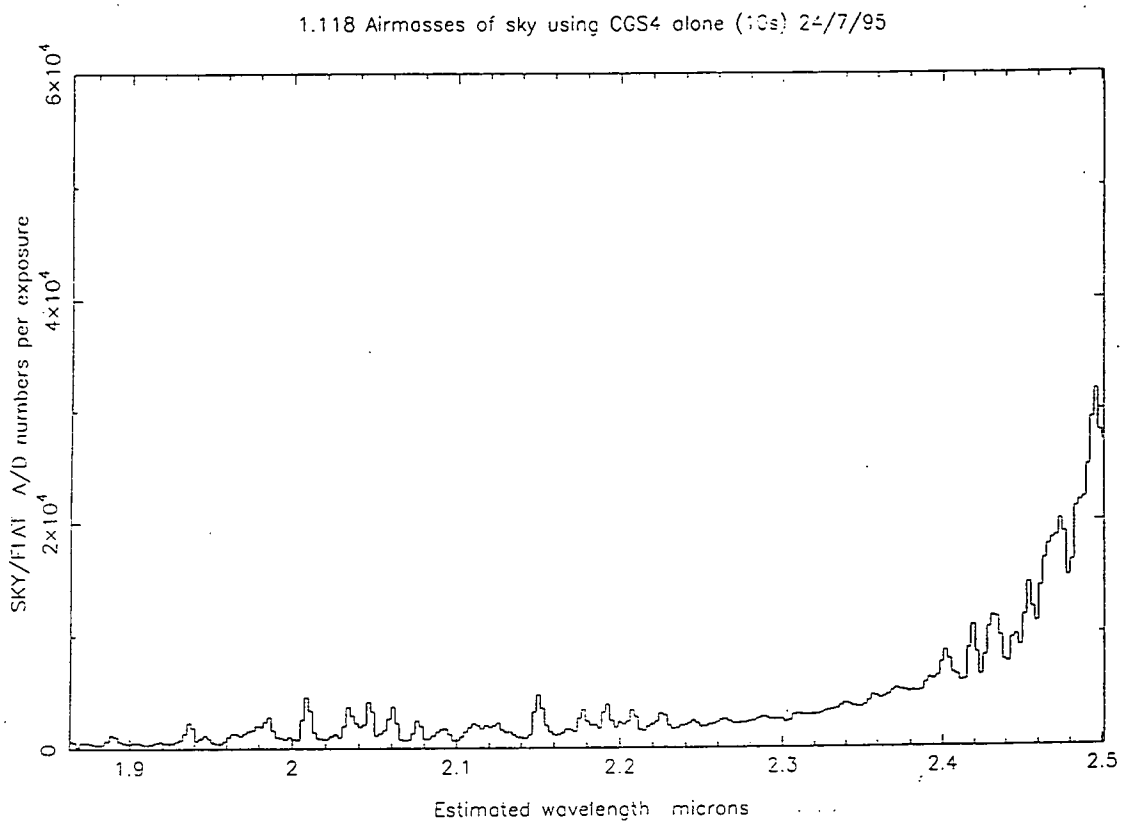

Figure 8.6 The signal extracted from rows 41-44 of a K-band sky exposure taken with CGS4 only.

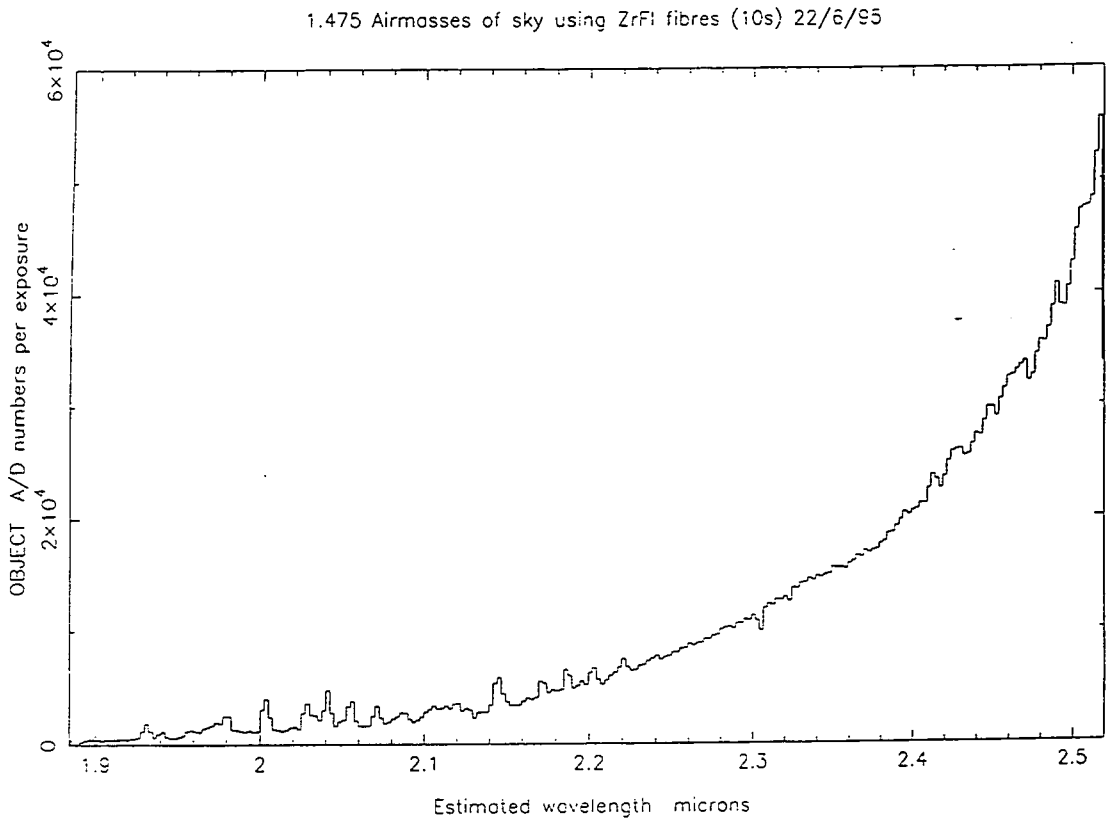

Figure 8.7 The signal extracted from rows 41-44 of a K-band sky exposure taken with SMIRFS.

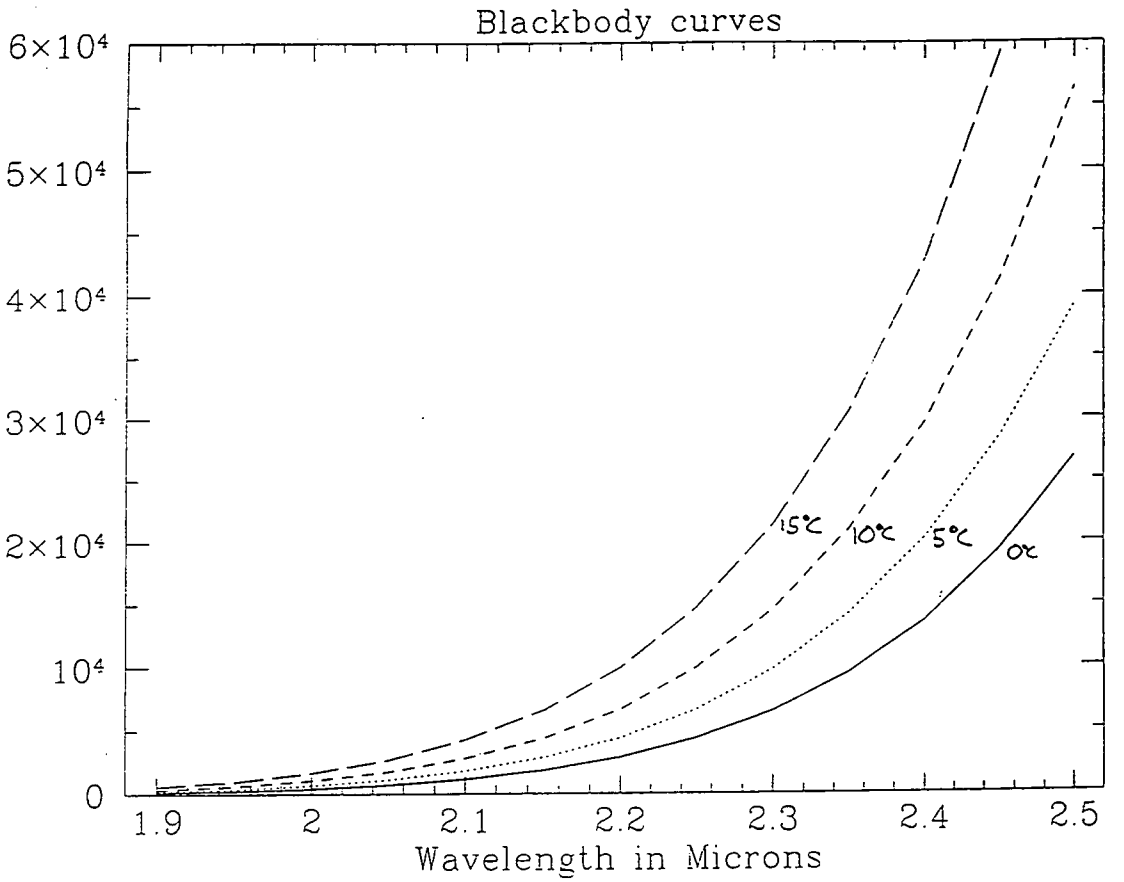

Figure 8.8 A plot of blackbody curves for a blackbody with a temperature ranging from 0 to 15°C. The vertical axis units are arbitrary.

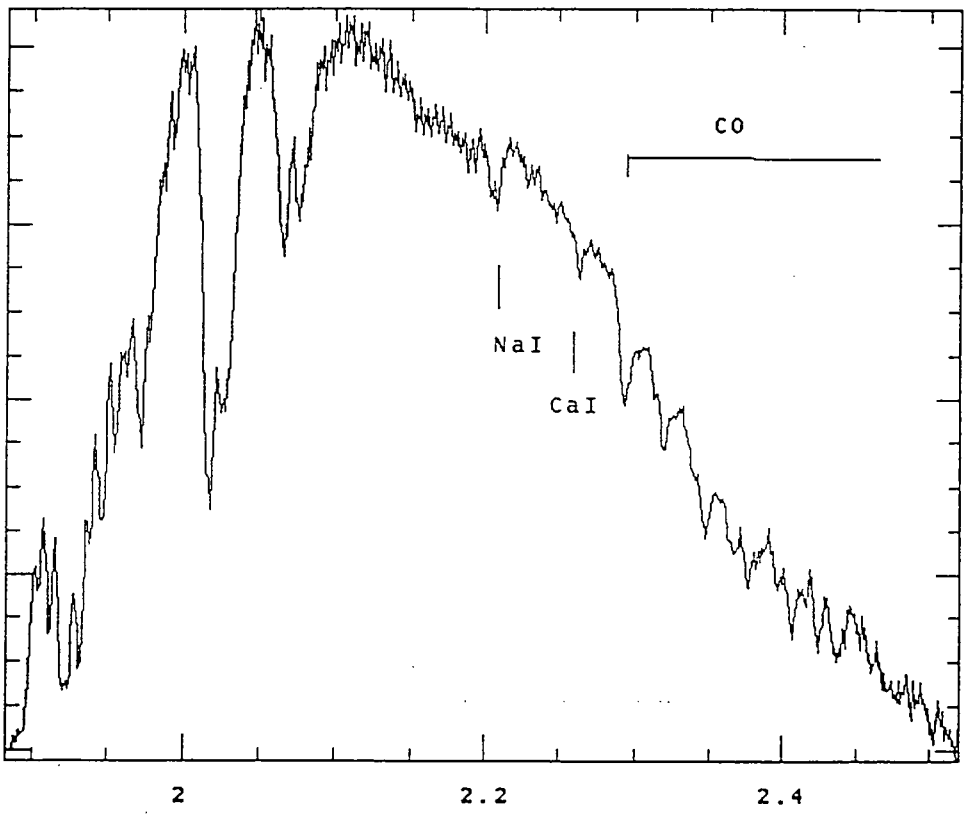

Figure 8.9 A K-band spectrum of a giant star in the globular cluster NGC6653. It shows the neutral metal absorption and CO lines.

Chapter 9: Further development of IR fibres

The potential for the development of fibres in infrared spectroscopy is very significant. The development of 2 dimensional infrared arrays, which are already in common use in a 256x256 format and will shortly be available in a 1024x1024 array format, permits such systems to be developed with a large number of fibres. Assuming detector sampling of the fibre in the region of 2-3 pixels per fibre, as suggested by sampling theory, and allowing a 1 pixel gap between the fibre spectra, to reduce the risk of spectral contamination from adjacent fibres, the fibres may be arranged on 5 pixel centres. For a 1024x1024 array more than 200 fibre spectra could be accommodated on one array, and over 50 on the current 256x256 arrays. This could lead to massive multiplex gains when taking multiple spectra in a limit field.

9.1 Multi-object spectroscopy

The wavelength region from 0.5-1.8μm is free from the thermal background constraints which tend to dominate the region beyond 2μm and is readily accessible using 'dry silica' fibres. These low OH^- silica have attenuation characteristics of less than 50dB/km (~ 1% loss/m) over the whole region and significantly less over most of this range (see chapter 2). This means that fibre bundles of tens of meters can be constructed without too great a throughput loss. This frees up the position of the spectrograph which can then be floor or bench mounted. This allows the development of more massive instruments which will not suffer the flexure problems traditionally associated with telescope mounted instruments. These 'dry silica' fibres can be handled and prepared in the same way as the current generation of silica fibre employed in the visible region. If a suitable spectrograph was available, it should be a relatively simple task to manufacture a fibre bundle for the near-IR J and H bands for the current generation of multi-fibre robotic positioners. Such a system could be developed for AUTOFIB2, for example. Ian Parry (I.O.A., Cambridge) has suggested a system using FOCAP and IRIS at the AAT. Fibres are also available that have both a blue and infrared enhanced response; these could possibly replace the current generation of fibres. However their UV response is not as good as some of the silica fibres in current use.

9.2 Integral field spectroscopy

Another area in which infrared fibres could be employed is in integral field spectroscopy in which a number of fibres are closely packed together at the telescope focal plane and are re-formatted at the fibre output into a slit. This then acts as the spectrograph entrance slit and enables the simultaneous gathering of spectra from the series of contiguous sub-apertures that divide up an extended source. As only one target is being studied accurate fibre positioning systems are not required. The fibre bundle can be fixed in the centre of the field plate and the target aligned using the telescope guiding system. Exact alignment is not critical since the pointing can be determined in the data reduction. These integral field units (IFU's) can give valuable information on internal dynamics and composition of the object. One such system, IR ISIS (Dallier *et al.* 1994), has been developed to work at the CFHT, utilising the RedEye camera as the detector for the spectrograph.

9.2.1 An IFU for UKIRT

Such studies can be achieved using conventional long slit spectroscopy but this can prove to be very time consuming as they can only sample a thin slice of the object in each exposure whereas the fibres can sample the whole object in one exposure. These integral field fibre bundles can be used to feed existing long slit spectrographs as well as purpose-built fibre spectrographs. Such a system has been proposed for UKIRT as an upgrade to the SMIRFS. This would provide the CGS4 spectrograph with an 2-dimensional spectroscopic option with very little operational overheads. Initially it would be designed for the J & H bands using 'dry' silica fibres with 0.8 arcsec sub-apertures. The output slit would be arranged such that adjacent fibres at the telescope focal plane would also be adjacent along the slit. This allows the spectra to be closely packed as any contamination from adjacent spectra would be from a region spatially adjacent and therefore likely to be very similar. This means that it is not necessary to leave any 'dead space' between the spectra.

If the 300mm camera is used in CGS4, the pixel scale is ~0.61 arcsec/pixel which allows a minimum fibre to fibre pitch of 2 pixels allowing a maximum of 128 fibres. At the moment a regular hexagonal array of 61 fibres at the input which has a pitch of 4 pixels per fibre is proposed. This would sample a roughly circular area ~ 7.2 arcsec across.

However, extended sources are not necessarily symmetrical, in which case a hexagon would not be the most effective arrangement of the fibres. A rectangular shape for example, would enable the major axis of the source to be aligned with that of the fibre array. This might provide more efficient sampling of the source than a hexagonal array made with the same number of fibres.

It has been noted previously within this thesis (chapters 5 & 6) that fibres are not suited to coupling slow optical beams, so it is necessary to couple the fibres to the telescope and the spectrograph using microlenses. At the telescope focal plane (~f/36) a lenslet array will be used to both couple the fibre at a fast beam speed (~ f/5) and remove the problem of dead space between the fibres that results from packing cylinders together. This also reduces the losses into the fibre cladding. The typical packing efficiency for an unlensed system is ~ 60% or less depending on the cladding thickness. With the microlens array it is possible to achieve ~ 100% filling factor so the light from the source is continuously sampled. The output from the fibres couples to the f/36 of the spectrograph via one or more linear microlens arrays forming a slit. The image of the fibre slit is then projected into CGS4 using the SMIRFS slit projection unit (see chapters 6 & 7) in the same way that the multi-object fibre bundles are imaged.

The technology for coupling microlens arrays to fibre bundles is a relatively new one and requires significant research and development. However, it appears feasible. Similar systems to the UKIRT IFU could be designed for the next generation of instruments: 8-10 meter class of telescopes with more fibres and finer sampling which could take advantage of the large arrays and better image quality. An example of an extended object (NGC 4151) being sampled by a 217 aperture lenslet array is shown in figure 9.1. The apertures are 0.25 arcsec across and are chosen to match the image quality that will be available with the ELECTRA adaptive optics system being developed by Durham University Astronomical Instrumentation group.

9.3 K band fibre spectroscopy

The use of infrared fibres in the K band is not as simple as in the J and H bands for two reasons. First, since silica fibres start to attenuate heavily beyond ~ 1.8μm it is necessary to use ZrF_4 glass fibres for this region unless only very short length fibres are required

and throughput can be compromised. These fibres display excellent throughput characteristics at these wavelengths but are currently about 30 times the price of silica fibres and require careful preparation and handling (see chapter 2). Secondly, and more significantly, is the problem of contamination from the thermal background from any 'warm' objects in the optical path (see chapters 4 & 8). With SMIRFS this contributed significantly to the signal during the first commissioning run in June 1995 and needs to be addressed further. The thermal emissivity calculations (chapter 4) suggested that the thermal background from the fibres themselves should not contribute significantly to the background but this has yet to be thoroughly tested and backed up with results. The area that did contribute significantly to the thermal background was the 'warm' material of the slit block between and around the fibres. It appears necessary to cool the fibre slit to reduce the thermal emissions from the slit block. A drop in temperature to ~ -30°C should be sufficient to reduce the background to negligible levels compared to that from the telescope. It may be advantageous to cool the whole slit projection unit as this will also reduce the emission from the mirrors. However, it is not yet clear if it will be necessary to cool the fibres themselves; further tests need to be carried out. The development of fibre systems based on ZrF_4 fibres would provide J, H and K bands coverage. These could be similar to the system developed for the J and H band using silica fibre. However, the cooling requirement adds an extra level of complexity that is not required in the J and H bands systems.

9.5 Summary

With advances in the large format infrared arrays it should be possible to develop multi-fibre systems with up to 200 fibres or more for the J and H bands which can utilise the current fibre robot manipulation systems. These can be used to feed infrared spectrographs designed for long slit spectroscopy or purpose built instruments. The same spectrographs could also be fitted with fibre integral field units providing area spectroscopy capability with minimal operational overheads. The multi-object fibre bundle and slit would be replaced by the IFU unit. The technology for J and H band fibre spectroscopy has already been proved. The spectral range of these instruments could be extended to the K band using ZrF_4 fibres but it is unclear whether it will be necessary to

cool the fibres, in addition to the relay optics, to reduce thermal emissions contributing to the background. Further experimentation is required in this area.

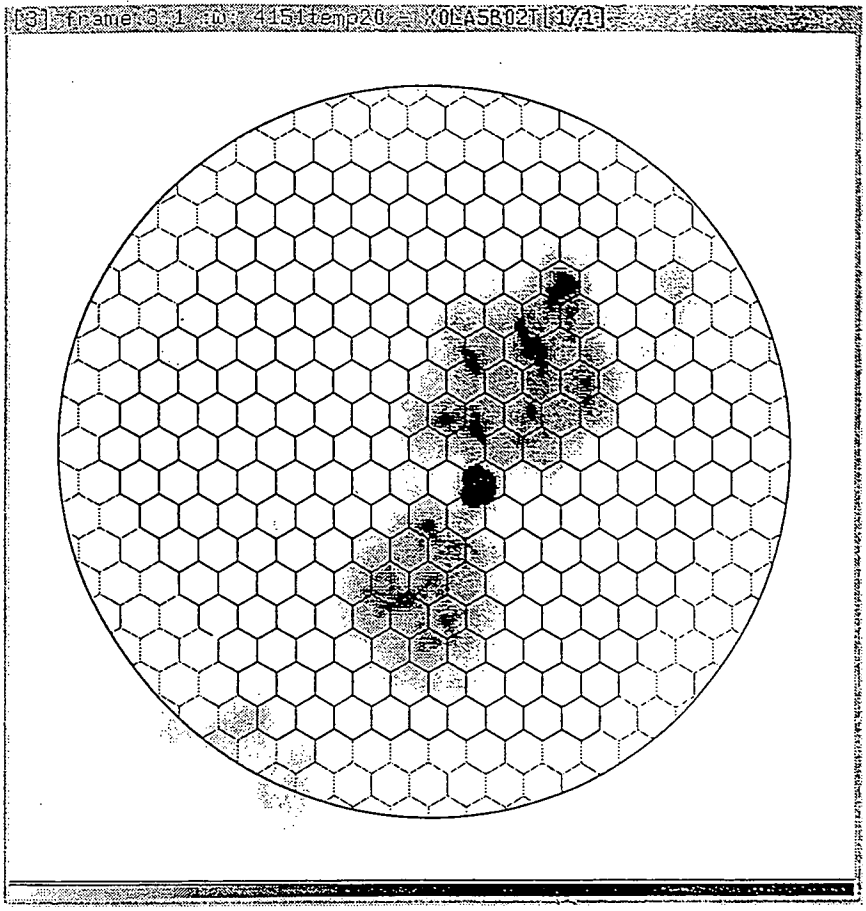

Figure 9.1 The nuclear region of NGC 4151 observed using the HST, at a resolution of 0.1", overlaid with a regular lenslet array of 217 apertures each 0.25" across.

Chapter 10: Conclusions

The aim of my research was to investigate the feasibility of using fibres for spectroscopy at near-IR wavelengths, primarily in the 1-2.5μm region. Conventional silica fibres, typically used for fibre spectroscopy in the visible region, are unsuitable for all the near-IR so different fibre materials were investigated. There are two fibre types that have good transmission characteristics in this region, they are Low OH^- Silica fibre which performs well from 0.4 ~ 2.0μm and zirconium fluoride (ZrF_4) fibre that performs well from ~ 1-3.6μm. Samples of these fibres were obtained and tested. Both fibres displayed favourable inherent throughput and FRD characteristics. For short lengths of fibre (< 10m), throughput losses are dominated by Fresnel reflection at the fibre ends. The fibre losses are also affected by the fibre end finish quality. However if care is taken with the polishing process these losses are minimal. For the 1.2m long SMIRFS fibres the mean throughput was measured to be 92.4% for the ultra low OH^- silica fibres and 86.2% for the zirconium fluoride fibres, at a wavelength of ~ 0.9μm. This is mainly accounted for by Fresnel reflection losses. These are approximately 3.1% for silica and ~ 4.0% for ZrF_4, at each surface. The FRD of the SMIRFS fibres was found to degrade an f/5 input beam to produce an output beam of f/4.4±0.3 for the silica and f/4.2±0.3 for the ZrF_4 fibres.

To couple the f/36.3 beam of UKIRT to the f/36.3 beam required by CGS4, microlenses were used at both the input and output of the fibres. These microlenses converted the focal ratio from f/36.5 to ~ f/5 at the fibre input and back to f/36.3 at the output. This reduced the amount of FRD induced in the fibre which is significantly worse with slow input beams. Two methods of microlens coupling were investigated: direct re-imaging in which the telescope focal plane image is re-imaged on the fibre input face and pupil imaging in which the telescope pupil is imaged onto the fibre face. For SMIRFS the pupil imaging had the advantage that it provided a well defined output focal ratio. Also it has the advantage over direct re-imaging in that the fibre's output image is sensitive to the input image size. However, the fibre aperture is poorly defined, being fixed by the numerical aperture of the fibre or the diameter of the microlens. This differs from direct re-imaging in that the fibre aperture is set by the fibre core diameter and magnification of the microlens.

Two fibre bundles were made for SMIRFS; one from the ultra low OH^- silica fibre for use in the J and H bands, and one of ZrF_4 for use in the K band.

The thermal emissions from the fibres in the K band needs to be considered. The emissivity of fibres is proportional to one minus their transmission and is typically a few percent. Thus, for short lengths of ZrF_4 fibre thermal emission should be small compared to that from the telescope and instrument structure. Data, from the commissioning of SMIRFS at UKIRT, was used to estimate instrument thermal background. At its peak, the background signal in the K band was about 4 times larger with SMIRFS installed than without. The contributions to the background signal were dominated by thermal emission from the fibre slit material which contaminated the fibre signal. The thermal emissions from the fibres alone needs to be investigated further so that a value can be derived without any contamination from the slit material.

The throughput of the SMIRFS system was also investigated during the commissioning run. The mean throughput using the ZrF_4 fibre bundle was ~62% which compared well with the minimum throughput estimate of ~60%. The mean throughput of the silica fibre bundle was ~41%, lower than the estimated minimum of ~61%. There were however significant fibre to fibre variations. These variations are unacceptably large and need to be reduced. I believe these are due to alignment errors from both fibre pointing and the fibre alignment at the slit, however further investigation is necessary to minimise the problem. Mis-alignment of the fibre slit is, most likely, the cause of the poor silica fibre bundle throughput results.

The SMIRFS commissioning results, on the whole, were very encouraging and it is planned to further develop the system. The thermal background contamination from the fibre slit, in the K band, needs to be reduced. This is likely to be achieved by cooling the fibre slit, and possibly the slit projection unit including slit projection optics. Also an integral field unit (IFU) is planned. This will consist of a compact array of fibres fed by a microlens array that will provide a means of doing 2 dimensional spectroscopy of extended sources. Initially, it will be made from 'dry' silica fibres for the J and H bands. It will have 61 sub-apertures, each 0.8" across, making it approximately 7.2" across in

total. Before a K band device is built the thermal emissions from the system need to be reduced.

Infrared IFU devices could be developed for the next generation of infrared spectrographs for the 8-10m class of telescopes, but fibre IFU's are a relatively new idea and a great deal of work needs to be carried out before such systems become readily available. However, if suitable spectrographs are available, an area in which infrared fibres could be used is in the current generation of multi-fibre systems. With relatively little investment it would be possible to build fibre bundles using 'dry' silica fibre, which when coupled to a suitable infrared spectrograph could provide a J and H band multi-object capability.

SMIRFS and ISIS-IR (Dallier *et al.*, 1993) are the first astronomical instruments to use fibres for infrared spectroscopy. Though such systems are still in their infancy, they have provided encouraging results. These suggest there could be considerable development of infrared systems based on both 'dry' silica and zirconium fluoride fibres.

References

Allington-Smith J., and Zhang J.,'Intergral field spectroscopy with the GEMINI multiobject spectrographs' *Proceedings of the International Symposium on the Scientific and Engineering Fronties for 8-10 m Telescopes*, M. Iye and T. Nishimura, Editors, Unverersal Academy Press Inc., Tokyo, Japan, 205-210, (1995).

Angel J. R. P., Adams M. T., Boroson T. A., Moore R. L.,'A very large optical telescope array linked with fused silica fibers' The Astrophysical Journal, no. 218, 776-782, (December 1977).

Barden S. C.,*Instrumentation for Ground Based Optical Astronomy*, L. B. Robinson, Editor, Springer Verlag, New York, 250, (1987).

Barden S. C., Elston R., Armandroff R., Pryor C.,'Observational Performance of Fiber Optics - High Precision Sky Subtraction and Radial Velocities' *Fiber Optics in Astronomy II*, Peter M. Gray, Editor, Astronomical Society of the Pacific Conference Series, Vol. 37, 223-234, (1993).

Baudrand J., Casse M., Jocou L., Lemonnier J.,'Fiber link for the FUEGOS high-resolution multiple fiber spectrograph' *Instrumentation in Astronomy VIII*, David L. Crawford, Eric R. Craine, Editors, Proc. SPIE 2198, 1071-1082, (1994).

Bingham R. G., Gellatly D. W., Jenkins C. R., Worswick S. P.,'Fiber-fed spectrograph for the 4.2m William Herschel Telescope' *Instrumentation in Astronomy VIII*, David L. Crawford, Eric R. Craine, Editors, Proc. SPIE 2198, 56-64, (1994).

Broadhurst T. J., Ellis R. S., Glazebrook K.,'Faint Galaxies: Evolution and cosmological curvature' Nature, no. 355, 55-58, (January 1992).

Carr J. S., Tokunaga A. T., Najita J., Glassgold A. E.,'Infrared spectroscopy of disks around young stellar objects' *Infrared Astronomy with Arrays: The next generation*, Ian S. McLean, Editor, 53-56, (Netherlands, 1994).

Carrasco B. E.,'Further developments of optical fibre techniques for astronomical spectroscopy' (University of Durham, PhD. thesis, 1992).

Chandler C. J., Carlstrom J. E., Scoville N. Z., Dent W. R. F., Geballe T. R.,'High resolution spectroscopy of infrared CO emission from young stars' *Infrared Astronomy with Arrays: The next generation*, Ian S. McLean, Editor, 57-60, (Netherlands, 1994).

Coude Du Foresto V., Maze G., Ridgway S.,'Stellar Interferometry with Infrared Single-Mode Fibers' *Fiber Optics in Astronomy II*, Peter M. Gray, Editor, Astronomical Society of the Pacific Conference Series, Vol. 37, 285-294, (1993).

Dallier R., Baudrand J., Cuby J. G.,'Near IR Fiber Spectroscopy: First Results' *Fiber Optics in Astronomy II*, Peter M. Gray, Editor, Astronomical Society of the Pacific Conference Series, Vol. 37, 310-321, (1993).

Dallier R., Cuby J. G., Czarny J., Baudrand J.,'ISIS IR: The first infrared fibre-fed spectrograph' *Infrared Astronomy with Arrays: The next generation*, Ian S. McLean, Editor, 343-344, (Netherlands, 1994).

Dallier R.,'Spectroscopie astronomique infrarouge par fibres optiques et detecteurs bidimensionels' (University of Paris VII, PhD. thesis, 1995).

Davidge T. J., Lilly S. J., Roche P.,'The Number of Faint Objects in the Near-Infrared' GEMINI Project Newsletter no. 7. (January 1994), 29-30.

Epchtein N.,'DENIS: a Deep Near-Infrared Southern Sky Survey' *Infrared Astronomy with Arrays: The next generation*, Ian S. McLean, Editor, 227-230, (Netherlands, 1994).

Fowler A. M., Gatley I., Vrba F. J., Ables H. D., Hoffman A., Woolaway J. T.,'Next generation in InSb arrays: ALADDIN-the 1024x1024 InSb focal plane array development project status report' *Instrumentation in Astronomy VIII*, David L. Crawford, Eric R. Craine, Editors, Proc. SPIE 2198, 623-629, (1994).

France P.W., Drexhage M. G., Parker J. M., Moore M. W., Wright J. V.,*Fluoride Glass Optical Fibres*, Blackie, Glasgow and London, (1990).

Graham J. R., Herbst T. M., Beckwith S., Matthews K., Neugebauer G., Serabyn E., Soifer B. T.,'Photodissociation regions in young PN' *Infrared Astronomy with Arrays: The next generation*, Ian S. McLean, Editor, 69-72, (Netherlands, 1994).

Gray P. M., *Instrumentation in Astronomy*, Proc. SPIE 445, 57, (1983).

Guerin J.,'Optical Fibres for Astronomical Applications', *Fiber Optics in Astronomy*, Samuel C. Barden, Editor, Astronomical Society of the Pacific Conference Series, Vol. 3, 52-62, (1988).

Haynes R., Parry I. R.,'SMIRFS: an infrared multifibre spectroscopic coupler for UKIRT' *Instrumentation in Astronomy VIII*, David L. Crawford, Eric R. Craine, Editors, Proc. SPIE 2198, 572-577, (1994).

Haynes R., Sharples R. M., Ennico K.,'SMIRFS-An Infrared Fibre Feed for CGS4' SPECTRUM Newsletter of the Royal Observatories, no. 7, 4-6, (September 1995).

Heacox W. D.,'On the application of optical-fiber image scramblers to astronomical spectroscopy' The Astronomical Journal, Vol. 92, 219-229, (1986).

Heacox W. D, and Connes P.,'Optica fibers in astronomical instruments' The Asrtronomy and Astrophysics Review, Vol. 3, 169-199, (1992).

Hill J. M., Angel J. R. P., Scott J. S., Lindley D., Hintzen P., Proc. SPIE 331, 279, (1982).

Hill J. M., Angel J. R. P, Richardson E. H.,'Optical matching for fiber optics spectroscopy' *Instrumentation in Astronomy*, Proc. SPIE 445, 85-92, (1983).

Hill J. M., and Lesser M. P., Proc. SPIE 627, 303, (1986).

Hill J. M.,'The History of Multiobject Fiber Spectroscopy',*Fiber Optics in Astronomy*, Samuel C. Barden, Editor, Astronomical Society of the Pacific Conference Series, Vol. 3, 77-92, (1988).

Hodapp K. W., Hall D. N. B., Vural K., Kozlowski L.J., Bostrup G. L., Chen A. C., Cooper D. E., Bailey R. B., Cabelli S. A., Kleinhans W. E.,'Status report on 1024x1024 HgCdTe detector arrays for low-background operation in the 1.0 to 2.5 μm range', *Instrumentation in Astronomy VIII*, David L. Crawford, Eric R. Craine, Editors, Proc. SPIE 2198, 668-673, (1994).

Katsuyama T., and Matsumura H.,*Infrared Optical Fibers*, Adam Hilger, Bristol and Philadelphia, (1989).

Kleinmann S. G., Lysaght M. G., Pughe W. L., Schneider S. E., Skrutskie M. F., Weinberg M. D., Price S. D., Matthews K. Y., Soifer B. T., Beichman C. A., Chester T. J., Jarrett T., Kopan G. L., Lonsdale C. J., Elias J., Liebert J. W., Seitzer P.,'The two micron all sky survey' *Infrared Astronomy with Arrays: The next generation*, Ian S. McLean, Editor, 219-226, (Netherlands, 1994).

Klocek P., and Sigel G. H. Jr.,*Infrared fiber optics* Vol. TT2, SPIE Optical Engineering Press, Washington USA, (1989).

Levin K. H., Tran D. C., Mossadegh R.,'Properties and Applications of Infrared Fiber Optics' *Fiber Optics in Astronomy*, Samuel C. Barden, Editor, Astronomical Society of the Pacific Conference Series, Vol. 3, 23-25, (1988).

Levin K. H., Tran D. C., Kindler E., Glenar D., Mumma M. J., Joyse R.,'Infrared Fiber Arrays for Low Background Infrared Astronomy' *Fiber Optics in Astronomy II*, Peter M. Gray, Editor, Astronomical Society of the Pacific Conference Series, Vol 37, 295-309, (1993).

Lund G., and Enard D., *Instrumentation in Astronomy*, Proc. SPIE 445, 65, (1983).

McCaughrean M. J., 'The astronomical application of infrared array detectors', Ph.D. Thesis Edinburgh University, 1987.

Mignoli M., and Cuby J. G.,'Sky subtraction with fibres' *Instrumentation in Astronomy VII*, David L. Crawford, Editor, Proc. SPIE 1235, 98-109, (1990).

Mountain C. M., Robertson D. J., Lee T. J., Wade R.,'Advanced cooled grating spectrometer for the UKIRT' *Instrumentation in Astronomy VII*, David L. Crawford, Editor, Proc. SPIE 1235, 25-33, (1990).

Nelson G. W.,' Introduction to Fiber Optics' *Fiber Optics in Astronomy*, Samuel C. Barden, Editor, Astronomical Society of the Pacific Conference Series, Vol. 3, 2-22, (1988).

Neugebauer G., Leighton R. B.,'The Two Micron Sky Survey', U. S. Government Printing Office, Washington, D. C., (1982).

Nicia A.,'Lens coupling in fiber-optic devices: effciency limits' Applied Optics, Vol. 20, no. 18, 3136-3145, (September 1981).

Parry I. R., and Sharples R. M.,'AUTOFIB - Current Status' *Fiber Optics in Astronomy*, Samuel C. Barden, Editor, Astronomical Society of the Pacific Conference Series, Vol. 3, 93-98, (1988).

Parry I. R., and Carrasco B. E.,'Deep fibre spectroscopy' *Instrumentation in Astronomy VII*, David L. Crawford, Editor, Proc. SPIE 1235, 702-708, (1990).

Parry I. R., Lewis I. J., Sharples R. M., Dodsworth G. N., Webster J., Gellatly D. W., Jones L. R., Watson F. G.,'Autofib-2: an automated fibre positioner for the prime focus of the William Herschal Telescope' *Instrumentation in Astronomy VIII*, David L. Crawford, Eric R. Craine, Editors, Proc. SPIE 2198, 125-133, (1994).

Powell J. R., *Instrumentation in Astronomy*, Proc.SPIE 445, 77, (1983).

Ramsey L. W.,'Focal Ratio Degradation in Optical Fiber of Astronomical Interest' *Fiber Optics in Astronomy*, Samuel C. Barden, Editor, Astronomical Society of the Pacific Conference Series, Vol. 3, 26-40, (1988).

Ramsey S. K., Mountain C. M., Geballe T. R.,' Non-thermal emission in the atmosphere above Mauna Kea' Mon. Not. R. Astron. Soc., Vol. 259, 751-760, (1992).

Spyromilio J., Allen D. A., Graham J. R., Pinto P. A., Eastman R. G.,'Infrared Spectroscopy of Supernovae' *Infrared Astronomy with Arrays: The next generation*, Ian S. McLean, Editor, 65-68, (Netherlands, 1994).

Steele I. A., Jameson R. F., Hodgkin S. T., Hambly N. C.,'Infrared spectroscopy of low-mass stars and brown dwarfs in the Pleiades' Mon. Not. R. Astron. Soc. no. 275, 841-849, (1995).

Taylor K., Gray P. M.,'2df: the AAT's planned wide-field multifiber spectroscopic facility-report on commissioning the 2df corrector/ADC' *Instrumentation in Astronomy VIII*, David L. Crawford, Eric R. Craine, Editors, Proc. SPIE 2198, 136-142, (1994).

Tokunaga A. T.,Toomey D. W., Carr J., Hall D. N., Epps H. W.,' Design for a 1 to 5 μm cryogenic echelle spectrograph for the NASA IRTF' *Instrumentation in Astronomy VII*, David L. Crawford, Editor, Proc. SPIE 1235, 131-143, (1990).

Watson F. G.,'Multi-object Spectroscopy with FLAIR' *Fiber Optics in Astronomy*, Samuel C. Barden, Editor, Astronomical Society of the Pacific Conference Series, Vol. 3, 125-132, (1988).

Watson F. G., Terry P.,*Gemini*, no. 42, 32, (1993).

Wyse R. F. G., and Gilmore G.,'Sky subtraction with fibres' Mon. Not. R. Astron. Soc., Vol 257, 1-10, (1992).

Zur A., Katzir A.,'Theory of fiber optic radiometry, emissivity of fibers, and distributed thermal sensors' Applied Optics, Vol. 30, no. 6, (February 1991).